In Vitro Astrocyte Remodeling of Extracellular Matrix Following Mild Traumatic Brain Injury

Laith Al-Jaouni

Thesis submitted to the Faculty of the
Virginia Polytechnic Institute and State University
in partial fulfillment of the requirements for the degree of

Master of Science
in
Biomedical Engineering

Scott Verbridge, Chair
Pamela VandeVord
Arina Korneva

May 3rd, 2023
Blacksburg, Virginia

Keywords: Traumatic Brain Injury, Extracellular Matrix Remodelling, Reactive Astrocytes
Copyright 2023, Laith Al-Jaouni

In Vitro Astrocyte Remodeling of Extracellular Matrix Following Mild Traumatic Brain Injury

Laith Al-Jaouni

(ABSTRACT)

Every year millions of individuals suffer from traumatic brain injury (TBI) leading to permanent disabilities and even death. Mild TBI (mTBI) is the most common form of TBI comprising about 80-90% of all occurrences. Following a CNS insult like an mTBI, astrocytes can undergo activation resulting in the transformation into reactive astrocytes (RAs). RAs also play an important role in brain remodeling following an mTBI. Research on the mechanical complexity of the brain has important implications for understanding brain function and dysfunction, as well as for the development of new diagnostic and therapeutic tools for neurological disorders. This study aimed to develop and utilize an *in vitro* mTBI platform to investigate the intricate mechanical interplay between the extracellular matrix (ECM) and astrocytes following a simulated mTBI. Cellular mechanisms underlying mTBI and the contribution of mechanical forces that result in prolonged brain damage are yet to be comprehensively understood. Successfully devised mechanical characterization techniques for tissue-engineered models were developed utilizing atomic force microscopy and rheology. Astrocyte exposure to high-rate overpressure revealed altered mechanical properties of the surrounding matrix and decreased expression of laminin and collagen IV, which are critical for brain function and may contribute to pathologies associated with mTBI. The developed platform and methods provide new insights into the mechanistic complexity underlying ECM-astrocyte interactions following an mTBI.

In Vitro Astrocyte Remodeling of Extracellular Matrix Following Mild Traumatic Brain Injury

Laith Al-Jaouni

(GENERAL AUDIENCE ABSTRACT)

Every year, millions of people suffer from traumatic brain injury (TBI), which can lead to permanent disabilities or even death. The most common form of TBI is mild TBI (mTBI), which accounts for 80-90% of all cases. After a mTBI, astrocytes, the most common cell type in the brain, can become activated and turn into reactive astrocytes (RAs). RAs play an important role in the brain's recovery following a mTBI. Understanding the mechanical complexity of the brain is crucial for developing new diagnostic and therapeutic tools for neurological disorders. This study aimed to investigate the mechanical interplay between the modeled tissue and astrocytes following a simulated mTBI using an *in vitro* platform. Development of mechanical characterization techniques allowed for any alterations caused by the astrocytes to their environment to be detectable. The astrocyte exposure to the simulated mTBI revealed altered mechanical properties of the surrounding environment and decreased expression of proteins laminin and collagen IV, which are critical to brain function and may contribute to pathologies associated with mTBI. This study provides new insights into the mechanistic complexity underlying the interaction between astrocytes and their environment, which could lead to the development of new treatments.

Dedication

First and foremost, I dedicate this thesis to my fiancé, Nadine Manna, whose unwavering support, encouragement, and steadfast belief in my abilities have been essential to my success. I am grateful for her love and companionship, and I am looking forward to creating a future together filled with love and happiness. Next, I would like to dedicate this thesis to my beloved father, Baher AlJaouni. His steadfast belief in my abilities, tireless encouragement, and wise guidance have played a pivotal role in shaping my academic journey and achievements. His love, support, and sacrifices have been a constant source of inspiration, and for that, I am forever grateful. Additionally, I dedicate this work to my beloved grandmother, Ferdaus Al-Jaouni, whose love and support have been a guiding light throughout my life. My siblings - Abraham Al-Jaouni, Aliya Al-Jaouni, Eleena Al-Jaouni, and Zaina Al-Jaouni have been with me every step of the way and huge support throughout my academic journey. Their love and encouragement have propelled me forward, and I am blessed to have them in my life. Lastly, Nadia Da'ana, your dedication to my success and your unwavering support and encouragement have been a great source of inspiration for me. I feel incredibly fortunate to have such loving and supportive family and friends in my life. Their unwavering support, guidance, and encouragement have been indispensable to my academic success, and I am truly grateful for their presence in my life.

Acknowledgments

Thank you to the Laboratory for Integrative Tumor Ecology, Dr. Scott Verbridge, Dr. Anand Vadlamani, Dr. Barath Udayasuryan, Dr. Zerin Khan, Savieay Esparza, Raffae Ahmad, Xiang Pan, Brian Parker, Shivanie Kumar, and Patrick Kruk.

Additional thanks is due to the Traumatic Nerve Technologies Laboratory, Dr. Pamela VandeVord, Kelsey Wilson, Ryosuke Yokosawa, Noah Showalter, Brendan Arnold, Jessica Wilkes, and others.

Finally, I must thank those who funded this work, the National Science Foundation Award 2141291 on Deciphering Mechanisms of Mechanotransduction in Astrocyte Reactivity.

Contents

List of Figures ix

List of Tables xi

1 Introduction 1

1.1 Mild Traumatic Brain Injury . . . 1

1.2 Role of Astrocytes in mTBI . . . 2

1.2.1 Physiological Function of Astrocytes . . . 2

1.2.2 Reactive Astrocytes . . . 3

1.2.3 ECM Remodelling . . . 5

1.3 Mechanobiology . . . 7

1.3.1 Understanding the Unique Strains and Trauma Resulting from mTBI Impacts . . . 7

1.3.2 Nanomechanical Characterization . . . 8

1.4 Motivation . . . 15

1.5 Objectives . . . 15

2 Development of Semi-Permanent 3D Platform to Encase a Hydrogel 17

2.1 Introduction . . . 17

2.2 Formulation, Concept and Feasibility 18
2.2.1 User Needs 19
2.2.2 Design Inputs and Outputs 23
2.3 Verification and Validation 31
2.3.1 Materials and Methods 31
2.3.2 Results 36
2.3.3 Discussion 39
2.3.4 Conclusion 40

3 Developing Method of Mechanical Characterization via Rheometric Analysis 41

3.1 Introduction 41
3.2 Materials and Methods 42
3.3 Results 48
3.4 Discussion 53

4 Development of Mechanical Characterization via Atomic Force Microscopy 57

4.1 Introduction 57
4.2 Materials and Methods 58
4.3 Results 63
4.4 Discussion 66

5 Evaluating the Mechanical Alterations of Reactive Astrocytes **68**

5.1 Introduction . . . 68

5.2 Materials and Methods . . . 69

5.3 Results . . . 73

5.4 Discussion . . . 81

6 Conclusion **88**

Bibliography **90**

Appendices **103**

Appendix A Collagen I Hydrogel Synthesis **104**

A.1 Protocol . . . 104

A.2 Equations . . . 104

Appendix B Collagen I - HA Hydrogel Synthesis **106**

B.1 Protocol . . . 106

B.2 Equations . . . 106

Appendix C ImageJ Anlaysis **109**

C.1 Cell Viability . . . 109

Appendix D 3D Surface Profilometer **111**

List of Figures

1.1 Diagram depicting the activation of astrocytes following an mTBI. Created with BioRender.com 4

1.2 Small Amplitude Oscillatory Shear Testing 10

1.3 Atomic Force Microscopy Diagram 13

2.1 Schematic of the SWG used to expose cultured cells to high-rate overpressure. The side view (A) and top view (B) of the SWG depicts how an experiment is set up to inflict a shock wave. The culture plate in (C) depicts how the culture plate can be used to hold the sample. An alternative option is to utilize a distinct holder within the SWG to incorporate a Petri plate. 20

2.2 Negative mold design 26

2.3 Membrane layer. A very thin layer of PDMS about 15 microns in height sitting on a silicon wafer is shown in (A). (B) portrays a spin coater that vacuums the silicon wafer down and subjects it to a rotation velocity of 3000 rpm. 27

2.4 Platform Assembly 30

2.5 Membrane Removal 33

2.6 Membrane integrity experimental setup 36

2.7 Platform Biocompatibility 37

2.8 Reproducibility and integrity of PDMS membrane 38

3.1 BCA Assay Experimental Setup 44

3.2 Blast Modulus Impact Experimental Setup 46

3.3 Quantification of the concentration of proteins within the cytosolic and membrane compartments 48

3.4 Optimizing Hydrogel Compatibility with Rheology 50

3.5 Optimized Rheology Protocol Yields Outcome with Minimal Deviation . . . 52

4.1 Modification of PDMS Platform for AFM 61

4.2 Utilization of AFM Platform 62

4.3 AFM Initial Phase Force Curve Generation 64

4.4 AFM Functioning Nanoindentation 65

5.1 GFAP Fluorescence in 2D and 3D 74

5.2 Analysis of GFAP Expression in 2D and 3D 76

5.3 Reactive Astrocytes Modulate Microenvironment 78

5.4 Reactive Astrocytes Alter Mechanical Integrity of Surrounding Matrix . . . 79

5.5 Collagen IV, Laminin and GFAP Expression Following High-Rate Overpressure 80

5.6 Analysis of RA ECM Protein Deposition 82

5.7 Human MMP Antibody Array 83

C.1 Cell Viability Analysis in ImageJ 110

D.1 Thickness Measurement 112

List of Tables

2.1 User Needs 19

2.2 Design Inputs 23

2.3 Pugh Matrix of Material Selection 24

3.1 Evaluation of Hydrogel Transfer to Peltier Plate 51

List of Abbreviations

AFM Atomic Force Microscopy

BBB Blood Brain Barrier

CNS Central Nervous System

ECM Extracellular Matrix

GFAP Glial Fibrillary Acidic Protein

HA Hyaluronan or Hyaluronic Acid

mTBI Mild Traumatic Brain Injury

RAs Reactive Astrocytes

TBI Traumatic Brain Injury

TBI is an injury causing brain dysfunction caused by an external force, usually a violent blow to the head.

mTBI is a classification of TBI severity that includes loss of consciousness of 30 minutes or less, a Glasgow Coma Scale score of 13-15, and post-traumatic amnesia not greater than 24 hours.

CNS is one part of the nervous system that consists of the brain and spinal cord.

BBB is a network of blood vessels and tissue that is made up of closely spaced cells and helps keep harmful substances from reaching the brain.

RAs are astrocytes that undergo morphological, molecular, and functional changes in response to pathological situations in the surrounding tissue.

ECM is a large network of proteins and other molecules that surround, support, and give structure to cells and tissues in the body.

GFAP is a marker of astroglial injury and a type III intermediate filament that forms part of the cytoskeleton of mature astrocytes.

HA is a primary component of the brain extracellular matrix and functions through cellular receptors to regulate cell behavior within the central nervous system.

AFM is a very high resolution type of scanning probe microscopy.

Chapter 1

Introduction

Every year millions of individuals suffer from traumatic brain injury leading to permanent disabilities and even death. In the United States alone, over 64,000 TBI-related deaths were reported in 2020 [1]. A TBI is typically classified into mild, moderate and severe categories [2]. Any severity of TBI has a high risk of long term disabilities as one third of individuals that survive suffer persistent neurological dysfunction. The long-term effects on the brain remain largely unknown, but TBI has been linked to neurodegenerative diseases such as Alzheimer's and Parkinson's [3]. A great majority of TBI occurs from falls, vehicle accidents and assaults. It is estimated that 1 in 6 Americans live with a TBI related disability causing an estimated 76.5 billion cost to society [4].

1.1 Mild Traumatic Brain Injury

Mild TBI (mTBI) is the most common form of TBI comprising of about 80-90% of all occurrences [5, 6]. A mTBI can be characterized by brief or no loss of consciousness and minimal duration of post-traumatic amnesia resulting from any type of mechanical force impacting the skull [7, 8]. Clinical pathophysiological diagnosis is difficult to determine due to the common absence of objective findings on standard clinical imaging [2]. One of the most recent widely used definitions of mTBI established by the World Health Organization (WHO) is based on review of literature. The WHO definition comprises of a Glascow Coma Scale

score of 13-15, post traumatic amnesia lasting less than 24 hours and loss of consciousness lasting 0-30 minutes [9].

The majority of those that experience a mTBI only encounter temporary brain dysfunction. Post mTBI symptoms include somatic, cognitive and emotional symptoms that gradually resolve in most patients within the first 3 months of injury. The short term symptoms associated with mTBI deceived many to believe that any damage to the brain had been reversed during the healing process. Data collected from autopsies, new imaging modalities and biomarkers in new reports suggest that structural and pathophysiological changes occurs with mTBI [10, 11]. Wide reports have also been made linking chronic traumatic encephalopathy with mTBI. Although structural brain changes were observed in the reports, the relationship between mTBI and post-concussive symptoms remains difficult to link and does not explain the persisting problems in most patients [2].

1.2 Role of Astrocytes in mTBI

1.2.1 Physiological Function of Astrocytes

Astrocytes are a type of specialized glial cells that constitutes the majority of all cells in the human brain. They are scattered throughout the entire central nervous system (CNS) with the responsibility for a wide variety of complex and essential functions [12]. Essential functions include but are not limited to CNS homeostasis, maintenance of the blood-brain barrier (BBB), signal transmission across synapses, and metabolic regulation [13]. The anatomical organization of astrocytes is such that no overlaps or regions are lacking the specialized cell. Astrocytes have a star-shaped morphology that extends to many branches. These branches allow individual cells to form gap junctions with other astrocytes using

their distal tips, extensive contact with blood vessels, contact with hundreds of dendrites, and envelop over 100,000 synapses [14, 15]. Astrocytes represent critical components in the multicellular response to trauma and disease within the CNS, playing a pivotal role in the response to brain damage. The occurrence of biochemical and morphological modifications is a characteristic feature of astrocytic response to brain damage [16].

1.2.2 Reactive Astrocytes

Following a CNS insult like a TBI, astrocytes can undergo activation resulting in the manifestation of two different histological phenotypes over time. First is the transformation into reactive astrocytes (RAs) and then scar-forming astrocytes (SAs) [13]. RAs can be defined as astrocytes that undergo alterations in molecular, morphological, and functional aspects in response to pathological stimuli from surrounding tissue [17]. Elevated glial fibrillary acidic protein (GFAP) expression and cell hypertrophy are the standards for defining RAs [18].

RAs can be further divided into subgroups: neurotoxic astrocytes and neuroprotective. While this binary classification of astrocytes is widely used and makes it easier to comprehend, the complex functional heterogeneity makes it much more difficult to label the true nature of the cells [17, 19]. The transformation into RAs is characterized by alterations in morphology, increased expression of the intermediate proteins GFAP and vimentin, and increased proliferation and secretion of inflammatory mediators and growth factors [20].

Astrocyte activation can be initiated via mechanosensitive channels in the plasma membrane through stretching [13]. The mechanical strain on the cells induces an activation response by stimulation of P2 receptors which causes activation in extracellular signal-related protein kinase [21]. When exposed to high-rate overpressure, astrocytes also exhibit changes in structural and junction proteins through the contributions of extracellular adhesion and

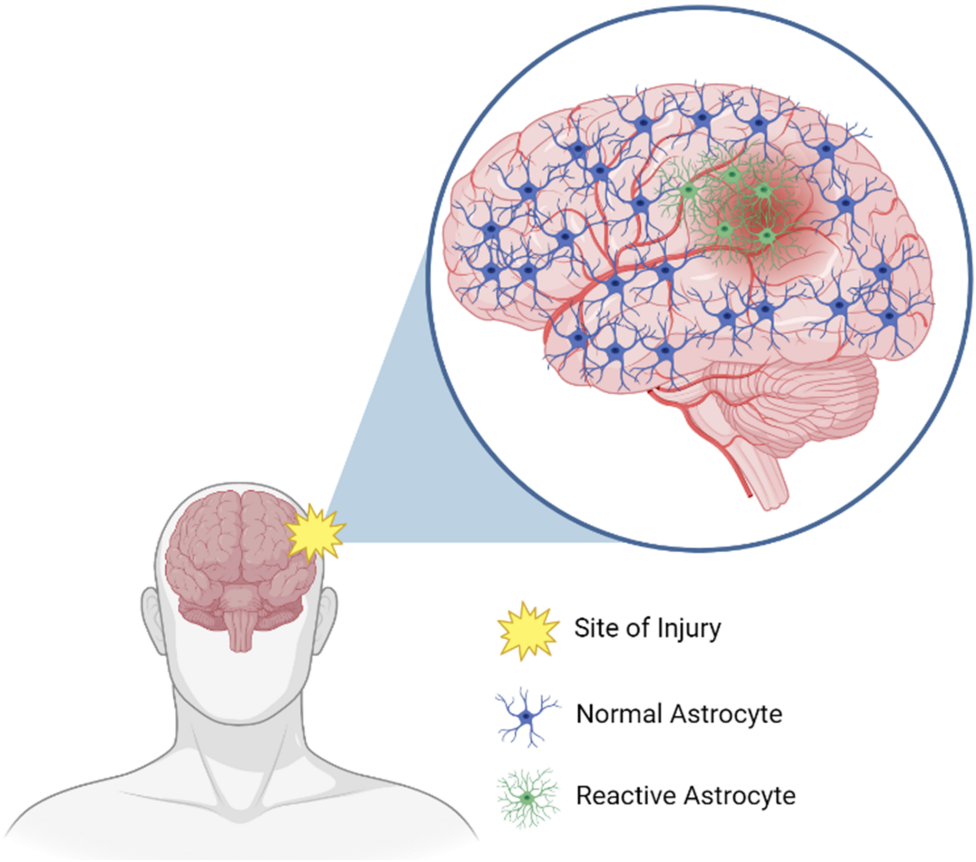

Figure 1.1: Diagram depicting the activation of astrocytes following an mTBI. Created with BioRender.com

cationic conductance [22].

Mechanical insult to the brain not only has immediate pathological effects but also secondary pathological processes. After the initial insult, a complex interaction between activated microglia and astrocytes recruited peripheral immune cells and the production of cytokines and chemokines creating cross-reactivity and feedback loops. Peripheral immune cells aid in the recruitment of additional cells to the injury site and promote activation of astrocytes which leads to further damage of surrounding tissue [23]. Cytokines that are significant in the activation of astrocytes include IL-1β, IL-6, and TNF-α which bind to their receptors and initiate downstream signaling pathways. Reactive astrocytes also secrete inflammatory

factors like HMGB1 and reactive oxidative species (ROS) promoting the positive feedback loop of activation [24].

1.2.3 ECM Remodelling

Brain extracellular matrix (ECM) is a macro-molecular network composed of proteins and polysaccharides occupying space between the neurons and glia that contributes approximately 20% of volume in the brain [25, 26]. The ECM contributes to proper brain function, providing structural support and modulating intercellular communication [27]. Unlike most regions of the body, the brain contains low levels of fibrous proteins like collagen and fibronectin. ECM in the brain is primarily composed of glycosaminoglycans, proteoglycans, and glycoproteins which provide the soft characteristic of brain tissue. The microenvironment modulated by the brain ECM exerts a significant influence on both normal and pathological conditions in the adult brain, playing crucial roles in processes such as neurite outgrowth, synaptogenesis, synaptic stabilization, and injury-induced plasticity [28].

RAs also play an important role in brain remodeling following a mTBI. The disruption of the BBB resulting from a head injury precipitates dysfunction that initiates a cascade of secondary injuries, including cell death, oxidative stress, and inflammation. These occurrences significantly impact the interaction between BBB endothelial and astrocyte cells, resulting in their further activation [29]. RAs leads to an upregulation of ECM molecule synthesis and the secretion of proteases, which contribute to the ongoing remodeling of the ECM [30]. Alterations from RAs can have both advantageous and unfavorable effects on the process of functional recovery [31].

A mTBI triggers the upregulation of additional ECM components that are primarily expressed in developing or pathological brain tissue [31]. Proteoglycans are a major component

of brain ECM that mediates cell to cell interaction and contribute to modulating growth factors during development and response to pathophysiological conditions in an adult [32]. Proteoglycans can be subclassified based on their glycosaminoglycan sugar chains. Chondroitin sulfate proteoglycans (CSPGs) and Heparan Sulfate Proteoglycans (HSPGs) are of interest due to their association with astrocyte deposition. CSPGS are the most studied proteoglycan in the nervous system, which following a TBI showed increased neurocan and aggrecan deposition by neurons and astrocytes [33, 34]. HSPGs have important roles as modulators of cell signaling in the brain. Agrins are core HSPG proteins in the basement membrane of brain microvasculature that maintains BBB integrity [35]. HSPGs that are upregulated or altered by astrocytes include Osteopontin, Laminin, Tenascin-C and Hyaluronan [31, 36]. Hyaluronan (HA) possesses physiological properties, such as maintaining biomechanical integrity, regulating tissue hydration, and facilitating tissue assembly, which are contingent upon its size, concentration, and localization. HA modifications resulting from mTBI have a significant impact on both the integrity of the ECM and signaling processes. HA is anchored to the ECM through the formation of exceedingly stable complexes with HA-binding proteins called hyaladherins, which can function as either adhesion proteins or receptors, including CD44 [37].

Matrix metalloproteinases (MMP) are a class of enzymes that execute diverse roles in the brain like brain remodelling and degradation [38]. Studies conducted have confirmed that following an ischemic stroke and TBI, RAs overexpress MMP-2 and MMP-9 leading to degradation of ECM and hyperpermeability of the blood brain barrier (BBB) [39, 40, 41, 42]. MMP-2 is primarily involved in the proteolytic degradation of the basement membrane, a specialized extracellular matrix (ECM) that provides structural support to cells and tissues. On the other hand, MMP-9 primarily modulates the dynamic equilibrium of the ECM by degrading and remodeling its various components [43]. It has also been observed that cy-

tokines secreted by RAs can induce modifications to the structural integrity and composition of the ECM. Additionally, alterations to the ECM can influence the functions of astrocytes [44].

1.3 Mechanobiology

Brain tissue is one of the most complex tissues in the human body due to its intricate network of billions of neurons and glial cells that communicate with each other through complex electrical and chemical signaling pathways [45]. Additionally, the brain's plasticity, or ability to adapt and change in response to experiences and stimuli, adds another layer of complexity to the already intricate nature of brain tissue [46, 47].

Despite being a soft and fragile organ, the brain is remarkably durable and resilient. It has unique mechanical properties can be contributed to its intricate physical structure. The mechanical complexity of the brain arises from its unique composition of various types of cells as well as the complex network of connections between these cells. In addition to its complex cellular structure, the brain is also a highly dynamic and constantly changing system, with neural activity patterns constantly shifting and adapting in response to internal and external stimuli. These dynamic changes in neural activity patterns are reflected in changes in the mechanical properties of the brain, such as changes in its elasticity and stiffness [45, 48].

1.3.1 Understanding the Unique Strains and Trauma Resulting from mTBI Impacts

Impacts to the head, such as a mTBI, result in the transfer of mechanical energy to the skull, leading to distinctive dynamic responses and characteristic brain tissue trauma. The

extent of impact and the mode of transmission give rise to a three-dimensional linear and rotational acceleration of the brain, leading to unique strains [49]. The exact mechanisms underlying the transformation of astrocytes into their reactive form in response to strain remains incompletely understood. However, emerging evidence sheds light on this process. Astrocytes have been shown to sense strains through mechanosensitive ion channels, stretch sensitive cation channels and plasma membrane stretching evoked by traumatic membrane deformation [21, 50, 51, 52].

1.3.2 Nanomechanical Characterization

Nanomechanical testing is a highly sophisticated technique that enables the precise measurement of mechanical properties at the nanoscale. It is a powerful tool that offers insights into the behavior of materials at the molecular level. In the context of tissue engineered hydrogels, nanomechanical testing is essential for characterizing the mechanical properties of these soft materials. A hydrogel are hydrophilic, three-dimensional networks that mimic critical features of a natural ECM. They can include ECM proteins that that replicate native cellular environments of soft tissues making them ideal for *in vitro* experiments. Changes in the composition and structure of the ECM can have a significant impact on the mechanical properties of a hydrogel, as well as on the behavior of cells and tissues that interact within it. Nanomechanical testing is a valuable tool for studying the effects of such changes, providing detailed information on the stiffness, viscoelasticity, and other mechanical properties.

In the context of astrocyte-seeded hydrogels, nanomechanical testing is particularly important for observing changes in the mechanical properties of a hydrogel induced by reactive astrocytes. Reactive astrocytes are known to modulate the ECM of the central nervous system (CNS), which may lead to alterations in its mechanical properties. By measuring

the mechanical behavior of the hydrogel at the nanoscale, insights into the interplay between reactive astrocytes and the ECM can be investigated, shedding light on the complex mechanisms underlying CNS pathologies.

Rheology

Rheometry refers to the experimental method utilized to measure the rheological characteristics of materials. A rheometer can perform various rheometric tests to determine the viscoelastic properties of a substance. A material that doesn't fit strictly into the categories of solid or liquid, but instead falls in a region between the two, is classified as a viscoelastic material. Viscoelastic materials exhibit both viscous and elastic behavior. The most widely used technique for measuring viscoelastic properties using rheometry is known as small amplitude oscillatory shear (SAOS) testing. During this process, the sample is oscillated around its equilibrium position in a continuous cycle. The amplitude of oscillation is equal to the maximum applied strain or stress, and the frequency is represented by the number of oscillations per second [53]. A diagram shown in figure 1.2 (A) shows how a sample is compressed between two parallel plates and subject to oscillatory strain by rotation of the top plate. The strain inflicted on the hydrogel can be calculated by applying equation 1.1 to the diagram shown in figure 1.2 (B).

Dynamic oscillatory tests apply a sinusoidal strain to the sample at a given frequency. The sample's response to stress gives informs the viscous and elastic behavior. The shift between the input strain and output stress shown in figure 1.2 (C) is called the phase angle. The phase angle ranges from 0 to 90 degrees and denotes whether the material deforms elastically like a solid or viscously like a liquid. A high phase angle would denote a viscous behavior. Using equations 1.6, 1.7 and 1.8 the elastic and storage modulus can be calculated. The complex shear modulus is the total modulus measured from the material.

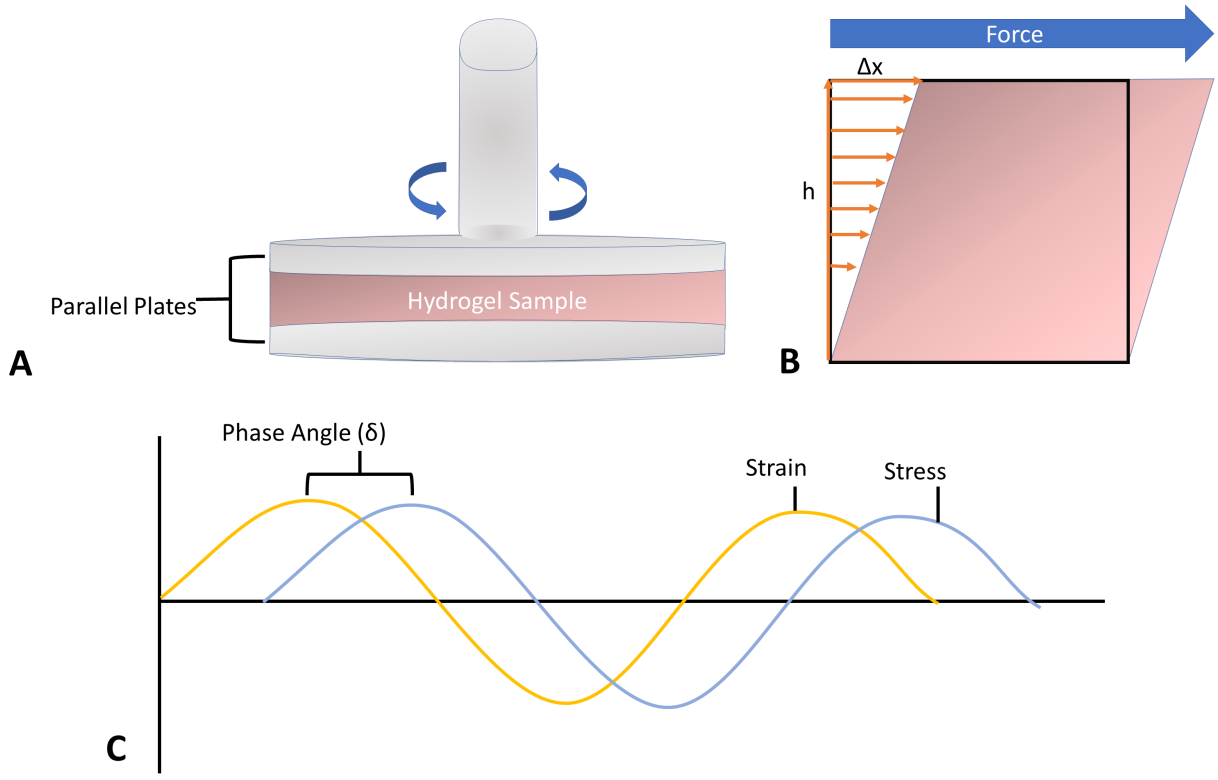

Figure 1.2: Small Amplitude Oscillatory Shear Testing. (A) the sample is placed between two parallel plates and compressed to a specified loading gap. The sample is then trimmed to the diameter of the top plate and SAOS testing oscillates the top plate to a specified strain at a specified frequency. (B) depicts how the rotation of the top plate causes a shear force to be applied to the sample causing deformation. Shear strain is dependent on both the height of the sample and displacement in direction of the force. (C) The phase angle informs how viscous or elastic the material is. Once a stress is applied to the sample, energy lost is contributed to the loss modulus and energy returned to the system contributes to the storage modulus. The phase angle can range from 0 to 90 degrees. All figures were adapted from [53] and [54].

$$\gamma = \Delta x/h \tag{1.1}$$

Where γ = strain, Δx = displacement in the direction of applied force (m) and h = sample height (m).

$$M = r * F \tag{1.2}$$

Where M = torque (N*m), r = radius (m) and F = force (N).

$$\sigma = M(N * m) * K_\sigma \tag{1.3}$$

Where σ = shear stress (Pa) and K_σ = stress constant dependent on measurement geometry.

$$\theta = s/r \tag{1.4}$$

Where θ = angular displacement (radians) and s = arc length (m).

$$\gamma = \theta * K_\gamma \tag{1.5}$$

Where K_γ = strain constant dependent on measurement geometry.

$$G = \theta * \gamma \tag{1.6}$$

Where G = complex shear modulus (Pa).

$$G' = Gcos(\delta) \tag{1.7}$$

Where G' = elastic storage modulus (Pa) and δ = phase angle.

$$G'' = Gsin(\delta) \tag{1.8}$$

Where G'' = viscous loss modulus (Pa).

Equations 1.9 and 1.10 are true when using parallel plate geometry.

$$K_\sigma = 2/(\pi * r^3) \tag{1.9}$$

$$K_\gamma = r/h \tag{1.10}$$

Where h = gap height (m).

Atomic Force Microscopy

Atomic force microscopy (AFM) is a type of scanning force microscopy that has the capability to reach resolutions sub nanometer. There are three primary modes at which it can operate: force measurements, topographic imaging and manipulation. Force spectroscopy is a powerful technique that allows for the characterization of the mechanical properties of materials at the nanoscale. In the context of hydrogels, AFM is widely used to measure the elastic modulus, which is a measure of the stiffness or rigidity of the material.

Hydrogels are soft materials that typically exhibit low stiffness and high elasticity, making

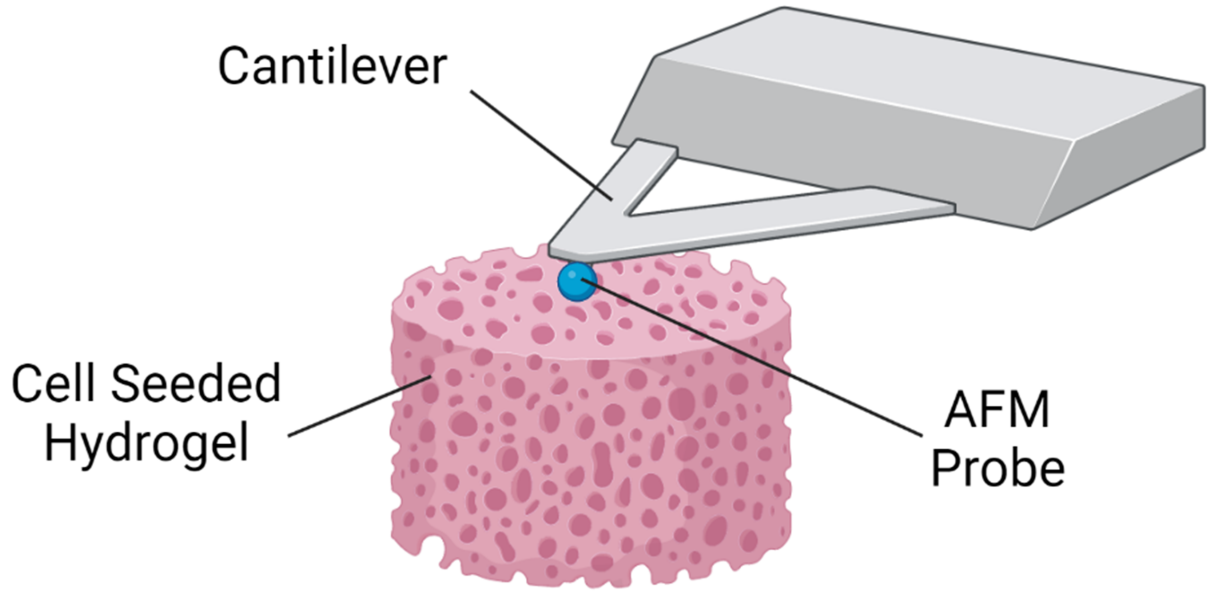

Figure 1.3: Depiction of a colloidal probe causing a micro indentation on a cell seeded hydrogel. Created with BioRender.com

them challenging to measure using traditional mechanical testing techniques. Rheology requires that the overall sample modulus be calculated, even if heterogeneity within the sample exists. AFM overcomes this limitation by using a colloidal probe to apply a small force to the surface of the hydrogel, allowing for the localized measurement of its deformation under the applied load. By analyzing the resulting force-displacement curves, AFM can accurately determine the elastic modulus of the hydrogel, providing crucial information about its mechanical behavior.

Motion of the probe as it interacts with the hydrogel is monitored by a laser beam that tracks its position through reflection off the cantilever. The projected laser beam bounces off the surface of the cantilever into a position sensitive photo detector (PSPD) that can read the motion of the probe. Deflection of the cantilever is calibrated by pressing the probe against a very hard surface like silicon and measuring the voltage at the known deflection [55]. The spring constant of the cantilever can be determined through photothermal excita-

tion. Photothermal excitation provides a wide frequency bandwidth excitation by inducing thermal expansion of the cantilever via excitation laser which provokes cantilever oscillation [56]. The amplitude of the oscillation is measured by the PSPD and the system uses that information to determine the spring constant.

The Hertz model is widely used to obtain elastic modulus with the data acquired from the AFM. The model assumes that the sample is isotropic, linearly elastic and that the indenter which is the probe in this case is not deformable. Tip geometry ultimately decides which equation is used as the surface indentation will vary across geometries [57]. For a colloidal probe, the Hertz equation is given by 1.11.

$$F = (4/3) * E * R * \delta^{(3/2)} \tag{1.11}$$

Where F = contact force between the probe and hydrogel (N), E = elastic modulus of material being probed (Pa), R = radius of colloidal probe (m) and δ = indentation depth of the probe into the material (m).

Equation 1.11 can be rearranged to solve for the elastic modulus shown in equation 1.12. The force is obtained by the AFM through indentation depth and spring constant measured.

$$E = (3/4) * F/(R * \delta^{(3/2)}) \tag{1.12}$$

A cell seeded hydrogel requires a hydrated environment and thus requires submerged AFM. Submerged AFM involves obtaining force curves of the hydrogel submerged in a liquid environment. While it is necessary to keep hydrogels hydrated, submerged AFM does create many difficulties. Liquid used can cause interference with the probe, cause thermal drift and affect the force between the probe and sample. Development of a protocol to measure soft

hydrogels submerged in liquid must be developed to obtain precise mechanical properties.

1.4 Motivation

It is crucial to investigate the cellular mechanisms associated with mTBI pathologies and the role of mechanics in causing prolonged damage. Understanding these mechanisms will help to identify injury thresholds and and to reveal unknown factors related to the pathophysiological outcomes of brain trauma. Development of an *in vitro* mTBI platform may provide a novel method for analyzing relevant molecular relationships and identifying potential therapeutic targets. Investigating the mechanical complexity of the brain has important implications for understanding brain function and dysfunction. For example, investigations into the mechanical characteristics of brain tissue may facilitate deeper comprehension of the fundamental mechanisms that contribute to mTBI and may potentially pave the way for the development of novel therapeutic interventions to preempt or alleviate the aftermath of such injuries. Overall, the study has significant implications for improving health outcomes for those experiencing mTBI and for the development of new diagnostic and therapeutic tools for neurological disorders.

1.5 Objectives

To investigate the mechanical impact reactive astrocytes have on their surrounding matrix, a novel platform to house the *in vitro* tissue engineered models needed to be developed. The first objective is to develop a platform that is able to house and protect a hydrogel being submerged in a custom built shock wave generator so that a high-rate overpressure similar to a mTBI may be inflicted upon the samples. The development of the platform is

detailed in chapter 2. The second objective of the study is to develop a method of mechanical characterization for the *in vtiro* models. By development of mechanical characterization methods, astrocytes can be analyzed for modulation of surrounding matrix mechanical integrity. Chapters 3 and 4 detail the methods used to characterize hydrogels. The third objective is to investigate the mechanical alterations astrocytes exposed to a high-rate overpressure impose on their microenvironment. The details surrounding this study is located in chapter 5.

Chapter 2

Development of Semi-Permanent 3D Platform to Encase a Hydrogel

2.1 Introduction

The aim of this thesis is to investigate the role astrocyte mechanotransduction plays on mTBI secondary injury cascades due to differential response to high-rate mechanical insult sensed through cell-matrix signaling. In previous studies, a custom-built shock wave generator (SWG) device shown in figure 2.1 was utilized to expose astrocytes to high-rate mechanical impulses. This process mimics the injury mechanisms associated with different types of TBI. The SWG produces characteristic pressure profiles with high-intensity spikes in pressure that occur on the micro-to-millisecond timescale. Select parameters of the mechanical impulses are of interest regarding their influence on the injury response of cells and tissue.

Utilization of the SWG in previous studies was limited to blasting cells in 2D. Cells would be grown on a petri dish, filled with sterile media and then wrapped in parafilm to create a sterile border from water in the tank. Due to the full submersion of the sample shown by figure 2.1, tissue-engineered *in vitro* hydrogels were not compatible with the device. Although two-dimensional cell culture is much cheaper and easier to execute, it is not an accurate representation of cellular behavior *in vitro*. The discrepancies between 2D and 3D cultures are numerous, with morphology being a significant factor. 2D cultures, which involve cells

growing in a monolayer on a flat surface, exhibit flattened and elongated characteristics. In addition, cell junctions are less prevalent and poorly represented, and cellular proliferation occurs at an unnaturally rapid rate. Furthermore, there are differences in gene and protein expression when compared to *in vivo* models, and cell differentiation is suboptimal. In particular, 2D cultures inadequately model the response of cells to mechanical stimuli, which is crucial in this study. [58].

To achieve compatibility between the SWG and 3D cell matrices, a novel platform was developed. This endeavor was motivated by the compelling ability of 3D cell cultures to emulate the typical cell-matrix and cell-cell interactions that occur in vivo, thus facilitating more accurate and reliable experimental outcomes. The brain microenvironment plays a crucial role in regulating astrocyte structure and function. A 3D cell matrix better mimics the in vivo brain environment because it provides a more physiologically relevant structure for cell growth and function compared to 2D cell cultures. In vivo, cells exist in a 3D matrix, and this environment plays a critical role in cell signaling, gene expression, and cell behavior. By contrast, 3D cell cultures allow cells to interact with each other more naturally and are typically more porous, allowing for the exchange of nutrients and gases. These conditions better mimic the in vivo brain environment, resulting in more physiologically relevant cell behaviors, gene expression patterns, and responses to mechanical stimuli. It is not clear how high-rate parameters contribute to micro-level strains in cells and their ability to differentially respond, thus motivating studies of astrocytes exposed to such impulses.

2.2 Formulation, Concept and Feasibility

The SWG is a specialized device designed to mimic TBI on cell cultures in vitro. The device works by employing an exploding bridge wire mechanism, which has been selected for its

economical and compact nature in generating blast waves via an electrical discharge. In particular, a high-voltage power source charges a capacitor to 5 kV, which is then discharged into the wire, causing it to be destroyed and generate a pressure wave characteristic of a blast. To measure the pressure wave, a strain gauge is utilized, and the results are recorded using an oscilloscope [59].

2.2.1 User Needs

Prior to the development of the platform, a comprehensive evaluation of user needs was undertaken. Table 2.1 delineates the specific needs, their corresponding metrics, and priority levels assigned on a scale of 1 to 5, with 5 indicating the highest priority. These needs were meticulously identified by accounting for the deficiencies of the existing platform, project financing limitations, experimental utilization, and post-processing analysis requirements.

Table 2.1: User Needs

User Need	Design Requirement	Metric	Priority (1-5)
UN 1	Biocompatible	Cytotoxicity	5
UN 2	Optically Transparent	Optical Transmittance	3
UN 3	High Reconfirgurability	Reconfiguration Complexity	3
UN 4	Robust/Reliable	Failure Rate	4
UN 5	Accessible for Imaging	Compatibility with Standard Imaging Systems	5
UN 6	Durability	Fatigue Life	3
UN 7	Semi-Permanent Membrane	Residue-Free Removal	4
UN 8	Ease of Use	Training Requirements	3
UN 9	Removable Hydrogel	Removability	5
UN 10	Inexpensive	Price of Production	2

Biocompatibility is the ability of the platform to not cause harm or have a negative impact on cell seeded hydrogels. Biocompatibility of the platform was given the highest priority due to the necessity that the platform does not interfere with the biological processes being

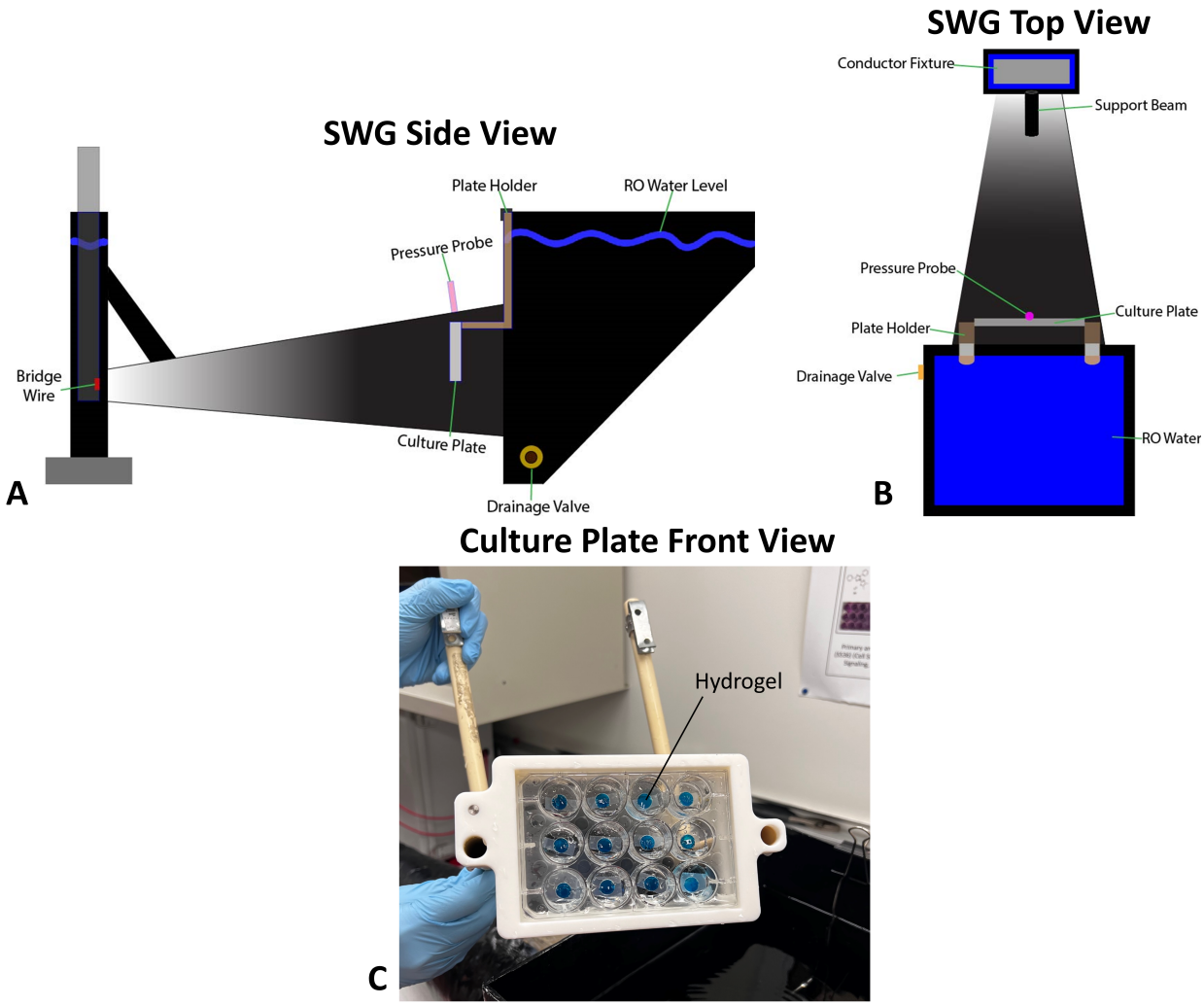

Figure 2.1: Schematic of the SWG used to expose cultured cells to high-rate overpressure. The side view (A) and top view (B) of the SWG depicts how an experiment is set up to inflict a shock wave. The culture plate in (C) depicts how the culture plate can be used to hold the sample. An alternative option is to utilize a distinct holder within the SWG to incorporate a Petri plate.

studied or cause harm to the sample being tested. Biocompatbility of the device can be evaluated by analyzing the cytotoxicity the platform has on the samples. As a user need, biocompatibility for research devices is important for ensuring the accuracy, reliability, and reproducibility of experimental results. Users need to have confidence in the results they obtain from their experiments, and this confidence can be enhanced by using biocompatible devices and materials that minimize the potential for artifacts or confounding factors.

Optical transparency refers to the ability of a material or device to transmit light with minimal absorption or scattering, which allows for clear and accurate visualization of the sample. It was ranked a three out of five due to the ability of the sample to be visualized under normal brightfield microscopy which may be helpful in many experimental procedures. Accessibility for imaging is a higher-priority user need that identifies the need for platform compatibility with conventional confocal and brightfield microscopes. The platform must be designed in a manner that ensures its dimensions can fit within all standard microscope incubation chambers, plates, and slide holders. Without meeting this need, the platform will be very limited in experimental analysis potential.

To submerge a hydrogel in the SWG it needs to be fully encased within the platform. To ensure that the hydrogel was also accessible after the blast, the platform also needed to incorporate a removable membrane making it open-faced. For this reason, a semi-permanent membrane needs to be incorporated that can detach without damaging the hydrogel or leaving residue behind. Incorporating a semi-permanent membrane feature onto the platform will have the highest correlation with the ease of use user needs, thus both must be taken into consideration when designing. Ease of use was given a priority of three because it is important for the device to be manufactured and utilized without much difficulty, but it should not be prioritized over functionality.

This study plans to investigate the effect astrocytes have on the mechanical integrity of their

microenvironment. As such, it is necessary to utilize an extracellular matrix that can be detached from the platform for mechanical assessment, while preserving the matrix's overall structural integrity. This user need is of utmost importance because the study's success hinges on it. Without a detachable hydrogel that maintains its structural integrity during removal from the platform, the study's objective would be unachievable. As a result, this user need must be met to guarantee that the study can yield reliable and accurate findings.

Reliability is a critical user requirement that virtually all devices or platforms seek to achieve, regardless of their intended application. Given its paramount importance in ensuring optimal efficiency and minimizing failure rates, this user need was assigned a priority rating of four. To satisfy this user need, the platform under development must be designed to guarantee the reliability of collected data and ensure that the number of experiment samples is not compromised by platform failure.

Given the prolonged experiments that the platform will need to conduct, as well as the ability to reuse it, durability was identified as another key user need. The platform will be frequently subjected to autoclaving as a sterilization method. Autoclaving employs saturated steam under pressure at approximately 15 psi and $121°C$ to sterilize materials. The ability of the platform to endure repeated use will enhance its durability and contribute to user need ten in Table 2.1, which pertains to cost-effectiveness. As project funds are limited, it is imperative to consider production costs when designing the platform. The priority of user need ten was assigned a rating of only two out of five, as it should not take precedence over the other user needs to be listed in the table.

Given the diverse range of applications that necessitate the collection of data regarding the various mechanisms by which astrocytes interact with their microenvironment following an mTBI, the underlying platform must be adaptable to meet the specific needs of each experiment. For this reason, the reconfiguration complexity of the platform must be kept to

a minimum. The design and manufacturing of the platform should be readily comprehensible, such that any modifications required by the user for a given experiment can be implemented with relative ease.

2.2.2 Design Inputs and Outputs

Once the user needs were identified, design inputs were formulated shown in table 2.2. The requirements set in the table are based on the needs of the platform, each with strict acceptance criteria.

Table 2.2: Design Inputs

Design Input	Requirement	Description	Acceptance Criteria
DI 1	Biocompatible	The platform must not result in a reduction of cellular viability	No statistical significance in the difference between cell viability in platform vs normal culture conditions
DI 2	Temperature	The platform's operational functionality must be upheld across various temperature environments	Performance of platform is maintained across temperatures ranging from 4-37°C
DI 3	Size	Must fit within standard microscope incubation systems	External dimensions smaller or equal to 85.4 mm width x 127.6 mm length x 20.2 mm height
DI 4	Lifespan	The platform must not degrade over one month during cell culture	Platform does not lose mass over 1 month period
DI 5	Moldable	The material should mold into any cavity designed	Material can cure into the shape of negative mold
DI 6	Optical Transparency	The platform should be able to transmit light	Material can pass over 85% of light through
DI 7	Resists Failure under High Pressure	The platform does not rupture during a blast from the SWG	Material maintains structural integrity
DI 8	Gas Permeable	The platform allows gas to permeate through surface	Material is gas permeable

Material Selection

A decision matrix shown in table 2.3 was employed to evaluate the optimal material for the platform. The criteria were adapted from [60] and adjusted based on the user needs 2.1 and design inputs table 2.2. The materials being compared are commonly used in research devices for *in vitro* modeling of various physiological mechanisms.

Table 2.3: Pugh Matrix of Material Selection

	Material				
Criteria	Polydimethylsixoxane (PDMS)	Polymethylmethacrylate (PMMA)	Polylactic Acid (PLA)	Polystyrene (PS)	Agarose
Ease of Fabrication	+	−	+	−	**0**
Robust Mechanical Properties	+	+	−	+	−
Ease of Sterilization	+	**0**	**0**	**0**	**0**
Gas Permeable	+	−	+	+	+
Biocompatible	+	+	+	+	+
Potential for Chemical Modification	+	+	+	+	+
Optical Transparency	+	+	−	+	+
Flexible	+	−	−	−	+
Bonding	+	**0**	−	−	**0**
Totals	9	1	0	2	4
Rank	**1**	4	5	3	2

Based on the analysis conducted using the Pugh matrix, it was found that polydimethylsiloxane (PDMS) was the only material that met all the specified criteria. Other materials were found to be unsatisfactory on multiple criteria or did not meet the required standards. Polystyrene (PS) and polymethylmethacrylate (PMMA) were identified as more challenging to manufacture than alternative materials. Additionally, PMMA's impermeability to gas could hinder the ability of a temporary 3D platform. This, in turn, may cause hypoxia and lead to skewed experimental results. Furthermore, all materials, except PDMS, had glass transition temperatures lower than $121°C$, making them unsuitable for autoclave sterilization. Given that the platform must be able to undergo deformation under stress to achieve physiologically relevant strain for mTBI experiments, rigid materials were not viable. Therefore, PDMS was selected for further experimentation [60, 61, 62, 63, 64, 65, 66].

Once PDMS was determined to be the material used in the platform, the limitations for the use of a negative mold could be determined. PDMS is a highly proficient material for the generation of micro features; nevertheless, its utilization in this platform would not prove advantageous. To design a cavity that is fully encased, there will need to be a minimum of two layers of PDMS bound to each other. The best way to bond PDMS is by utilization of a plasma cleaner. This method requires that both surfaces of PDMS being bound together

are completely flat, void of surface defects, and without surface contaminants like dust. For this reason, traditional rapid prototyping using both SLA and FDM 3D printing techniques could not be utilized due to the surface artifacts they produce as a byproduct of their manufacturing technique. A negative mold must be manufactured with a material with a smooth surface and could easily be manufactured for rapid prototyping. PDMS also cures much quicker at higher temperatures adding additional requirements for the negative mold to be made from a material with a glass transition temperature higher than $80°C$. Cast acrylic met all of the conditions listed above and was chosen to be the primary component of the negative mold. With a smooth surface and glass transition temperature ranging from $100 - 115°C$, it was suitable for the application [67].

Platform Design

The negative mold was designed in a manner that allowed high reconfigurability and rapid prototyping. Because acrylic was selected as the material of choice for the negative mold, laser cutting was used as part of the manufacturing process. Laser-cutting cast acrylic provides clear-cut edges, fast speeds, and high accuracy [68]. The negative mold was designed to be compatible with a laser cutter shown by the drawings in figure 2.2.

The negative mold geometry was designed so that the outer borders of the PDMS fit snugly inside a Falcon 12-well cell culture plate (catalog number 353043, Corning Inc., Somerville, MA). A secure fit was deemed necessary to prevent adverse effects on the hydrogel due to floating or detachment of the PDMS platform from the well. The top and bottom layers of the negative mold were fabricated from 3 mm cast acrylic, while a 0.8 mm Polyethylene terephthalate glycol (PETG) was employed for the hydrogel cut out, given the unavailability of acrylic with such thickness. The three layers of the negative mold were bonded using super glue (part number 1299292831, Loctite, Westlake, Ohio), which was found to be the most

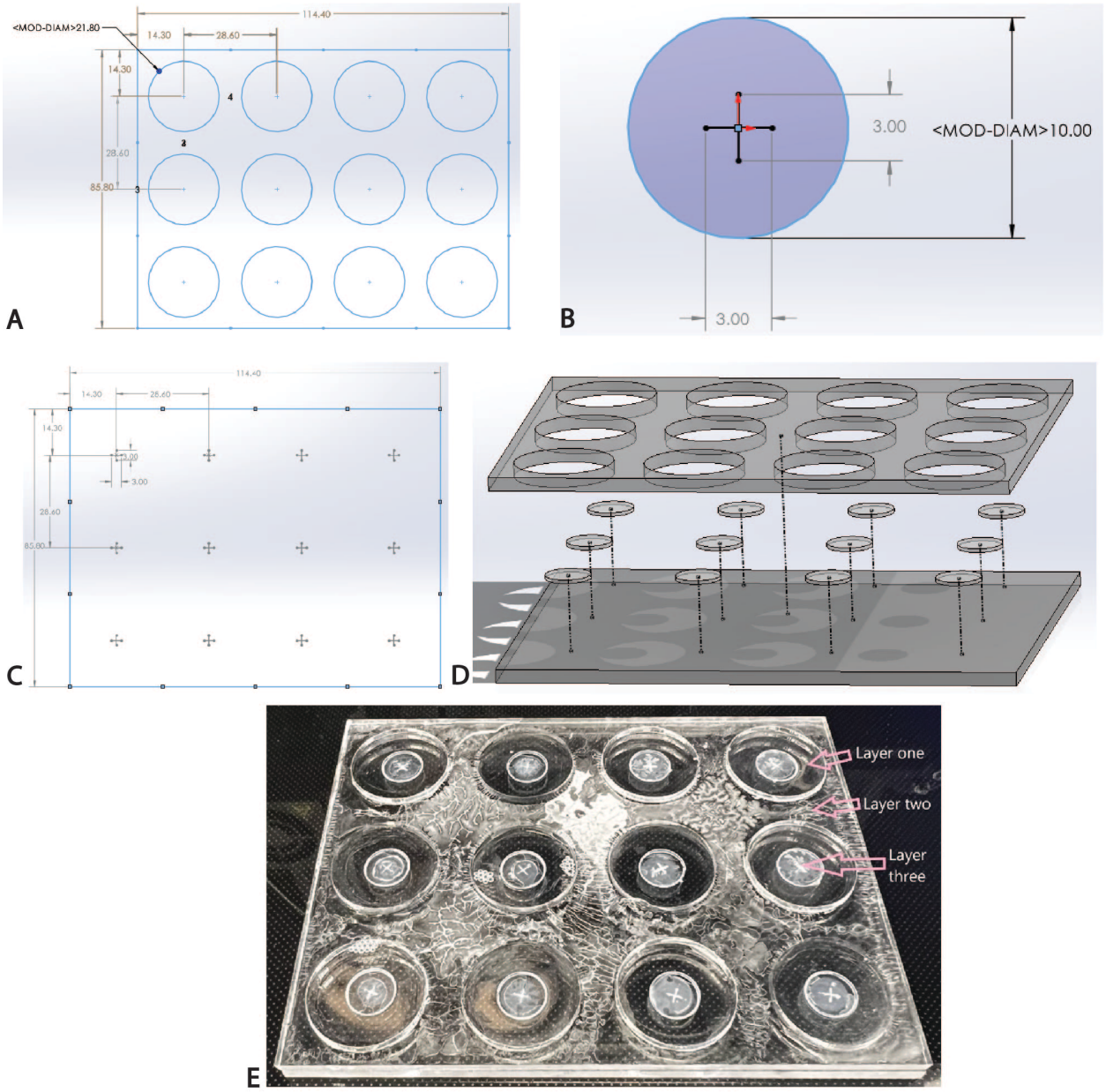

Figure 2.2: Negative mold design. (A), (B) and (C) are drawings used for the top layer, hydrogel cutout, and bottom layer respectively. Dimensions for each part are provided in mm which were based on a standard 12-well tissue culture plate. The circles in (A) create cavities for the PDMS to be poured into. Blue lines indicate what should be cut while the black and grey plus signs in (B) and (C) are engraved to aid in the alignment of the hydrogel cavity to the middle of the mold. (D) illustrates how the individual layers were assembled to produce the final part. The assembled negative mold is displayed in (E).

efficient adhesive for rapid prototyping, given cost and ease of use. It is critical to prevent any superglue from seeping out of the edges, as it may lead to toxic effects leeching into the PDMS surface. Leeching can be readily detected on PDMS by observing the formation of a sticky surface and a cloudy region. In future iterations, a biocompatible adhesive may be considered.

Producing the PDMS platform for compatibility with the SWG requires additional steps and components than just pouring PDMS into a negative mold. The hydrogel must be protected from the unsterile hypotonic water, thus incorporation of another layer is necessary. A thin membrane layer was designed to temporarily cover the hydrogel. Figure 2.3 displays how a thin layer of PDMS is subjected to a high centrifugal force which reduces the thickness to tens of microns high. The membrane layer mustn't be thick so that it allows the SWG to subject strain on the hydrogel, accurately mimicking an mTBI.

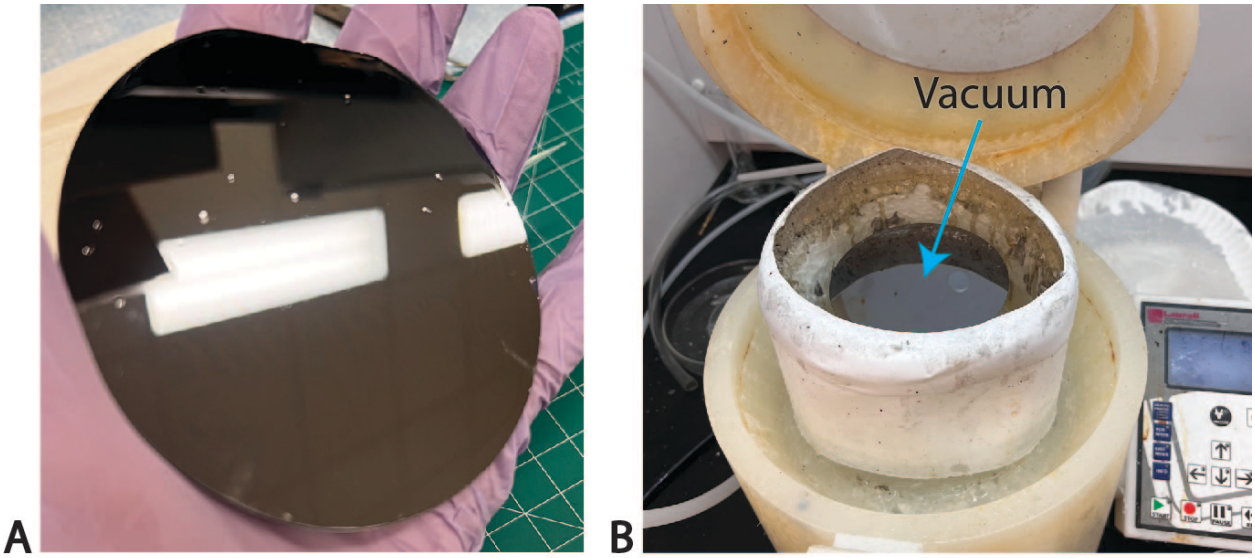

Figure 2.3: Membrane layer. A very thin layer of PDMS about 15 microns in height sitting on a silicon wafer is shown in (A). (B) portrays a spin coater that vacuums the silicon wafer down and subjects it to a rotation velocity of 3000 rpm.

Manufacturing and Assembly Procedure

Manufacturing of the PDMS platform used to encase a hydrogel during a simulated blast mimicking an mTBI required that the negative mold shown in figure 2.2 (E) be assembled. The original drawing files were created in SOLIDWORKS and saved as .dxf files were later modified in AutoCAD Mechanical. AutoCAD Mechanical was used to communicate with the laser cutter (VLS3.60DT, Universal Laser Systems, Scottsdale, Arizona) which lines should be cut and which should be engraved. As mentioned in 2.2.2The membrane layer mustn't besuper glued together and any residual glue on the surface was removed with isopropyl alcohol (IPA) and a Kim wipe.

PDMS bond strength is determined by chemical and physical interactions at the surface-to-surface interface [69]. The surfaces of both the negative mold and the silicon wafer were chemically modified using Trichloro(1H,1H,2H,2H-perfluorooctyl) silane (448931-10G, Sigma-Aldrich, St. Louis, Missouri) to decrease the bond strength of PDMS to the corresponding surface. Silane consists of hydrophobic molecules that can reduce surface energy by deposition of self-assembled monolayers via chemical vapor deposition [70, 71]. Additionally, the silane coating can create a barrier between the substrate and the PDMS that can prevent direct contact between the two materials. This barrier layer can further reduce the adhesion of PDMS to the substrate, making it easier to manipulate and remove the PDMS material. The surfaces coated with a silane monolayer were placed in a vacuum chamber along with a small piece of PDMS. 100 μL of silane was then pipetted onto the surface of the PDMS and the chamber was closed for 3-5 hours.

Once a silanized negative mold and silicon wafer are produced, production of the two platform layers can begin. SYLGARD 184 Elastomer Kit (material number 2065622, Dow, Midland, Michigan) was used to synthesize the PDMS by mixing the elastomer base and curing agent

at a 10:1 ratio. The mixture was then placed into a vacuum chamber for 30 minutes to degas. For the base layer, PDMS was slowly poured into the negative mold to avoid air bubble formation. The membrane layer was manufactured by first placing a silanized wafer into the spin coater shown in Figure 2.3 (B). The wafer was then suctioned down in place and rotated to ensure that it was centered. The lid was then closed and a custom cycle was selected that subjects the wafer to 3000 rpm for 45 seconds. During the first cycle, 70% IPA was sprayed on the surface to remove any contaminants. Before starting the second cycle, PDMS was poured onto the center of the wafer until forming a 1 cm radius. The second cycle induces a high centrifugal force on the PDMS until an equilibrium is met creating a very thin layer on the surface. Both the wafer and the negative mold are left to cure at $70°C$ for 30 minutes. PDMS should not be sticky on the surface during removal, if so, allow additional time for curing.

Before bonding the two layers, the base layer requires access points for the hydrogel to be injected. Two 1 mm holes are created using a biopsy punch at diametrically opposed locations of the hydrogel cavity. This creates an inlet and outlet allowing a hydrogel to be injected into the platform and air to escape. The layers can then be bonded by utilizing a plasma cleaner shown in figure 2.4 (A). A plasma cleaner can activate the surface through a mixture of energetic particles including electrons, ions, and UV. By means of surface activation, terminal methyl groups may be replaced by silanol groups, which are capable of establishing covalent siloxane bonds with a corresponding silanol group on another activated PDMS surface [72]. This creates a permanent bond between the two PDMS layers.

It was determined that injecting fluid into the platform needed to be performed prior to removing the platform from the silicon wafer as shown in figure 2.4 (B). The pressure increase when injecting fluid into the cavity causes the membrane layer to expand, increasing volume and trapping in air. When the platform is kept bound on the wafer, the cavity is unable to

expand and mitigates the problem.

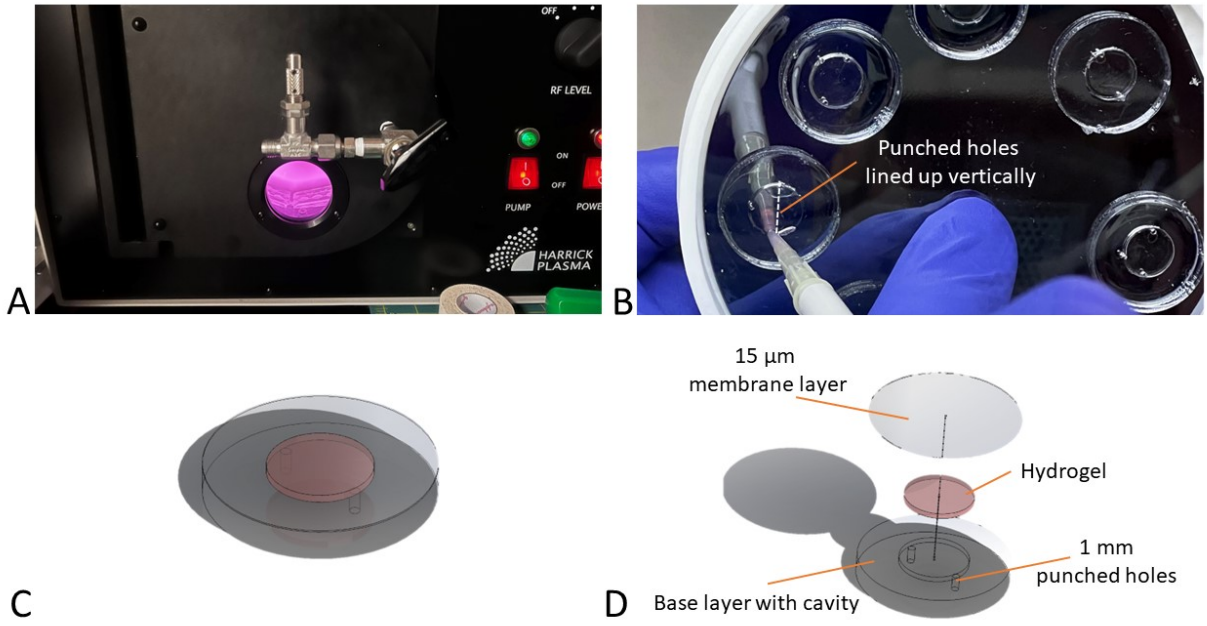

Figure 2.4: Platform Assembly. (A) PDMS-coated wafer and platform base layer are placed face up in a plasma cleaner to activate the surface for bonding. (B) both layers are bound together completing the 3D platform. Hydrogel is dispensed into the circular biopsy punched inlet hole and allowed to undergo crosslinking prior to extraction from the silicon wafer. (C) Cell-seeded hydrogel encapsulated by the 3D PDMS platform can be placed in a 12-well culture plate and subjected to a simulated blast. (D) Exploded view of the platform.

The hydrogel is introduced into the biopsy punched apertures and allowed to undergo crosslinking prior to extraction from the silicon wafer.

Before injecting the hydrogel into the 3D platform, the surface must be sterilized and chemically modified to allow adhesion of the ECM. A 21 gauge blunt tip needle that has been autoclaved is used to dispense each reagent. First 70% ethanol is used to fill the cavity and aspirated to sterilize the inner surfaces. Next Polyethyleneimine (PEI), a cationic organic polymer that effectively binds to DNA is used to treat the surface [73]. (add material used) was diluted to a 1% (v/v) solution by dilution in deionized water (DIW) and sterilized in

an autoclave. The PEI solution was incubated at room temperature in the platform for 10 minutes. Following PEI, glutaraldehyde was diluted to 0.1% (v/v) in DIW and was incubated at room temperature for 20 minutes in the platform. DIW was then used to wash the hydrogel cavity removing any residual cytotoxic reagents [74]. Once the surface treatments improving hydrogel adhesion to the PDMS were administered, the device was completed and ready for experimental use.

2.3 Verification and Validation

Verification of design inputs listed in table 2.2 was conducted to ensure the device met the required specifications. Many inputs from the table were accomplished through the material properties of PDMS. These inputs include DI 2, DI 4, DI 5, DI 6 and DI 8. DI 3 was accomplished by the design parameters of the platform shown in figure 2.2. For inputs requiring further testing, experiments were planned and conducted to ensure those needs.

2.3.1 Materials and Methods

SWG Blast procedure

The SWG is prepared by first filling the tank with RO water. A heating block is then used to warm the water to $37°C$. A NiCr40 bridge wire is then hooked up to the electrical discharge system and submerged in water. The sample is placed in a holder like the one shown in 2.1 and submerged in water. The capacitor is charged using a high-voltage power source which is then discharged into the NiCr40 bridge wire, causing it to be destroyed and generate a pressure wave characteristic of an mTBI. The pressure probe reads the magnitude of the blast using an oscilloscope.

Biocompatibility

A study on biocompatibility was verified by first analyzing the impact keeping a cell-seeded hydrogel in a closed platform starved of nutrition has on cell viability. Due to the limitation of available cells during the first experiment, 4T1 cells were used to carry out the study. A follow-up experiment was later conducted using normal human astrocytes (NHAs) to investigate if the assembly of the platform in 2.2.2 has a significant impact on cell viability.

For the first experiment, the 3D platform was assembled and a hydrogel was injected into the cavity. The hydrogel comprised of 4T1 cells seeded at $1x10^6$ cells / mL in a 3 mg/mL collagen ECM. Volumes for each reagent used to synthesize the gels were calculated through equations in A.2. The protocol A.1 was followed to make the gel. 12 PDMS molds were not bonded to a membrane layer as a control and 12 PDMS molds were bonded, creating the closed platform. All molds were injected with the cell-seeded hydrogel and left to crosslink in an incubator for 30 minutes. Once crosslinked, the hydrogels acting as a control were immediately placed in a sterile 12-well plate. The inlet and outlet holes were taped shut in the encapsulated gels to inhibit any air from seeping in during removal from the silicon wafer. Once removed, they were transferred to a sterile 12-well plate and left encapsulated for 1 hour and 24-hour time points. Once time points were met, the membrane layer was carefully removed using a pair of sterilized tweezers shown in figure 2.5 (B). The gels were immunostained for 45 minutes in calcein green 1:500 (v/v) in PBS (lot 2420629, Thermo Fisher Scientific, Waltham, MA) and propidium iodide 1:66.6 (v/v) in PBS (lot 2015554, Thermo Fisher Scientific, Waltham, MA) solution to determine viability. Fluorescence was captured using a confocal microscope and analyzed using ImageJ following the steps listed in C.1.

The second experiment assessing if the assembly of the platform has a significant impact on

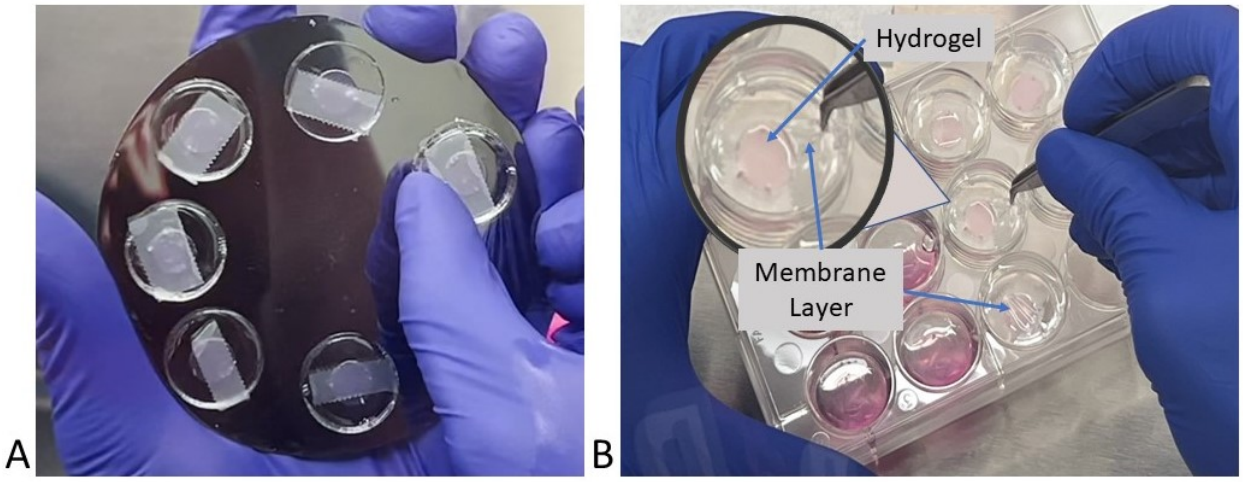

Figure 2.5: Membrane removal. The thin PDMS membrane is removed from the platform to expose the gel to the external environment. To remove the platform from the silicon wafer, the inlet and outlet holes must first be taped to prevent any air from entering the cavity (A). Once taped, tweezers are dragged along the perimeter of the mold to create a tear in the thin PDMS layer that sits on the wafer making it easier for the platform to be removed. Then the platform is carefully pulled from all directions until the platform pops off. Following a blast from the SWG, the membrane layer is sterilized and the membrane layer is removed using sterile tweezers (B). It is best to start from an edge and pull the membrane around the circumference until it peels off.

cell viability was conducted similarly to the initial experiment. In the first experiment, 4T1s were used which is a malignant immortalized breast tumor cell line. For this experiment, NHAs were used which are much less likely to survive harsh environments. The NHAs were seeded at $1x10^5$ cells / mL which was shown to be the optimal concentration in this experiment 3.3. The hydrogel also comprised of collagen I (catalog number CB-40236, Fisher Scientific Company LLC, Waltham, MA) and hyaluronic acid (catalog number GS1004, Advanced Biomatrix Inc, San Diego, CA) which better mimics the brain's microenvironment and keeps the NHAs in their quiescent state [75]. Details on the hydrogel synthesis can be found here B. 6 open platforms were acting as a control and 6 3D platforms were used to test the impact on viability. All molds were injected with the cell-seeded hydrogel and left to crosslink in an incubator for 30 minutes. Once crosslinked, the hydrogels acting as a control were immediately placed in a sterile 12-well plate. The inlet and outlet holes were taped shut in the encapsulated gels to inhibit any air from seeping in during removal from the silicon wafer. Once removed, they were placed in a non-sterile culture plate and submerged underwater in the SWG to simulate similar conditions to a blast procedure. After being submerged, the platforms were transferred back to the biological safety cabinet and dipped in 70% ethanol to sterilize them. Following sterilization, the molds were transferred to a sterile 12-well plate and left encapsulated for 1 hour after the seeding of the gel. Once an hour had passed, the membrane layer was carefully removed using a pair of sterilized tweezers as described in the first study. The gels were immunostained for 45 minutes in calcein green 1:500 (v/v) in PBS and propidium iodide 1:66.6 (v/v) in PBS solution to determine viability. Fluorescence was captured using a confocal microscope and analyzed using ImageJ, once again following the steps listed in C.1.

Membrane Efficacy

A study investigating the reproducibility and efficacy of the semi-permanent membrane was conducted. First, the thickness of the PDMS membrane that acts as a thin barrier between the hydrogel and water in the SWG was measured for its thickness. To begin, the PDMS membrane layer was manufactured according to 2.2.2 and left to cure before proceeding. The base layer was then plasma bonded on different areas of the wafer to asses if the membrane thickness changed upon removal. Using a Keyence VK-X3000 3D Surface profilometer, the thickness of the membrane was measured at different locations on a silicon wafer shown in figure 2.8 according to the procedure described in D. The 3D platforms were then removed from the wafer and the membrane layer was measured once again to determine the effects strain during removal has on thickness.

Additionally, the membrane was subjected to simulated blasts in the SWG to determine if it could withstand the high peak pressures generated by the instrument. 3D platforms were assembled and injected with dyed water to represent a hydrogel using the method shown in figure 2.4 (B). The inlet and outlet holes were taped and the platforms were transferred to a 12-well plate shown in figure 2.6. The plate was then inserted into the plate holder and submerged in the $37°C$ water. Three blasts were conducted with peak pressure readings of 16, 11, and 42 PSI. The plate holder was then removed from the SWG and rupture analysis was conducted.

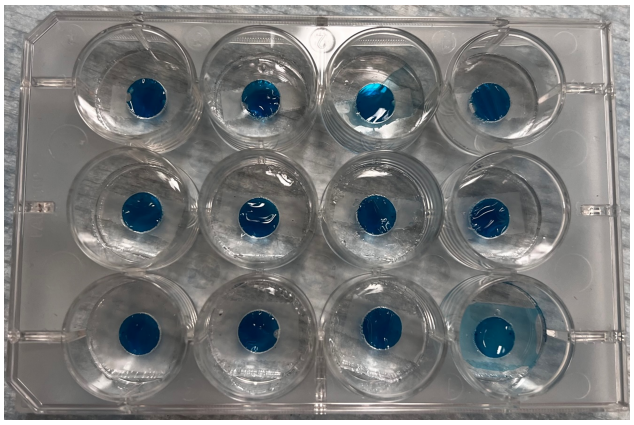

Figure 2.6: Membrane integrity experimental setup

2.3.2 Results

Biocompatibility

Results of both experiments testing the biocompatibility of the platform and blast procedure are shown in figure 2.7. Calcein green and propidium iodide was used to quantify the number of live and dead cells. The viability of 4T1 cells significantly decreases the longer they are kept within the 3D platform and starved of nutrients. Removal of the membrane layer at 1 hour opposed to 24 hours showed much higher cell survival as shown in (A). Results for the control where no membrane was present at both time points were not obtained due to siphoning of media out of the wells. It was originally thought that keeping the hydrogels closer to the surface of the 12-well plate would help create a more predictable blast profile, but due to siphoning of media, the inserts that raised the platform were removed from further experiments. Figure 2.7 (B) indicates that the blast procedure has no impact on cell viability.

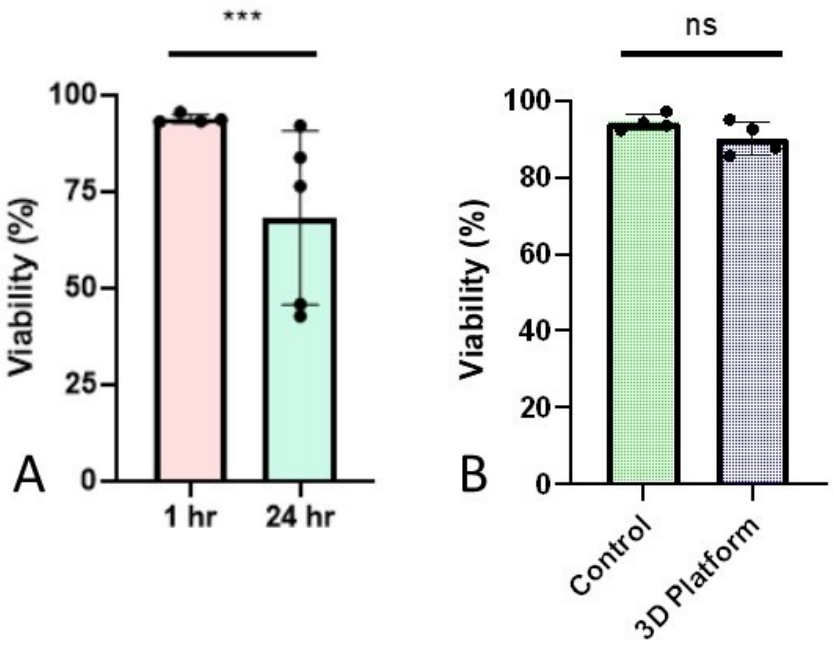

Figure 2.7: Platform Biocompatibility. (A) 4T1 cells were seeded in the closed 3D platform without removal of the membrane for 1 and 24 hours. (B) Viability of NHAs when subjected to SWG blast procedure.

Membrance Efficacy

Using the parameters outlined by 2.2.2 to create the PDMS membrane layer leads to an even coating on the wafer shown in figure 2.8 (A). No significant variation in thickness was observed with all measurements with an average of 15.58 μm across all readings. During the removal of the platform from the wafer, the membrane experiences some stretching that causes the thickness to decrease to an average of 13.63 μm. The new thickness of the membrane only showed a range of 1.47 μm across all samples.

3D platforms filled with dyed water and taped at the punched inlet and outlet showed no sign of rupture when subjected to high magnitudes of peak pressure. Well C4 shown in the bottom right of figure 2.8 (D) does appear to have some discoloration underneath the platform due to leakage of water around the tape.

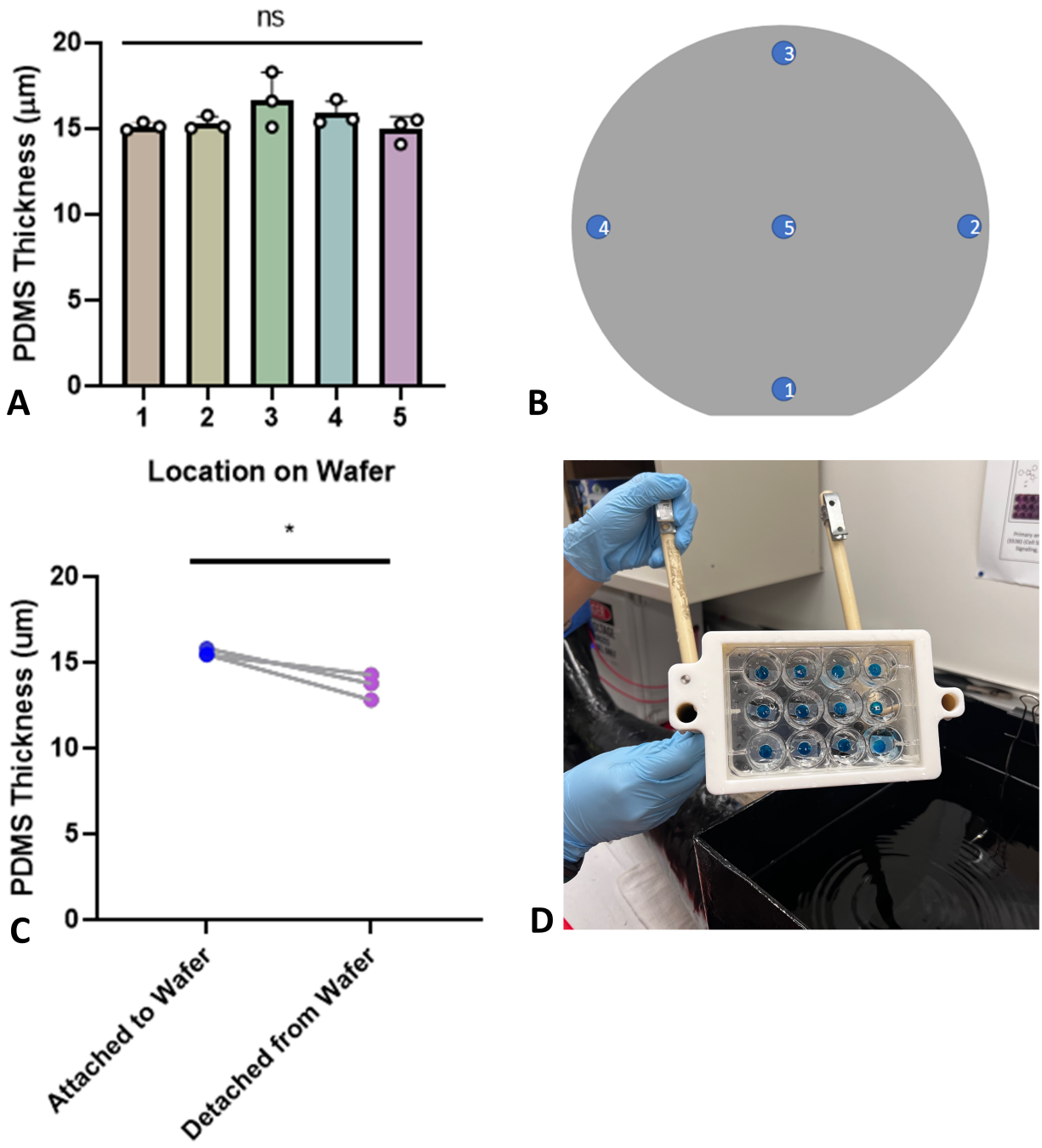

Figure 2.8: Reproducibility and integrity of PDMS membrane. (A) and (B) the thickness of the PDMS at multiple locations on the coated wafers. (C) changes in membrane thickness before and after removal from the wafer. (D) 3D platform filled with dyed water following a simulated mTBI at peak pressures of 16, 11, and 42 PSI.

2.3.3 Discussion

Biocompatibility

Decreased viability between 1-hour and 24-hour time points indicates that cells within the encapsulated hydrogel are starved of nutrients that are contained within the media. Therefore, incubation and exposure to blast should ideally occur within 1 hour of seeding the hydrogel in the platform. Conducting all steps of the blast procedure can be time-consuming, especially when transferring each individual mold. Not too many plates must be blasted in succession to not exert the hydrogels to nutrient starvation for too long. The blast procedure as described in the 2.3.1 second experiment does not impact cell viability and shows to be an effective method of blasting the hydrogels without sacrificing sterility. The procedure took into account the 1-hour window cells have before potentially decreasing in viability shown in figure 2.7 (A).

Membrance Efficacy

Figure 2.8 (A) and (B) show that the method used to produce the membrane layer is effective with insignificant variation between samples. Spinning the wafer at such a high angular velocity causes an equilibrium point where the PDMS evenly coats the surface. Air bubble formation on the surface is not common but should be avoided when bonding the base layer to ensure consistent membrane thickness.

The membrane layers in each platform should not cause any variation to the pressure profile subjected to the hydrogels. Additionally, the membrane has been shown to effectively protect the sample from the surrounding water within the SWG as shown in figure 2.8 (D). With a zero percent failure rate, the membrane has proven to be a reliable component of the

platform. The membrane developed may also apply to other applications that require a semi-permanent layer with easy accessibility and reliability.

2.3.4 Conclusion

Verification confirmed that all design input requirements were met by the design outputs implemented. Most standards were met through the material properties of PDMS which is a widely used material for *in vitro* modeling of various physiological mechanisms. Experiments also confirmed that biocompatibility and resistance to failure of the platform were met.

By revisiting the user needs in table 2.1, we can validate that the platform adheres to the requirements originally set. Although ease of use for the manufacture and use of the platform is not as simplistic as intended, any new user can learn how to use the platform for their experimental use. All other user needs are adequately met or excelled.

Chapter 3

Developing Method of Mechanical Characterization via Rheometric Analysis

3.1 Introduction

The brain is an extremely complex organ that is poorly understood at the mechanical level. Mechanical response of the brain has been linked to development and diseases, but further understanding has been challenging. This challenge is largely in part due to the organ being fully enclosed making it difficult to probe. The brain is also one of the softest organs in the body which make its response influenced by a fluid phase contributed by cerebrospinal fluid. Regional variation of the mechanical properties of the brain makes it especially difficult to detect changes due to mechanical insult [45].

Glia in the brain express mechanosensitive receptors that link the ECM to the cytoskeleton making the cells sensitive to external forces [76]. Astrocytes, a sub-type of glia are known to develop into a reactive phenotype when subjected to strain like a TBI. Reactive astrocytes (RAs) play an important role in brain remodeling following a mTBI. RAs lead to an upregulation of ECM molecule synthesis and proteases which contribute to ECM remodeling and

changes in the mechanical characteristics of the microenvironment.

To work around the issues associated with *in vivo* brain testing, an *in vitro* method of testing tissue-engineered brain models was developed to study the mechanical disparities between extracellular matrices encapsulating normal astrocytes against reactive astrocytes. There is a need to establish a method that quantifies very small changes in these *in vitro* models so that mechanical changes in the ECM due to astrocytes exposed to high-rate mechanical insults can be detected.

3.2 Materials and Methods

Cell Culture

Human astrocytes (catalog number 1800, Sciencell Research Laboratories, Carlsbad, CA) were cultured in complete Astrocyte Medium (catalog number 1801, Sciencell Research Laboratories, Carlsbad, CA). Cell passaging was performed when the confluency reached 80% or higher, accompanied by media exchanges occurring at intervals of 2-3 days. Cells were passaged by first removing media and washing with 5 mL of D-PBS. The D-PBS was then removed and 5 mL of trypLE was pipetted on the surface where the flask was then incubated for 7-10 minutes until all cells detached from the surface. 5 mL of complete astrocyte medium was then added to neutralize the trypLE, then the cell suspension was transferred to 15 mL where it was centrifuged at 150 x g for 5 min. The supernatant was then removed and 5 mL of media was added to resuspend the cells. The cells were passaged at a 1:3 split so 1.67 mL was added to each T-75 flask followed by 12 mL of media.

BCA Assay

A Bicinchoninic acid (BCA) assay was executed to extract cytosolic and membrane protein. First, the PDMS platform was manufactured and assembled according to 2.2.2 without the use of the membrane layer. Different cell concentrations were seeded within the gels to find the optimal seeding density. The hydrogel was then synthesized according to B with 63 μL/well with varying cell concentrations shown in 3.1. The hydrogels were left to incubate for 5 days before beginning the protein extraction.

Reagents used came from the Mem-PER Plus Membrane Protein Extraction Kit (catalog number 89842, Thermo Fisher Scientific, Waltham, MA). Each gel was placed in a 5 mL microcentrifuge tube along with 4 mL of cell wash solution and vortexed briefly, then the wash was discarded. The gels were then transferred to a 24-well plate containing the permeabilization buffer to sit. The gel and buffer were then transferred to a glass mortar and pestle tissue homogenizer to be shredded. The homogenate was transferred to a new tube where it was then incubated for 10 minutes at $4°C$. The tubes were then centrifuged for 15 minutes x 16,000 g at $4°C$. The supernatant containing the cytosolic proteins was then transferred to a new tube. The remaining pellet was resuspended in 1 mL of solubilization buffer and incubated for 30 min at $4°C$. The tubes were centrifuged once more for 15 minutes x 16,000 g at $4°C$. The supernatant containing the solubilized membrane and membrane-associated proteins was transferred to a new tube. The cytosolic and membrane supernatant was placed in a 96-well plate with each sample in triplicate. The absorbance was detected in a plate reader at 562 nm.

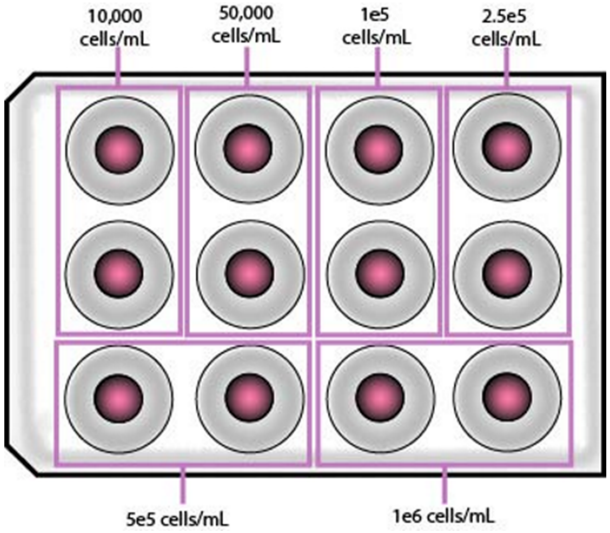

Figure 3.1: BCA Assay Experimental Setup. Hydrogels seeded with 6 different seeding densities to investigate the optimal concentration of cell/mL of gel.

Establishing Rheology Compatibility

The PDMS platform was manufactured by first using SYLGARD 184 Elastomer Kit (material number 2065622, Dow, Midland, Michigan) to synthesize the PDMS by mixing the elastomer base and curing agent at a 10:1 ratio. The mixture was then placed into a vacuum chamber for 30 minutes to degas. The degassed PDMS was then carefully poured into the negative mold shown in figure 2.2 (E) and left to cure for 30-40 minutes at $80°C$. The PDMS was removed from the mold and autoclaved for sterilization. Unlike the procedure described in section 2.2.2, the membrane layer was not manufactured because the hydrogels will not be blasted. The molds were placed in a sterile 12-well plate and the surface was first treated with polyethyleneimine at a 1% (v/v) solution in DIW for 10 minutes. Next, glutaraldehyde was left to incubate on the surface of the mold at a 0.1% (v/v) solution in DIW for 20 minutes. DIW was then used to wash the hydrogel cavity removing any residual surface treatments. The hydrogel did not contain any cells and was synthesized following the protocol in B with 63 μL/well. The hydrogel was left to crosslink in the incubator for

30 minutes and then filled with 1 mL of PBS.

A Discovery HR-30 rheometer was used with a temperature-controlled Peltier plate and an 8 mm parallel plate. Transferring the hydrogel from the PDMS mold was attempted using a transfer pipette, spatula, tweezers, and fine-tip paintbrush. Once the paintbrush was found to work best, it was utilized moving forward. A transfer pipette was used to transfer media to the Peltier plate. The gel was then placed on top of the liquid and spread out using two fine-tip brushes. The gel was then compressed to the loading gap where any excess liquid was removed using a Kim wipe.

For both strain and frequency sweeps, a 50 μm gap was used with a 0.03 N axial compression force being applied to the gel. An initial temperature of 37°C was set which was later modified to 21°C. A strain sweep was applied from 0.1 to 100% with a constant frequency of 6 rad/s. A frequency sweep was also applied from 0.1 to 100 rad/s with a set strain of 1.35%. Starting parameters for the sweeps were based on values presented in [77]. The rheometer can produce the storage and loss modulus by utilizing the equations listed in 1.3.2.

Assessing Modulus Discrepancies Between Blasted and Non-Blasted Hydrogels

An experiment was conducted that investigated the impact that blasting hydrogels in the SWG had on the shear modulus. First, the PDMS platform was manufactured and assembled according to 2.2.2. For the conditions without a simulated TBI blast, no membrane layer was bound to the base layer and the platform remained open. The collagen I-HA hydrogel was then synthesized according to B with a seeding density of 100,000 cells/mL based on the BSA assay results. Two 12-well culture plates contained all conditions for the experiment shown in 3.2. After the application of high-rate overpressure, the gels were subjected to a 4-day incubation period, during which fresh media was replenished every 2 days. The gels were

transferred using two paintbrushes with media coating the surface of the Peltier plate. Once the gel was spread out, the plates compressed it at the loading gap and any excess media was removed via Kim wipe. Stress sweeps were initially performed with a temperature of $21°C$, angular frequency of 0.25 rad/s, axial force of 0.05 N, and strain of 1.35%. Extremely high variability of the stress sweeps prompted the switch to strain sweeps. All parameters remained the same and a strain sweep from 0.1 to 5% was applied.

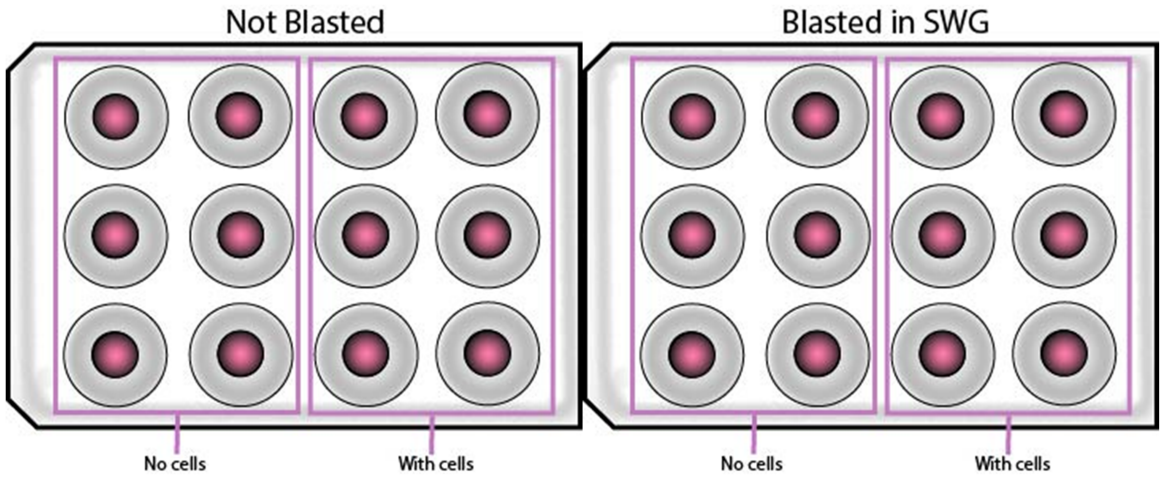

Figure 3.2: Blast Modulus Impact Experimental Setup. The two 12-well plates contain four conditions for the experiment. The conditions aim to identify the impact mimicking an mTBI has on both hydrogel integrity and astrocyte remodeling of the ECM

Adjusting Experimental Procedure to Decrease Modulus Variability between Samples

The high variability between results shown in figure 3.5 (A) prompted many changes to be made to the experimental procedure. The primary aim is to decrease variability between samples so that shear modulus differences between conditions can be detected, even if subtle. First, the hydrogel was designed to be much larger in volume, increasing from 63 μL to 170 μL. The increase in hydrogel diameter and thickness was prompted after observing the very thin gels in the original mold degrade over time and become much thinner causing rips and

tears when transferring 3.1. The thin nature of the gels is also thought to contribute to some variability due to the very small 50 μm gap height required when testing. This gap height is significantly smaller than any other experimental setup found in the literature. The new cavity within the PDMS mold was designed to be 12 mm in diameter and 1.5 mm in height which are both an increase from the original 10 mm diameter and 0.78 mm height. To implement the changes, the sketch shown in figure 2.2 (B) was modified to a diameter of 12 mm, and a piece of 1.5 mm thick acrylic was used when laser cutting. The negative mold was then assembled described in 2.2.2 using the new hydrogel cutout. The PDMS platform was then manufactured and assembled according to 2.2.2 without the use of the membrane layer making it an open platform. The collagen I-HA hydrogel was synthesized according to B without cells. The new, thicker gel used a gap height of 400 μm which is an 8-fold increase to the original parameters.

Initially, the fluid surrounding the hydrogel was removed before starting the analysis. It was hypothesized that the fluid volume surrounding the gel may increase variability hence the removal via Kim wipe. Later it was discovered that a reservoir of media surrounding the hydrogel during a strain sweep allows volume change by fluid flow across the free edges which aids in variability reduction [78]. This experiment dispensed a few drops of media on the Peltier plate surface via transfer pipette and spread the liquid using a brush which reduced the surface tension forces acting on the gel and created a thin even coating.

The hyaluronic acid (HA) component of the hydrogel is naturally clumpy and can crosslink prematurely when stored at $-20°C$. This was thought to cause localized clusters of HA within the gels and increase variability between readings. To mitigate this issue, a newly reconstituted vial of HA was made at a lower concentration than directed in the protocol. The 5 mg/mL was thought to decrease clumping within aliquots and help create a more homogeneous hydrogel during synthesis.

The number of samples for each condition shown in figure 3.5 (A) also made it difficult to detect any differences between hydrogels if any exist. Experimental error also may cause samples to be lost causing the number of samples available for testing to be reduced further. To mitigate this problem, the total number of samples for each condition was increased to 12.

3.3 Results

NHA Concentration Optimization

A BCA assay was performed which consisted of collecting total protein concentrations from each concentration of gels and displayed in figure 3.3. The membrane proteins showed little variation between samples and indicated that cell density has little impact. The cytosolic protein concentration is similar for the lowest 4 concentrations and then significantly decreases at 500,000 and 1 million cells/mL. The variation in cell densities 10,000, 50,000, and $2.5 * 10^5$ cells/mL are very high as densities $1 * 10^5$, $5 * 10^5$ and $1 * 10^6$ cells/mL show little variation.

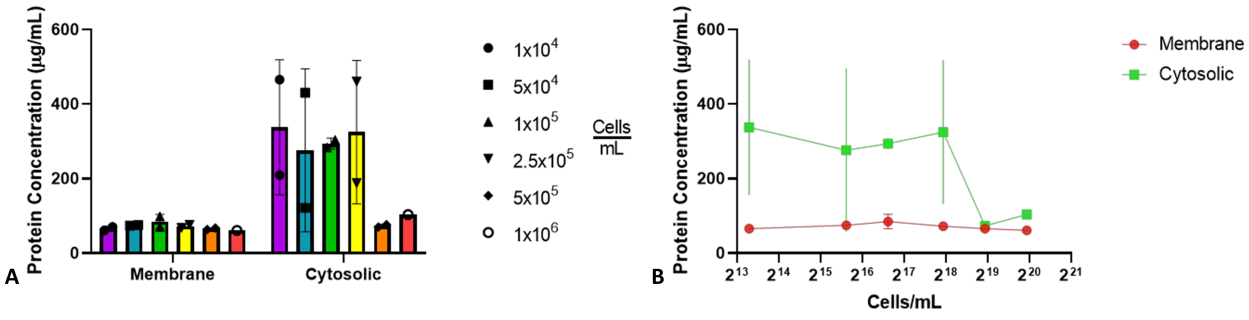

Figure 3.3: Quantification of the concentration of proteins within the cytosolic and membrane compartments. Both (A) and (B) display the membrane and cytosolic protein concentration but in two different forms.

Transfer of Soft Hydrogel

The hydrogel is a viscoelastic material that has a modulus in the order of tens to hundreds of pascals which made transferring the hydrogel challenging. The transfer pipette produced too much of a pressure gradient with a small nozzle making it very difficult to transfer the hydrogel without impacting its mechanical integrity. Due to the soft nature of the gel, using tweezers to pick it up was troublesome and often ended in cleavage at the site of contact. Fine-tip paint brushes were found to work best with picking up and transferring the gel shown in figure 3.4 (A). The most effective method for eliminating gel residue from the brush involves the utilization of a secondary brush, which facilitates the downward displacement of the gel towards the Peltier plate. The hydrogel was able to retain its original geometry shown in figure 3.4 (B) making it compatible with the rheometer. Correct sample loading for a parallel plate rheometer requires that the sample be filled only until the edges of the plate. It was found that the hydrogels cannot be trimmed without being displaced due to the strong crosslinked network.

Strain and Frequency Sweeps

The results of the strain sweep performed are shown in figure 3.4 (C) according to the parameters detailed in 3.2. The strain sweep shows that the detection limitations of the instrument occurs near strains of 0.1%. The hydrogels exhibited linear behavior until about 8% strain indicating that the matrix starts to breakdown at higher strains and starts to exhibit more viscous behavior. For subsequent sweeps a strain of 1.35% was selected.

The frequency sweep shown in figure 3.4 (D) utilized the updated strain constant of 1.35% from the strain sweep plot. At low frequencies up until about 0.3 rad/s, the hydrogel exhibits a linear behavior where the sample behaves as a gel. This corresponds with figure 2 found in

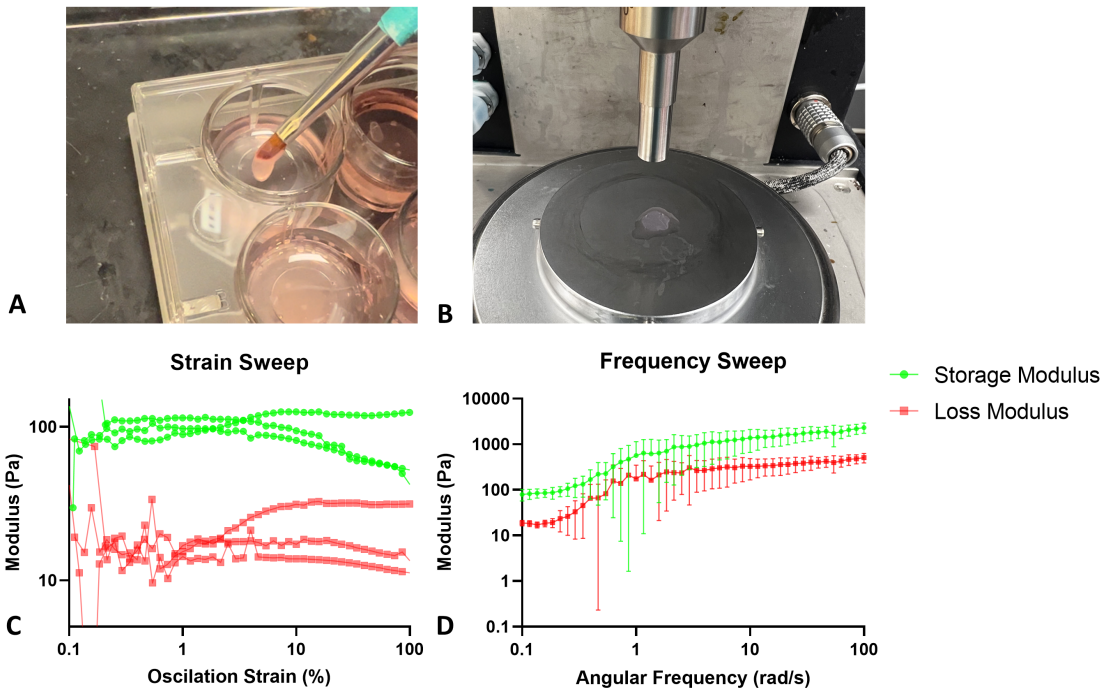

Figure 3.4: (A) the hydrogel adheres well to the paintbrush bristles allowing for transfer between culture plate and parallel plates. (B) using a second brush, the hydrogel was carefully spread out to its initial geometry and ready to be tested. (C) The linear-viscoelastic limit was determined from 0.1 to 100% by performing a strain sweep. (D) The linear equilibrium modulus plateau was determined from 0.1 to 100 rad/s by execution of a frequency sweep.

[77] describing how at low frequencies, the shear modulus can be obtained. For subsequent measurements, a value of 0.25 rad/s was used to stay within the solid behavior region.

Characterization of Blasted Hydrogels

Transferring the hydrogels with a brush, which was determined to be the optimal method was implemented in this experiment. Not all gels transferred remained fully intact after transferring to the rheometer's Peltier plate as shown in table 3.1. Each condition started with 6 gels, but some were damaged during experimental processing. The condition which was not blasted and did not contain any cells exhibited partial ripping in one of the four gels. Hydrogels that were cell seeded without a simulated blast showed partial tears in two of the six gels. The condition without cells that were blasted contained one gel with small rips within after transfer. Lastly, gels that contained cells and were blasted all looked to be fully intact after transferring. Best transfer results were obtained when using a technique to pull gel up from a side where there was already some loss in adhesion to the PDMS. Only intact specimens were tested, and specimens damaged by human error were discarded.

Table 3.1: Evaluation of Hydrogel Transfer to Peltier Plate

Condition of Gel	Without cells not blasted	With cells not basted	Without cells blasted	With cells blasted
Intact Transfer of Gel	3/4	4/6	2/3	4/4

Complex modulus factors in both the storage and loss modulus of a material. The hydrogels analyzed were fully crosslinked and thus exhibited a very low loss modulus that was considered negligible while the storage modulus was almost identical in magnitude to the complex modulus. Moving forward, only the value of the complex modulus was chosen to represent the properties of the specimens as it was already determined that elasticity dominates. Although a trend that the non-blasted gels have a higher modulus is observed in figure 3.5 (A), there is no statistical significance observed when subjecting the groups to a two-way

ANOVA with a 95% confidence level. Among each group, there is much variation apart from the blasted cell-seeded hydrogel condition. The decreased variation may be influenced by astrocytes within the hydrogel becoming reactive and remodeling their matrix. No decisive conclusion can be made due to the high variation between conditions. The results indicated that further changes to the rheology protocol needed to be applied to detect any differences if they exist. Variations due to the blast may also exist. Variations in readings which may also be caused by rips within the surface of the hydrogel make any conclusions futile.

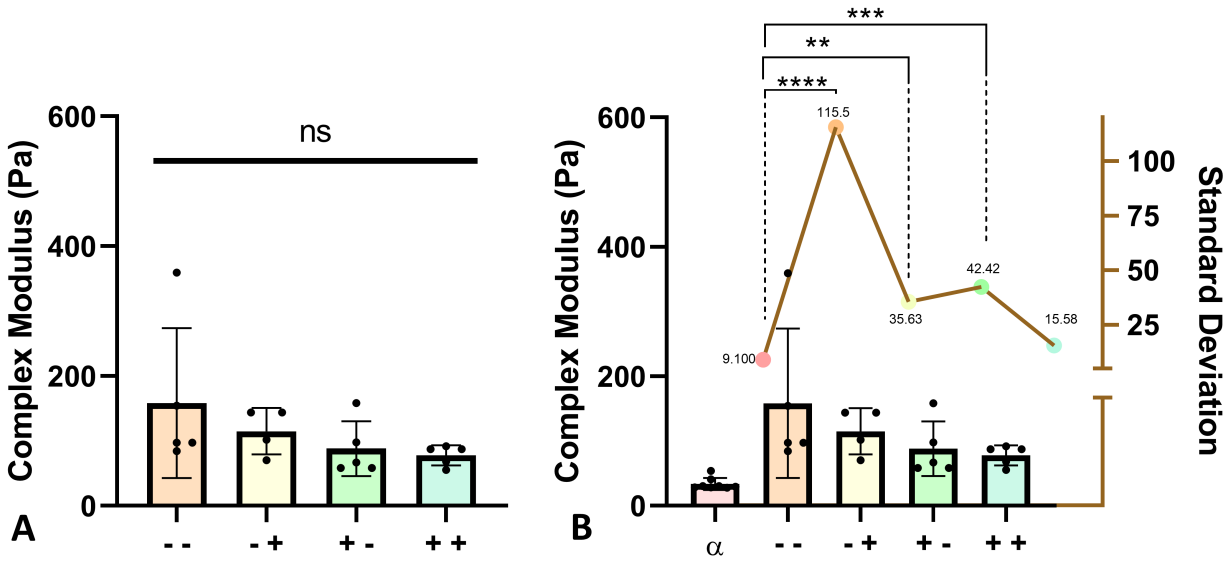

Adjusted parameters	Cell seeding in hydrogel	Exposure to HROP
α	±	/ ±

Figure 3.5: Optimized Rheology Protocol Yields Outcome with Minimal Deviation. The complex shear modulus produced by the characterization of hydrogels exposed to high-rate overpressure (HROP) with and without cell seeding (A). Adjusted parameters reduced variation when compared to the characterization of blasted hydrogels (B).

Improved Rheology Procedure

The implemented changes described in 3.2 made a large impact on decreasing variability between samples. Of the gels originally observed for tears after transferring, only 76% remained fully intact. After implementing the procedural changes, 100% of the gels remained fully intact after transferring to the Peltier plate.

The standard deviation comparing the modulus readings for the adjusted parameters to the original data set is shown in figure 3.5 (B). There is much less variation as the data points cluster to a mean close to 34 Pa. It is not known if this decreased mean is closer to the true value of the gel, but the interest of this study is primarily to detect changes between samples. The standard deviation of each condition is plotted above the bar graphs and compared using an F test. A significant difference was detected between the set of samples with adjusted parameters applied and three out of the four conditions from the prior experiment.

3.4 Discussion

The BCA assay was conducted to serve two purposes. The first was to maximize the total protein concentration extracted from each hydrogel. A high total protein concentration is needed when conducting western blots. The second purpose is to estimate what the optimal seeding density of the cells is for viability. If cell concentrations are too low or too high, the NHAs can die via apoptosis. The results indicate that there is a cutoff where the seeding density is too high and the overcrowded cells start to decrease in viability. The hydrogels containing 500,000 and 1 million cells/mL have much lower cytosolic concentrations hypothesized to be from cell death. Cytosolic protein is found within the cytosol of a cell. They are distinct from membrane proteins, which are embedded in the cell membrane. The

incubation period of 5 days allowed time for the astrocytes to proliferate which may explain why the cytosolic protein concentrations are similar across all conditions. Variation between samples may be caused by experimental error as well. During homogenization, a droplet of the homogenate was unable to be extracted from the homogenizer which can contribute to the variation observed. Moving forward the 100,000 cells/mL seeding density was selected because it provided high total protein with little variation detected. It's believed that the seeding density is high enough for cell survival, but also low enough to allow proliferation of cells if needed.

The initial tests to establish compatibility between the collagen-HA hydrogels served as the fundamental basis for the subsequent development of a comprehensive protocol. Following extensive experimentation with various transfer methods of the soft, viscoelastic hydrogel, it was determined that the employment of a fine-tip paintbrush was optimal for achieving transfer without compromising the hydrogel's structural integrity. The preservation of hydrogel integrity is crucial for the acquisition of precise rheometric analyses. The use of an additional brush also proved useful to spread the hydrogel back to its original form. One approach to mitigating the presence of bubbles on the gel's surface involves applying force to gently propel the bubbles away from the surface, thereby promoting a more uniform and optimal gel layer. The hydrogels were not trimmed to the edges of the parallel plates due to displacement that occurred during trimming. Moving forward, the samples were left to their original diameter creating an overfilled sample. An overfilled sample can cause additional stress from drag along the edges which should be noted when obtaining results [79].

Strain and frequency sweeps revealed the linear viscoelastic region and the linear equilibrium modulus frequency. Knowing the linear viscoelastic region helps inform when the deformation of the gel starts to occur. A reliable shear modulus value can be obtained by staying within that region. Similarly, the frequency range where the hydrogel exhibits solid behav-

ior is identified with the linear equilibrium modulus, which is necessary when measuring the shear modulus.

The variation between samples for each condition shown in figure 3.5 (A) made it impossible to detect a difference between samples if one existed. The collection of the high variability data prompted changes in the rheology data collection procedure. The first of these changes was an increase in hydrogel volume. This volume helped created a thicker gel, which increases the loading gap. As shown in equation 1.10, a larger gap height contributes to a lower strain constant. This means that the parallel plate can have more rotational displacement and achieve the same level of strain. This decreases variations detected between samples because the displacements measured are near the detection limitations of the instrument. Increasing the gap height allows the instrument to take readings that are well within its detection capabilities. To mitigate variation, the fluid surrounding the hydrogel was also spread along the surface of the Peltier plate which aids in volume change by fluid flow along the free surface.

HA localized clumping was evident when initially synthesizing the collagen I-HA hydrogels. The glycosil would often crosslink over time during storage which caused uneven distribution within the final gel composition. When creating the gels, some gels likely received much more HA than others which contributed to modulus differences. Changes were made to the reconstitution of glycosil which changed the final concentration from 10 mg/mL to 5 mg/mL. The change to lower concentration glycosil reduced the clumping over time. Using the glycosil closer to the reconstitution date is advised as the crosslinking of glycosil only increases over time. The last improvement to the procedural change was increasing the number of samples run for each condition. Initially, only an n of 6 was cultured for each of the conditions. This number was increased to 12 samples per condition to maximize the potential for detecting differences.

The adjusted parameters applied to decrease variation between samples were applied and the collected data is shown in figure 3.5 (B). During the transfer of the thicker gel, all samples were still intact which proved that the gels were initially too thin to carry out rheological measurements. The graph shows that the standard deviation (SD) of the adjusted parameters is significantly reduced when compared to the conditions of the prior experiment. A reduced SD validates the changes that were made and enhances the potential to detect differences between conditions in future studies. The modulus for the adjusted parameters was also observed to be lower than the conditions from the previous experiment. This change may be due to the difference in diameter, compression of the sample, and increased sensitivity from the instrument from the increased gap height.

Chapter 4

Development of Mechanical Characterization via Atomic Force Microscopy

4.1 Introduction

AFM is a type of microscopy that can obtain extremely high-resolution force measurements that allow for the characterization of mechanical properties. Force spectroscopy operates by using a small probe to indent the surface of the sample and measures the deformation under the applied load. In the context of this study, force spectroscopy can be utilized to characterize the soft *in vitro* hydrogels to detect any mechanical impacts RAs may have on their environment.

Unlike most samples that are characterized using an AFM, the hydrogel must remain submerged in liquid throughout testing to ensure that it retains its mechanical properties. However, submerged AFM presents several technical challenges such as probe interference, thermal drift, and force distortion due to the liquid medium.

Although rheology is a good technique for measuring shear modulus, there are areas where it falls behind. AFM allows localized measurements with high spatial resolution on the order of

nanometers. This allows for the measurement of mechanical properties with very high precision and accuracy, even on small features or inhomogeneities within a material. In contrast, rheology typically offers lower spatial resolution, typically on the order of micrometers, and is better suited for measuring the bulk properties of a material. AFM can either be used as a substitute or in conjunction with rheology to better characterize the hydrogels. There is a need to establish a method of elastic modulus characterization that exceeds the resolution of traditional rheometry techniques.

4.2 Materials and Methods

Hydrogel Synthesis

Development of the AFM protocol involved the synthesis of hydrogels without cells or the HA component. The decision to exclude both was made to maximize time and cost efficiency. Although stiffer, a collagen I hydrogel has very similar material properties to a collagen I-HA hydrogel without the increased cost associated with glycosil. To synthesize the hydrogel, protocol A was followed without the addition of astrocytes.

Probe Surface Coating

For all probes used in this development, a coating of Trichloro(1H,1H,2H,2H-perfluorooctyl) silane (448931-10G, Sigma-Aldrich, St. Louis, Missouri) was deposited on the surface. Silane was coated on the surface to reduce the adhesion strength between the hydrogel and probe by creating a hydrophobic monolayer on the surface. To apply the saline, the probe was placed onto a glass coverslip and transported to a vacuum chamber located in a fume hood. A small piece of PDMS was also placed in the chamber and 100 μL of saline was pipetted

onto the surface. The AFM is very small and fragile so it was important to ensure that it does not get damaged during the process. The tubing connecting the chamber to the vacuum pump was connected while the valve remained closed. The valve was then slowly turned to minimize the opportunity for the probe to become displaced. The probe was silanized for 3-5 hours. Once ready for removal, the valve was closed and the tube connecting to the pump was removed. The valve was once again slowly turned to reduce the influx rate of gas and ensure the safety of the probe. The probe was then carefully transferred back to its casing.

Initial Testing and Development

The development of the AFM protocol was executed according to the procedure described below. This procedure paved the way for what later became a fully functioning method to characterize hydrogels with high resolution. The collagen I hydrogel synthesized and seeded within the PDMS platform developed 2.2.2 without assembly of the membrane layer. Following crosslinking, the hydrogels were stored in an incubator at $37°C$ and 5% CO_2 until ready for use.

All AFM studies were performed on the Oxford Jupiter XR AFM. Before calibrating, the probe and sample are placed into the AFM. For the initial testing, a circular symmetric probe with 7 μm height and 10 nm radius was utilized (qp-SCONT-10, NanoAndMore, Wetzlar, Germany). The beam has a force constant of 0.01 N/m and a resonance frequency of 11 kHz. To calibrate the probe, a silicon wafer is used because it is extremely hard and does not compress. When initiating testing, a drop of DIW is placed on the surface of the wafer and around the cantilever. The meniscus of fluid on both the probe and wafer are lined up and brought together until conjoined. The laser is then lined up at the end of the cantilever and the tip position is identified. Because this experiment is being conducted in DIW, it is important to change the refractive index to water. A virtual deflection of the cantilever is

calibrated to detect deflection while the cantilever is not physically touching the sample. If the virtual deflection is not able to fit on a straight or polynomial curve, the sample must sit for at least 30 minutes to allow the fluid to thermally equilibrate. The probe is then brought close to the surface and a tip approach slowly descends the tip until a set trigger point is met. For this step, a setpoint of 0.5 V was used. Once the surface of the silicon wafer is identified, a trigger point is set and the cantilever is deflected a known distance on the surface which then corresponds to the voltage detected. Calibrating the probe on the wafer has given the constant of nm/V. Photothermal excitation of the cantilever is then used to obtain a spring constant. This concludes the calibration of the AFM probe.

The wafer was then removed from the AFM and the PDMS mold containing the hydrogel was suctioned onto the stage. A drop of DI was placed onto the hydrogel and the meniscus of fluid surrounding both the sample and probe were conjoined. To obtain force measurements, the probe was brought to the surface of the hydrogel and a trigger point was set in either voltage or indentation distance. A force-distance plot was then generated by the software.

Modification of PDMS to Meet AFM Needs

The results in 4.3 indicated that the current PDMS platform was not compatible with the AFM. The hydrogel could also not be transferred to a glass slide as it was observed to float once it was submerged in fluid. To combat this, the PDMS platform developed in 2 was modified to fit the needs of the AFM. The hydrogel required culturing for extended periods as well as access to the AFM probe. To adhere to this restriction an additional removable piece was added to the platform. A coverslip was chosen as the additional component of the platform as it is easily removable and biocompatible. Once a negative mold for the platform was made, the only additional modifications to the manufacturing process included coating the coverslip with polyethyleneimine and glutaraldehyde instead of the PDMS itself. This

ensured that the hydrogel would stay adhered to the coverslip during testing and that it does not adhere to the surrounding walls.

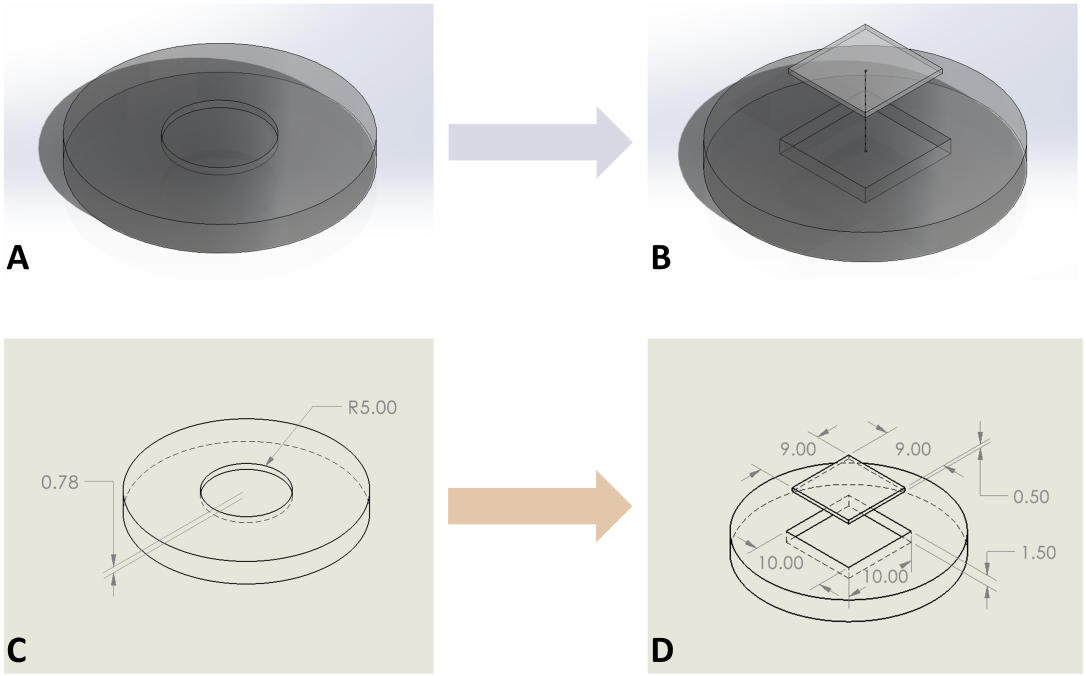

Figure 4.1: Modification of PDMS Platform for AFM. The geometry of the PDMS platform was modified from (A) to (B). The corresponding sketches with dimensions in mm of each platform are detailed in (C) and (D).

Final Testing and Development

It was hypothesized that the circular symmetric probe with a 10 nm radius was far to indent the surface of the hydrogel. Moving forward, a colloidal probe was utilized with a diameter of 10 μm (CP-qp-SCONT-BSG-B-5, NanoAndMore, Wetzlar, Germany). Similar to the initial probe, the force constant is 0.01 N/m with a resonance frequency of 11 kHz. Calibration and setup of the experiment were unchanged from 4.2. Once the probe was calibrated, the modified PDMS platform was utilized to transfer the hydrogel onto a glass slide as shown in figure 4.2.

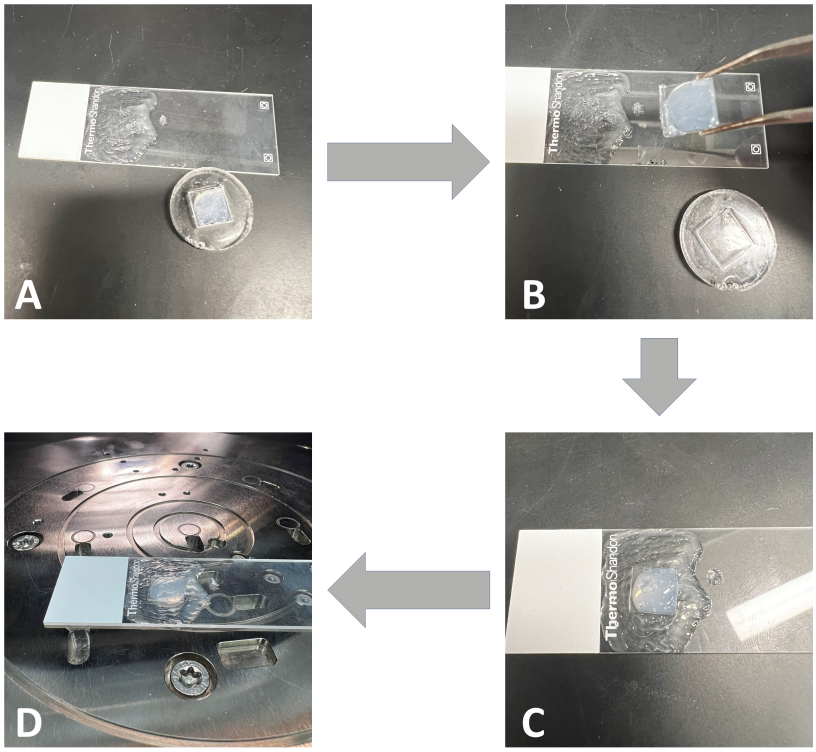

Figure 4.2: Utilization of AFM Platform. A thin coating of vacuum grease is applied to a glass slide to help adhesion with the coverslip (A). The coverslip is easily transported to the glass slide and adhered to the vacuum grease (B & C). DIW is then pipetted onto the hydrogel and the slide is vacuumed down onto the stage (D).

Due to the transparent nature of the hydrogel, the objective in the microscope is unable to detect the surface. For this reason, the height of the gel is estimated based on previous experiments with similar hydrogel volumes. The height of the sample is then set a few hundred microns above the estimated height. A slow controlled tip approach follows which ensures that the probe does not crash into the hydrogel.

The large mass of the colloidal probe paired with the very low spring constant of the cantilever made the development of this protocol especially challenging. The rate of false positives detected when probing for the surface was much higher than the circular symmetric nm probe. To combat this, approach parameters were optimized to decrease noise associated with slow speeds and false positives associated with high speeds and low detection voltages. It was found that a virtual deflection approach of 518.36 nm/s worked best. Any virtual deflection curves that were unable to fit a line meant the fluid surrounding the sample likely needed additional time to thermally equilibrate. Generation of the force curve on the surface of the hydrogel was optimized at an approach rate of 100 nm/s and voltage trigger of 0.5 V.

4.3 Results

Initial Testing and Development

During the initial phase of AFM development for the mechanical characterization of soft hydrogels, a very small probe on the order of nanometers was utilized. The deflection of the probe was first calibrated by fitting a line to the virtual deflection plot generated shown in figure 4.3 (A). The deflection of the probe when making contact with the silicon wafer at a known displacement was then determined as shown in (B). The plot was then able to determine a value for the inverse optical lever sensitivity with the units nm/V. Photothermal

data was then used to determine a spring constant for the cantilever. Once these values were determined, the silicon wafer was switched with the hydrogel sample.

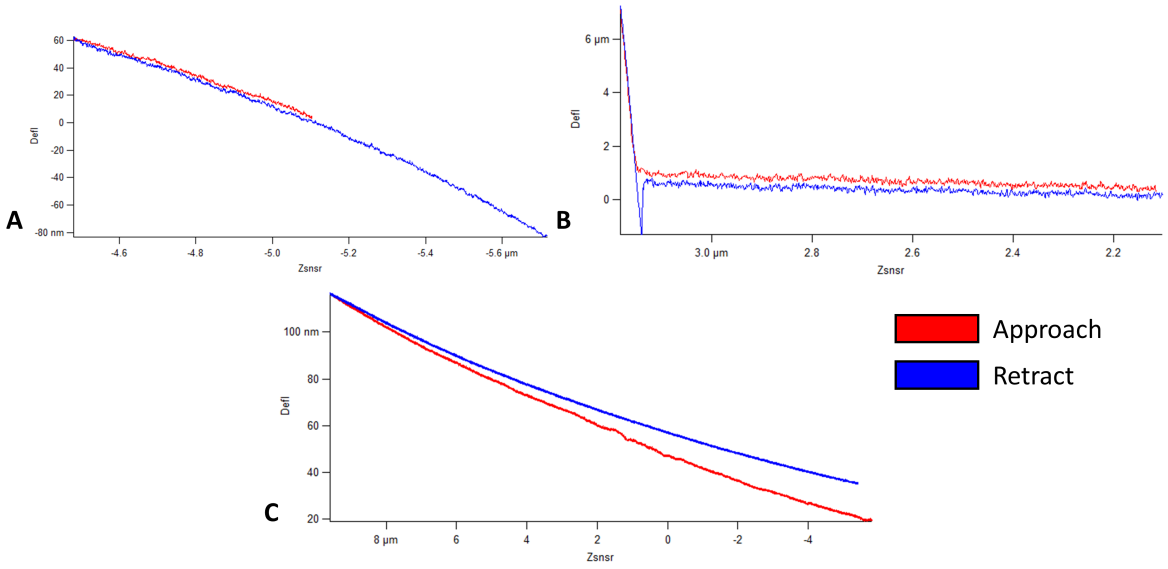

Figure 4.3: AFM Initial Phase Force Curve Generation. All plots generated detailed cantilever deflection in the y-axis of cantilever deflection and movement in the z-direction in the x-axis. During the tip approach toward the sample, the plot on the graph moves left and returns during retraction. Virtual deflection plot used to calibrate movement of the cantilever during non-contact movement (A). The plot of probe displacement when making contact with the silicon wafer was used to correlate distance and voltage (B). Indentation curve of probe making contact with hydrogel sample.

Hydrogel shrinking over time due to degradation cause the sample sitting within the PDMS cavity to be unreachable by the AFM probe. It was also observed that the hydrogel was undetectable to the AFM objective due to its optical transparency. Without clear identification of the hydrogel boundaries, the probe can crash into the sample and irreversibly damage the cantilever. When the probe was able to identify where the surface was located without crashing, a proper force curve was unattainable. Figure 4.3 (C) shows that there is no spike in deflection which is typically observed when striking a surface. (B) shows how the cantilever should deflect when making contact.

Final Testing and Development

Using the optimized platform, probe and scanning parameters, force curves of the hydrogel were obtained shown in figure 4.4 (D). The AFM protocol developed can produce virtual deflection plots and calibrate the probe as performed with the circular symmetric nm probe. The plot shown in figure 4.4 (C) shows how the deflection of the cantilever is inaccurately measured when the virtual deflection plot does not produce an accurate representation of the movement of the cantilever.

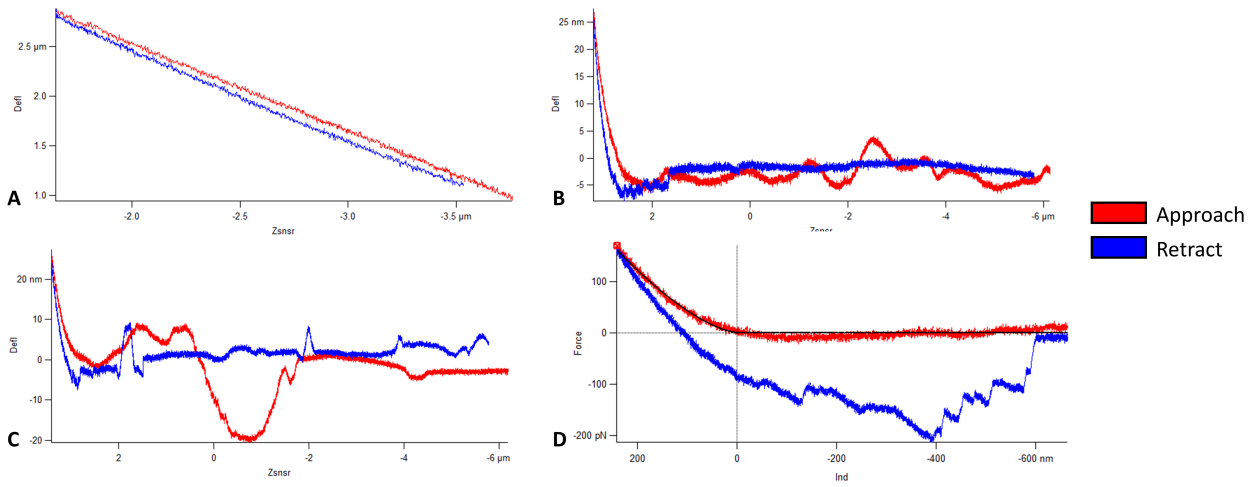

Figure 4.4: AFM Functioning Nanoindentation. Plot (A-C) details cantilever deflection in the y-axis of cantilever deflection and movement in the z-direction in the x-axis. Plot (D) details the force measured on the y-axis and surface indentation on the x-axis. During the tip approach toward the sample, the plot on the graph moves left and returns during retraction. Virtual deflection plot used to calibrate movement of the cantilever during non-contact movement (A). The plot of probe displacement when making contact with the silicon wafer was used to correlate distance and voltage (B). The plot displayed in (C) is the probe attempting to calibrate on the silicon wafer but is unable due to inadequate virtual deflection fitting. Indentation curve of probe making contact with hydrogel sample (D).

Unlike the deflection plot in figure 4.3 (C), the improved protocol can obtain a force measurement based on indentation into the sample. Assuming the hydrogel is isotropic, linearly elastic, and an incompressible colloidal probe, the elastic modulus of the hydrogel can be

calculated. The Hertz model can be adapted for the colloidal geometry and rearranged to produce 1.12. The software used to operate the Oxford Jupiter XR AFM can generate the elastic modulus using the force curve obtained along with probe geometry, size, material, and sample Poisson value. Using the force curve generated in figure 4.4 (D) the elastic modulus was measured to be 299.44 Pa.

4.4 Discussion

The initial phase of AFM development involved the utilization of circular symmetric probes with a diameter of about 10 nm. Although the virtual deflection and calibration plots were achievable, the probe was never able to produce a force curved that could measure the elasticity of the hydrogel. Due to the extremely small geometry of the probe, it is thought that it may slice right through the gel and thus never achieve a reliable force curve. This prompted the switch to much larger colloidal probes that could make contact with a much larger surface area.

It was also observed during the initial phase of testing that the objectives used in the microscope are unable to see the surface of the hydrogel due to its transparent nature. This issue can cause a probe to crash into the surface damaging the cantilever. To combat this issue, the surface height of the gel was estimated based on previous studies, and the probe was given a buffer of a few hundred microns above the estimated height. A tip approach is then conducted which can safely find the surface of the gel. One drawback to this is the added time it takes to find the surface. This added time is necessary given the high cost and time associated with damaging probes.

Another issue observed during the initial phase of testing was the interference of the PDMS platform when the hydrogel would degrade causing it to no longer be accessible by the probe.

A modification to the PDMS platform was made to incorporate a removable coverslip that is adhered to the gel. The modification allowed the probe access to the sample no matter the degree of degradation. If necessary, the coverslip and hydrogel can also be returned to the PDMS platform.

It was found that letting the sample sit for at least 30 minutes helped with obtaining a valid virtual deflection curve. Over time the fluid reaches a thermal equilibrium a creates a much smoother curve. If the virtual deflection does not accurately describe the deflection of the cantilever during motion, the calibration curve will not be used as shown in figure 4.4 (C).

Application of the larger colloidal probe, modified PDMS platform and updated scanning parameters yielded the ability to obtain force curves like the one shown in figure 4.4 (D). The approach of the tip to the hydrogel shows that no deflection occurs until the probe hits the surface. Then, the indentation of the probe yields a force curve that can be used to obtain the elastic modulus of the sample. The retraction of the probe from the surface shows that the probe is stuck onto the surface of the hydrogel until it is moved far enough away from the surface. Adhesion between the gel and probe cause the cantilever to bend in the opposite direction generating a negative force on the plot. Once the probe detaches from the gel, it snaps back in place and the force returns to 0. The modulus generated using the Hertz model was also able to obtain a value that is within the expected range of values for collagen I[80].

Chapter 5

Evaluating the Mechanical Alterations of Reactive Astrocytes

5.1 Introduction

Following a mechanical insult like an mTBI, astrocytes can undergo activation resulting in the transformation to a reactive phenotype. Astrocyte transformation can cause alterations in morphology, increased expression of the intermediate proteins GFAP and vimentin, and increased proliferation and secretion of inflammatory mediators and growth factors [20]. During a mechanical insult, activation of the cells is thought to be caused through the stretching of mechanosensitive channels in the plasma membrane [13]. RAs play an important role in brain remodeling following a mTBI. They have been observed to upregulate ECM molecule synthesis and secretion of proteases *in vivo*.

This study will investigate the influence a high-rate impulse has on astrocyte behavior *in vitro*. Astrocytes are known to modulate their environment and interact with many different cell types, but it is currently unknown how they can mechanically impact their environment when isolated and subjected to a mimicked mTBI.

The experiments conducted in this study consisted of astrocytes being blasted in 2D on a culture plate as opposed to being blasted 3D in a hydrogel. This change was implemented

to evaluate the astrocytes' capacity to restructure their matrix and nullify the likelihood of the shock wave imposed by altering the mechanical characteristics of the gels.

The study entailed subjecting astrocytes to a 2D blast on a culture plate instead of a 3D blast in a hydrogel. This change was implemented to evaluate the astrocytes' capacity to restructure their matrix and nullify the likelihood of the shock wave imposed by altering the mechanical characteristics of the gels.

5.2 Materials and Methods

Cell Culture

Human astrocytes (catalog number 1800, Sciencell Research Laboratories, Carlsbad, CA) were cultured in complete Astrocyte Medium (catalog number 1801, Sciencell Research Laboratories, Carlsbad, CA). Cell passaging was performed when the confluency reached 80% or higher, accompanied by media exchanges occurring at intervals of 2-3 days. Cells were passaged by first removing media and washing with 5 mL of D-PBS. The D-PBS was then removed and 5 mL of trypLE was pipetted on the surface where the flask was then incubated for 7-10 minutes until all cells detached from the surface. 5 mL of complete astrocyte medium was then added to neutralize the trypLE, then the cell suspension was transferred to 15 mL where it was centrifuged at 150 x g for 5 min. The supernatant was then removed and 5 mL of media was added to resuspend the cells. The cells were passaged at a 1:3 split so 1.67 mL was added to each T-75 flask followed by 12 mL of media.

Blasting Cells in 2D

After reaching 80% confluency in a T-75 flask, normal human astrocytes were transferred to a 100 mm petri dish at a 1:3 split. 12 mL of complete astrocyte medium was added and exchanged every 2 days until reaching 100% confluency. Once ready for blasting, the petri dish is filled to the top and wrapped in parafilm. It is then placed in a petri dish holder and submerged in the SWG which was used to carry out the high-rate overpressures mimicking a mTBI. The SWG was set up using a NiCr40 bridge wire and 37°C RO water. See section 2.3 for additional detail on the SWG. The petri dish would be placed back in the incubator following the blast. A collagen I-HA hydrogel was synthesized 24 hours after blasting following B and seeded in the PDMS platform manufactured according to 2.2.2 without the use of the membrane layer.

Measuring Influence of RAs on Shear Moduli

The thickness at the center of each hydrogel was measured using a Keyence VK-X3000 3D Surface profilometer. Details on the instrument operation can be found in D. On the rheometer, an 8 mm parallel plate geometry was used in conjunction with a temperature-controlled Peltier plate. Media from the culture plate was transferred onto the Peltier plate and spread across the surface with a paintbrush. The brush was then used to transfer the hydrogel to the rheometer and spread it out to its original circle geometry using a second fine-tip brush. The hydrogel was centered under the 8 mm parallel plate and subject to the 400 μm gap height. A linear strain sweep was performed from 0.1 to 5% at 0.2% increments. The parameters for the sweep included an angular frequency of 0.25 rad/s, 21°C temperature with 30-second soak time, and 400 μm gap height.

Matrix Metalloproteinase Array

A human MMP antibody array (ab134004, Abcam, Cambridge, UK) was used to detect the presence of MMPs secreted by the astrocytes. Normal and blasted astrocytes were seeded in collagen I-HA hydrogels and left to crosslink for 30 minutes. Following crosslinking of the gel, 1.5 mL of complete astrocyte media was added to each well and left to incubate for 3 days. The supernatant was collected after 3 days and transferred to low protein binding microcentrifuge tubes (88379, Thermo Fisher Scientific, Waltham, MA). The supernatant was then flash-frozen in liquid nitrogen and stored at $-80°C$ until use. Once ready for use, all samples for each condition were thawed and pooled into an Ultra-15 centrifugal filter unit (UFC900308, MilliporeSigma, Burlington, MA). The filter unit was centrifuged at 2400xg for 30 minutes. The supernatant concentrate was then diluted to a 5X concentration. The membrane containing the array was first blocked and then the concentrated supernatant was added. The membrane was washed and the biotin-conjugated anti-cytokines were added next. Washes were repeated and the HRP-conjugated streptavidin was dispensed on the membrane. The membrane was then put through one more set of washes and prepped for imaging. Any residual wash on the membrane was removed by tapping the bottom on a Kim wipe. A mixture of detection buffer was then added to each membrane for 2 minutes. After 2 minutes passed the membrane was moved to a glass slide and inserted into a slide scanner. Acquisition of the membranes was taken with a 4X objective using BFmono and 5.65 ms exposure time.

The images were analyzed in ImageJ by drawing a circle around the positive control and measuring the mean intensity within that region. Without changing the dimensions, the circle was dragged to each spot on the membrane and the mean intensity was measured. The average intensity for each enzyme was used for the analysis. Using equation 5.1, the average mean intensity was quantified and normalized across membranes.

$$X_N(\%) = ((x_a - n_a)/(p_a - n_a)) * 100 \tag{5.1}$$

Where X_N = normalized percentage intensity of positive control, x_a = average mean intensity of the enzyme on membrane a, p_a = average mean intensity of positive control on membrane a, and n_a = average mean intensity of negative control on membrane a.

Immunocytochemical Staining of Hydrogel

For analysis of reactivity using GFAP and protein deposition, each hydrogel was fixed using 4% Paraformaldehyde (PFA). The hydrogels were immunostained with either rabbit anti-human laminin (PA1-16730, Thermo Fisher Scientific, Waltham, MA) or rabbit anti-human collagen IV (PA5-104508, Thermo Fisher Scientific, Waltham, MA) in solution with mouse anti-human GFAP Alexa Fluor 488 conjugate (3655, Cell Signaling Technology, Danvers, MA). A goat anti-rabbit Cyanine5 conjugate secondary followed. For the repeated study investigating protein expression 4 days after hydrogel synthesis, an alternative GFAP antibody was used. A rat anti-human GFAP (13-0300, Thermo Fisher Scientific, Waltham, MA) primary was used followed by goat anti-mouse Alexa Fluor 488 conjugate (A-11001, Thermo Fisher Scientific, Waltham, MA). All primary and secondary antibodies were used 1:100. A confocal microscope was used to capture the images using a z-stack and ImageJ was used to analyze them. The expression of each protein was quantified by looking at total fluorescent intensity and the area covered using a threshold cutoff. The number of cells in each hydrogel was quantified by counting nuclei stained with DAPI.

5.3 Results

GFAP Expression 2D vs 3D

The expression of GFAP was investigated in both 2D and 3D to determine if an environment that closely mimics *in vivo* physiological conditions has an impact on the level of expression. Blasted astrocytes were seeded in either a 2D monolayer on a chamber slide or in a 3D hydrogel 24 hours after exposure to the high-rate overpressure. 2D monolayer images (A) and (B) in figure 5.1 differ greatly in terms of the spatial arrangement of cells compared to (D) and (E). The GFAP expression was analyzed at 2 and 5 days after seeding for each condition.

It can be observed in images (A), (B), (D), and (E) of figure 5.1 that the 2D monolayer promotes much more proliferation between days 2 and 5 compared to the 3D hydrogel. This information is also reinforced by figure 5.2 (D). While the astrocyte membranes were not specifically stained, observation of the most responsive cells from each condition suggests a higher degree of cellular branching in the hydrogel-seeded cells. The images taken in the 3D condition are also z-stacks converted into a max projection while the 2D condition images were acquired by acquiring a single focal plane. Unlike the cells seeded on the chamber slides, the astrocytes in the hydrogel can span about 100 μm in height.

Due to the different spatial arrangement of cells, the 2D and 3D conditions were not comparable to each other in figures 5.2 (B) and (D). Figure (A) shows that the GFAP expression relative to DAPI on day 2 in 2D significantly differed from day 5 in both 2D and 3D. The ratio of expression at day 5 in both conditions also showed a decrease in variability. Figure (B) shows that there is no significant difference between total GFAP expression on days 2 and 5. In (C), the level of GFAP expression for each cell that is expressing the protein is significantly different showing a decrease from day 2 to 5. In (D), the cell count was measured

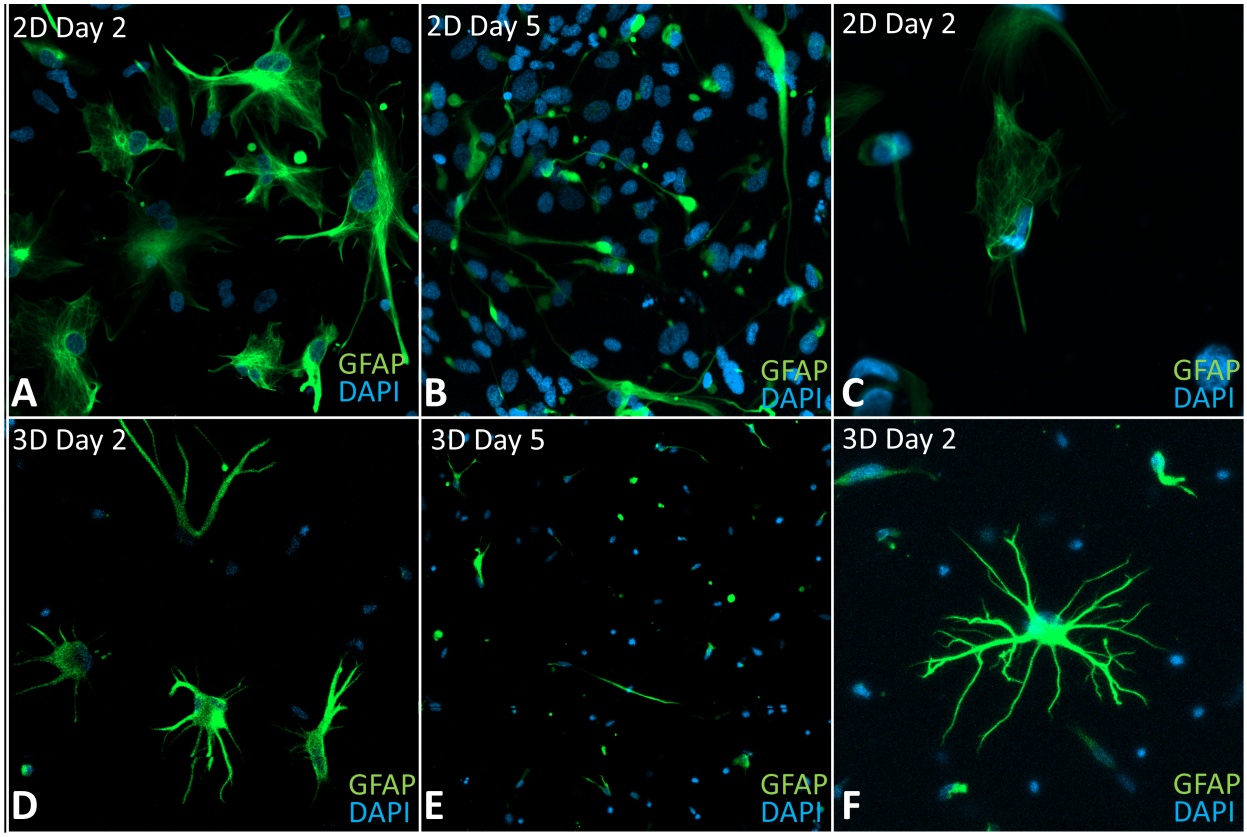

Figure 5.1: GFAP Fluorescence in 2D and 3D. For the images shown, green represents GFAP, and blue represents DAPI. (A) 2D monolayer fixed on day 2. (B) 2D monolayer fixed on day 5. (C) Single reactive cell from 2D monolayer fixed at day 2. (D) 3D hydrogel fixed on day 2. (E) 3D hydrogel fixed on day 5. (F) Single reactive cell from 3D hydrogel fixed at day 2.

by counting the number of nuclei present. From day 2 to 5 the cell count is shown to increase almost 3 fold in 2D whereas there is no significant change in cell count for cells seeded in a hydrogel. Figure (E) shows the percent of reactive cells for each image by dividing the number of nuclei showing GFAP expression over the total nuclei count. It was observed that no significant difference in reactive cell % was detected.

Understanding the Interplay of Reactive Astrocytes, Shear Modulus, and ECM Protein Deposition

The interplay between reactive astrocytes, hydrogel shear modulus, and ECM protein deposition was investigated. Blasted cells in the initial experiment were exposed to 16.3 PSI shock waves and analyzed at days 5 and 17 after seeding. A follow-up experiment was performed with blasted cells being exposed to a 12.46 PSI shock wave and analyzed on day 4.

The hydrogels housing human astrocytes underwent mechanical testing to determine the impact blasted astrocytes have on the mechanical integrity of their surrounding matrix. In figure 5.3 (A) the hydrogels seeded with normal and 16.3 PSI blasted astrocytes were measured across two days due to equipment reservation constraints. We can see that the hydrogels seeded with blasted cells have a higher modulus at day 4 for both the 16.3 PSI and 12.46 PSI experiments. This trend is not shared at day 17 amongst the 16.3 PSI blasted and control gels. The control hydrogels at day 17 exhibit a changed geometry shown in figure 5.4 (A) which may have impacted experimental readings. Differences in shear modulus were detected between the control hydrogels for each condition while the gels seeded with blasted cells show no statistical discrepancies when subjected to a 2-way ANOVA with a 95% confidence interval.

The center of each hydrogel was measured for thickness shown in figure 5.3 (B). Data is

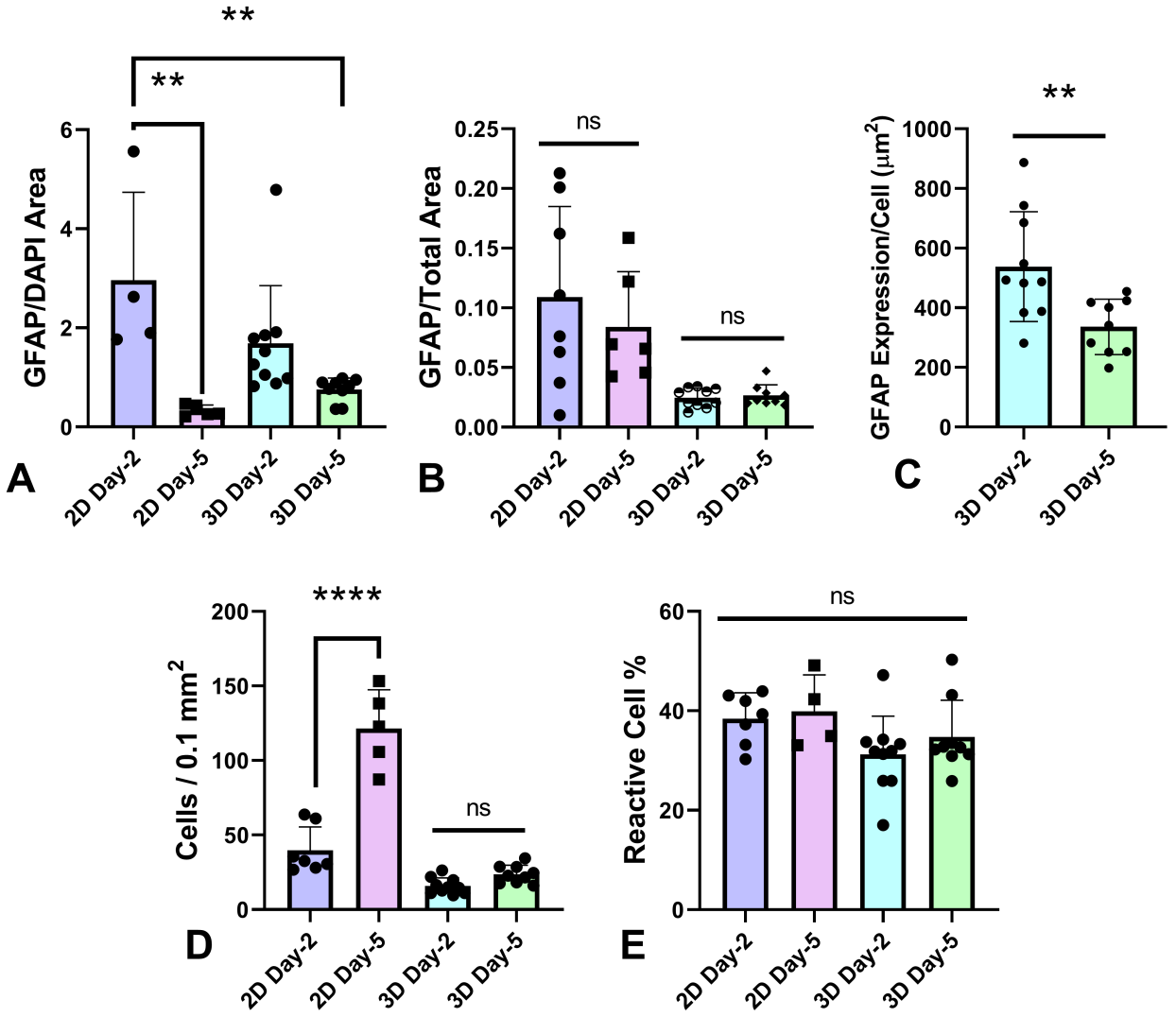

Figure 5.2: Analysis of GFAP Expression in 2D and 3D. (A) The ratio of area covered by GFAP to DAPI for each image acquired. (B) Fraction of total area covered by GFAP for each image. (C) The average intensity of GFAP across an image is divided by the number of cells present in 3D. (D) Cell count of each condition for a fixed area. (E) Percent of cells expressing any level of GFAP. (A), (B), (D), and (E) were analyzed using a two-way ANOVA with a 95% confidence level. (C) was analyzed using an unpaired t-test with a 95% confidence level.

missing for control at day 5 due to the method being developed after testing the modulus. It is observed that the day 4 and 5 gels show similar thickness regardless of blast magnitude or condition. Thickness between conditions at day 17 shows no difference and the gels degrade at the same rate regardless of astrocyte reactivity. Figure 5.3 (C) shows that there is no significant correlation between hydrogel thickness and complex shear modulus measured by the rheometer.

Figure 5.4 (A) and (C) show hydrogels in a 12-well tissue culture plate at day 17. The hydrogels in the control plate were observed to start detaching from the PDMS on day 14 while the blasted plate's gels remained intact. Detachment from the PDMS causes gradual folding of the edges over time shown clearly in row two of (A). Detachment of the hydrogel from the PDMS mold is also associated with a decrease in diameter. The hydrogel in (B) is observed to be much larger than in (D). At day 17, 11 out of the 12 gels for the control were detached from the PDMS while only 7 were detached in the blasted plate.

Hydrogel seeded with both normal and 16.3 PSI blasted astrocytes were stained for either (collagen IV-GFAP-DAPI), (laminin-GFAP-DAPI) or (GFAP-DAPI) at days 5 and 17. Acquisition of images is different between time points due to the detachment of the hydrogels by day 17. Gels stained at day 17 were mounted onto a coverslip and acquired as a single slice in contrast to the z-stack used for the day 5 gels. The gels fixed at day 5 exhibit a lower cell density as shown by figure 5.5 (A-B, D). Qualitatively, little difference is observed between blast and control conditions for any of the proteins analyzed (A&B, E&F). Images (B, G, H) show that cells can express both GFAP and laminin as well as GFAP and collagen IV. Although cells can express both simultaneously, the great majority of cells expressing either collagen IV or laminin do not express GFAP and vice versa.

Cell count and expression of GFAP, laminin, and collagen IV were quantified in ImageJ using the fluorescent images acquired. Due to the different methods of acquisition, hydrogels fixed

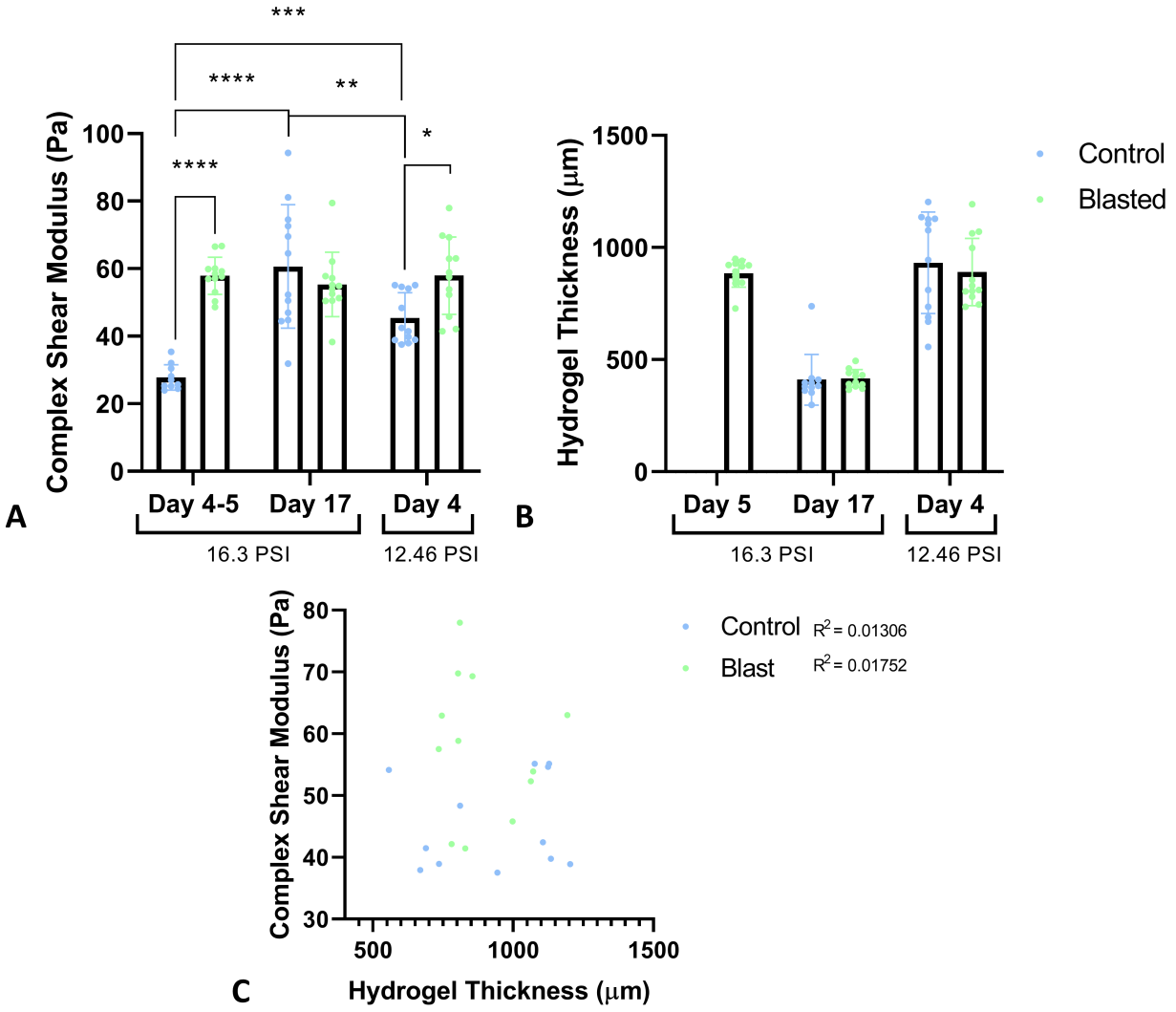

Figure 5.3: Reactive Astrocytes Modulate Microenvironment. Two experiments were conducted by subjecting human astrocyte cells to high-rate overpressures of 16.3 PSI and 12.46 PSI, respectively, using the SWG. (A) complex shear modulus was measured on days 4-5 and 17 and later repeated on day 4. Hydrogels analyzed for shear modulus were also measured for thickness at the center (B). (C) correlation between hydrogel thickness and complex shear modulus was investigated.

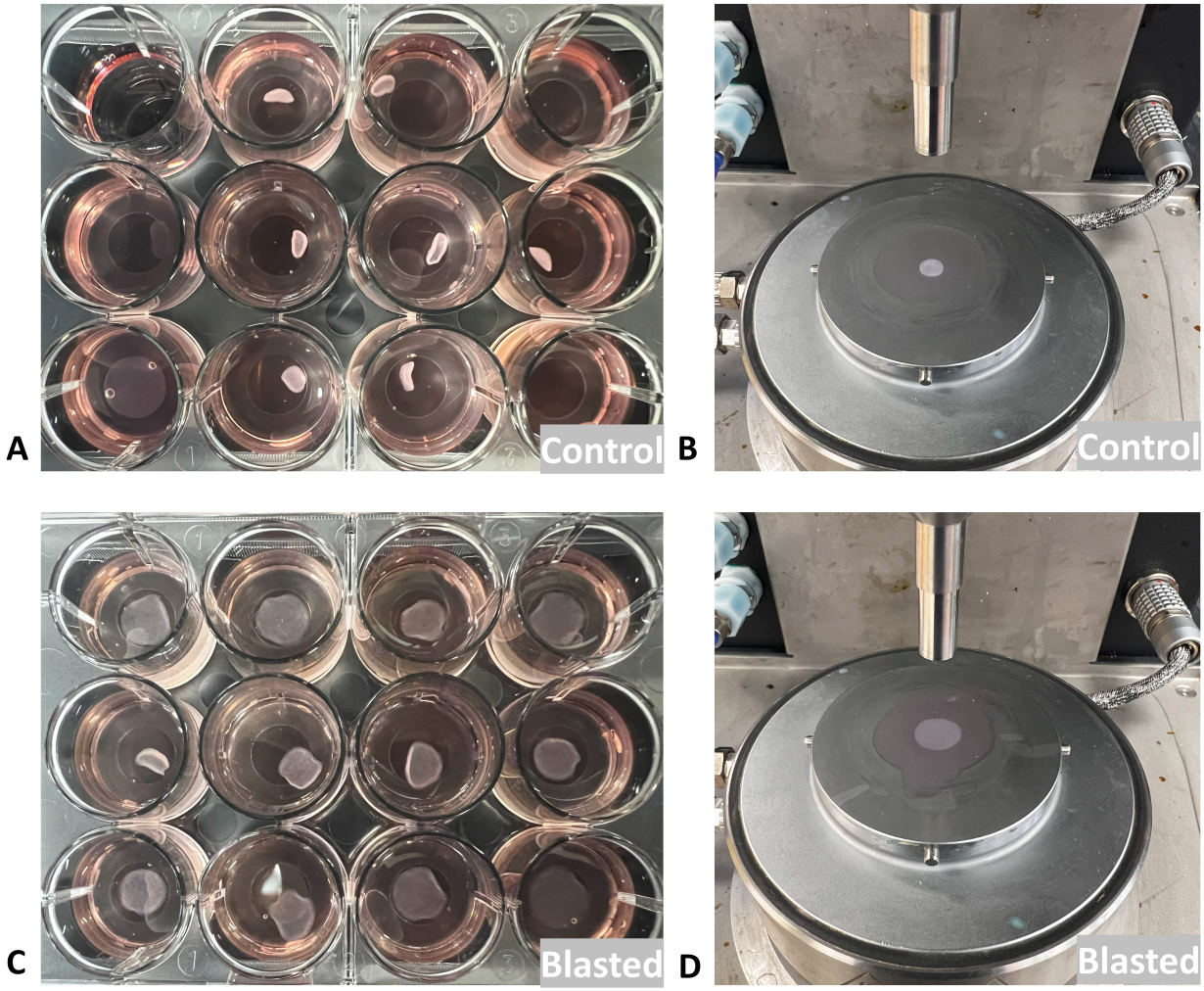

Figure 5.4: Reactive Astrocytes Alter Mechanical Integrity of Surrounding Matrix. Adhesion of the hydrogel to the PDMS mold was pictured on day 17 for each condition. Hydrogels from the control condition are shown in the 12-well plate and transferred to the rheometer (A-B). Similarly, the hydrogel seeded with blasted astrocytes are imaged in their 12-well plate and after transfer to the rheometer (C-D).

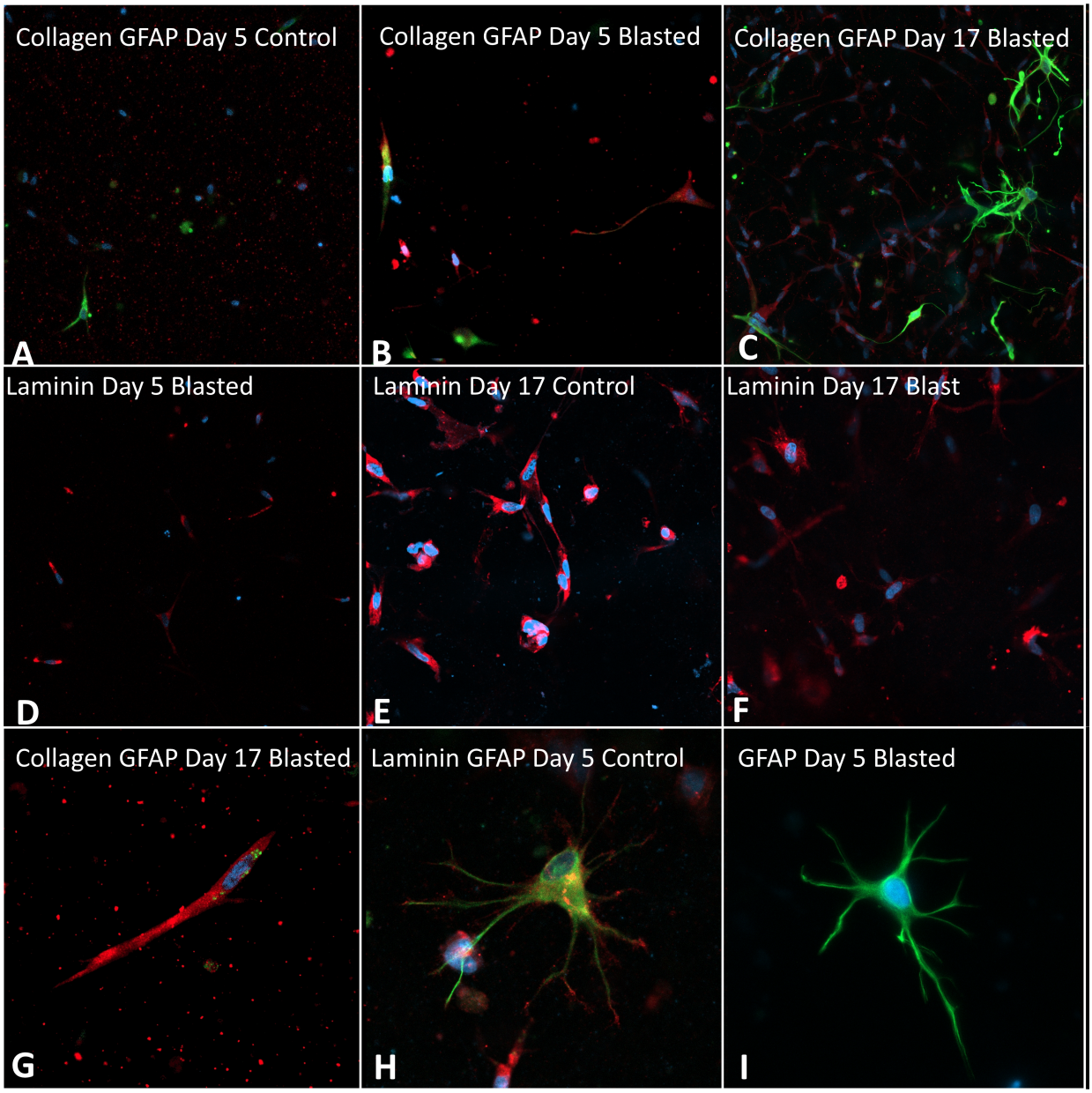

Figure 5.5: Collagen IV, Laminin and GFAP Expression Following High-Rate Overpressure. Confocal microscopy of hydrogels immunostained with either collagen IV & GFAP (A-C, G), Laminin and GFAP (D-F, H), or only GFAP (I). Images were obtained as a z-stack from normal hydrogel geometry in day 5 images. Hydrogel was mounted onto a glass slide on day 17 due to detachment from PDMS requiring images to be taken as a single slice. All hydrogels stained were synthesized during the initial experiment of 16.3 PSI blast magnitude.

on day 5 were not comparable to those fixed on day 17. For day 5 gels, a z-stack was taken which captured a total volume of 0.31 mm^3. For day 17 gels, a single slice measuring 0.1 mm^2 was acquired. The average fluorescent intensity for either the single slice or max projection is shown in Figure5.6 (B) and (C). Figure 5.6 (A) shows that the number of cells in the control gels is significantly greater than the blasted condition on both days 5 and 17. The cell count at day 17 for the control gels has much higher variation than compared to other conditions. In figure 5.6 (B & C) GFAP expression is similar between blast and control. No difference was detected between control and blast conditions at 5 days, but on day 17 the control hydrogels showed increased expression of laminin. Expression of collagen IV between the control and blast hydrogels showed to be elevated on both days 5 and 17.

Supernatant used to culture hydrogels for the first three days following hydrogel synthesis was collected and used to detect an array of enzymes secreted by astrocytes shown in figure 5.7 (C). Contrary to the initial hypothesis, almost no MMP expression was detected apart from MMP-1. TIMP-1 showed expression within both conditions with slightly more being detected in the blasted group. TIMP-2 exhibited high expression on membranes (A) and (B) in figure 5.7. Supernatant from the control groups showed a slight elevation of TIMP-2 compared to the blast groups. No detection of MMP-2, MMP-3, MMP-8, MMP-9, MMP-10, MMP-13 and TIMP-4 was detected.

5.4 Discussion

The effects of exposing human astrocytes to a high-rate overpressure on reactivity were investigated in both 2D and 3D. GFAP is one of the primary markers typically used to asses if an astrocyte is reactive or not. In figure 5.2the levels of GFAP expression for both 2D monolayers and 3D hydrogels can be observed. Graphs (A) and (C) indicate that the

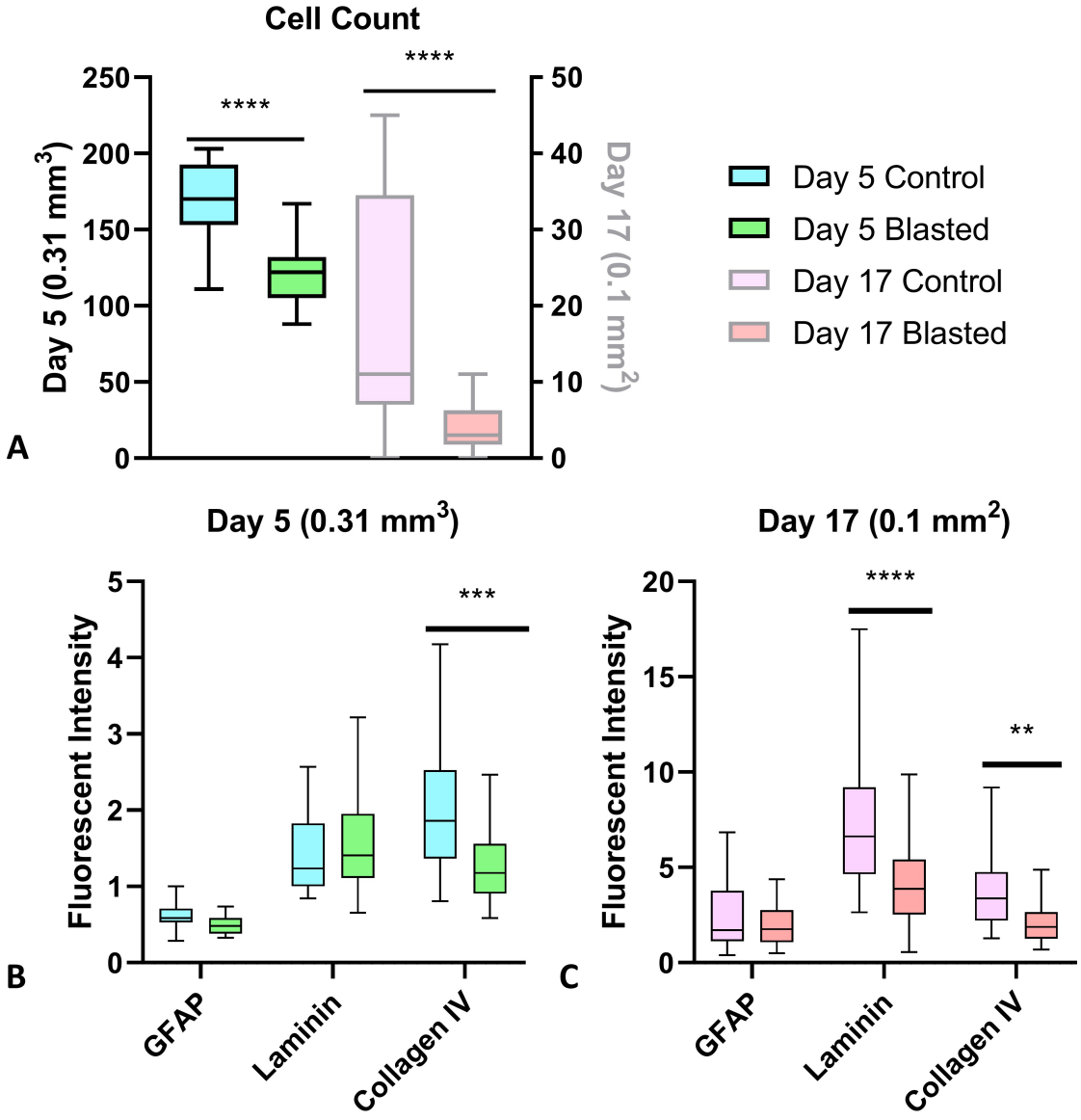

Figure 5.6: Analysis of RA ECM Protein Deposition. Normal and blasted astrocytes were seeded in collagen I-HA hydrogel and immunostained stained for collagen IV, laminin, and GFAP. The cell count was determined by counting the number of nuclei and subjecting each time point to an unpaired t-test with a 95% confidence interval (A). Images at the day 5-time point were acquired as a z-stack and the average fluorescence was determined from the max projection (B). Images at the 17-day time point were acquired as a single slice and the average fluorescence was determined (C). A 2-way ANOVA was used to compare the mean of each tagged protein between conditions at a 95% confidence interval. All hydrogels analyzed were synthesized during initial experiment of 16.3 PSI blast magnitude.

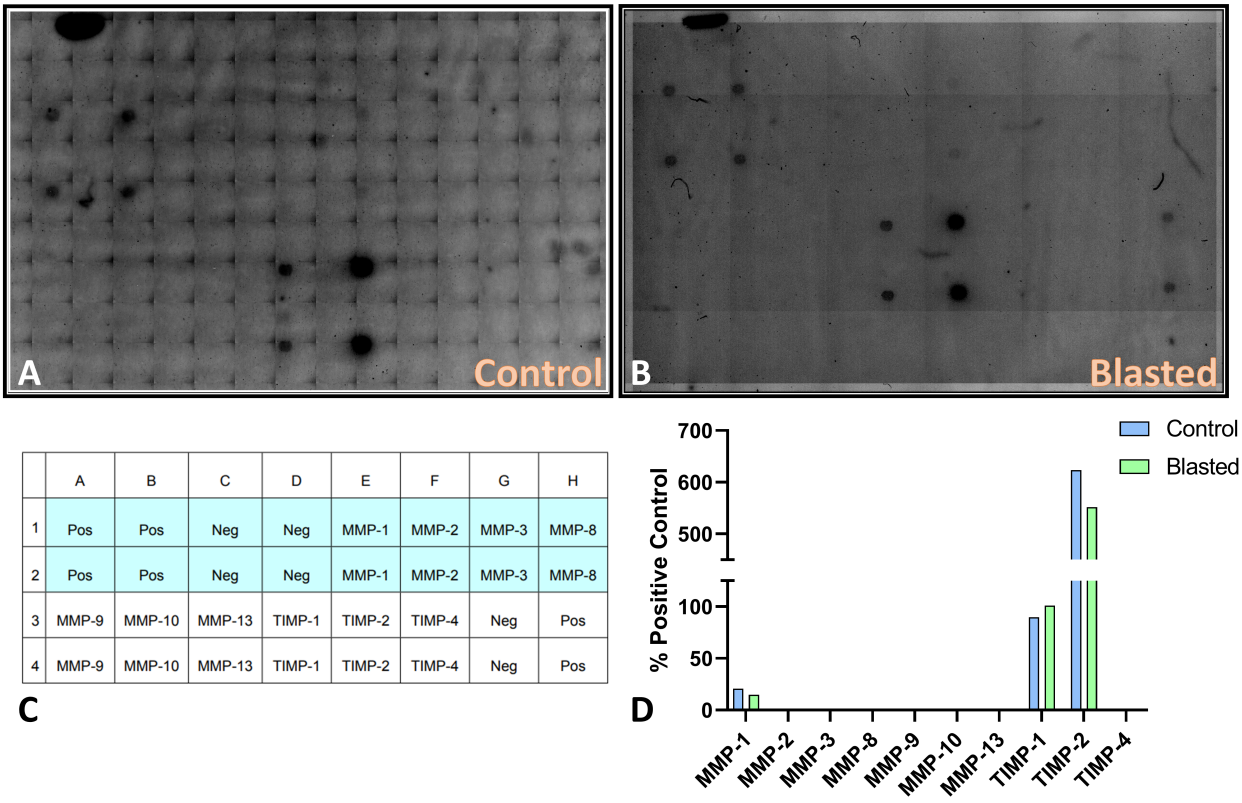

	A	B	C	D	E	F	G	H
1	Pos	Pos	Neg	Neg	MMP-1	MMP-2	MMP-3	MMP-8
2	Pos	Pos	Neg	Neg	MMP-1	MMP-2	MMP-3	MMP-8
3	MMP-9	MMP-10	MMP-13	TIMP-1	TIMP-2	TIMP-4	Neg	Pos
4	MMP-9	MMP-10	MMP-13	TIMP-1	TIMP-2	TIMP-4	Neg	Pos

Figure 5.7: Human MMP Antibody Array. Membrane chemiluminescent detection of an array of enzymes secreted by astrocytes cultured in hydrogels (A & B). The layout of antibody deposition on the surface of the membrane (C) [81]. Expression of enzymes was quantified in ImageJ and normalized to compare blasted and normal astrocyte supernatant (D).

overall GFAP expression for each cell decreases over time in both 2D and 3D. The drop in GFAP expression may be explained by the increase in cell count. The number of reactive cells does not change over time as shown by figure 5.2 (E), as well as the total level of expression shown by (B). This indicates that the cells expressing GFAP are likely splitting it among the two new daughter cells. The figure also shows that the hydrogel closer mimics an *in vivo* environment in contrast to the 2D monolayer. In figure 5.2 (D) the cell count in 2D almost triples from days 2 to 5. This rapid proliferation of astrocytes is not realistic to physiological conditions and advocates that the hydrogel is a much better model. This experiment validated the use of hydrogels as an *in vitro* model to better mimic physiological conditions. The method of immunocytochemical staining was also validated along with fluorescent image acquisition and analysis.

The impact of reactive astrocyte remodeling on the ECM was determined through mechanical testing, immunocytochemical staining, and an MMP antibody array. Mechanical testing was executed using a rheometer with a parallel plate geometry to test the complex shear modulus of hydrogels seeded with blasted and normal cells. The hydrogels with blasted astrocytes were shown to exhibit a higher modulus than those seeded with normal astrocytes shown in figure 5.3 (A). It is also observed that the modulus between hydrogels with blasted cells is very similar across all conditions. This indicates that the control hydrogels are decreasing in shear modulus over time while the blasted hydrogels are remaining constant due to the RAs modulating their environment. A future experiment can be conducted to compare the modulus of hydrogels one-day following seeding and compare how gels with blasted and normal gels compare over time. This would inform whether or not the blasted astrocytes retain the original modulus, or find an equilibrium similar to the value shown in figure 5.3 (A).

Over time it was observed that the shape and volume of the hydrogels changed. The decrease

in thickness over time shown by figure 5.3 (B) is likely due to the degradation of the hydrogel over time. Degradation may occur over 3 different modes: hydrolysis, non-cellular enzymatic, and cell-mediated degradation [82]. However, the change in thickness has little correlation to complex shear modulus as shown in figure 5.3 (C). To better understand the changes in mass over time thermogravimetric analysis can be performed which will provide better insight into the degradation caused by each condition over time. It is also unknown if the same effectors that degrade the matrix also change the modulus of the gel.

Detachment of hydrogels from their PDMS molds was observed in the longer time point studies shown in figure 5.4. It is unclear if the detachment stems from degradation or if there is another factor at play that influences the adhesion of the gel. Detachment from the PDMS was also observed to be decelerated in the hydrogels seeded with blasted astrocytes. Detachment also caused the shape of the hydrogel to change due to the folding of the edges. Folding causing changes in the geometry and likely impacting the modulus acquired in figure 5.3 (A) for the control day 17 condition. In this case, AFM can provide a more accurate measurement as the probe used to obtain readings requires less than 10 μm of surface area. A force map of the surface may also be obtained to investigate the heterogeneity of the hydrogel.

Images in figure 5.5 indicate that the majority of cells expressing GFAP do not express collagen or laminin and vice versa. This trend can be interpreted as a decrease in collagen and laminin production in reactive astrocytes. Collagen IV protects neurons from toxicity of amyloid-βpeptides. A decrease in the ECM protein is associated with increased spontaneous apoptosis and has shown impairment of motor and memory task performances in collagen IV deficient aged mice [83]. Laminin primarily serves the role of formation, stability, and architecture of basement membranes. The ECM protein helps maintain BBB integrity and provide adjacent cells with mechanical integrity [84]. Decreased production of collagen IV

and laminin is further supported in figure 5.6 (B) and (C). A decrease in collagen IV and laminin production follows the same trend observed in a TBI mouse model that saw a decrease in expression following a cortical impact [85].

Figure 5.6 (A) shows that the number of astrocytes present in the control is greater than that in the blasted gels. This difference may be due to the blasted astrocytes not proliferating as much or that the seeding density of the normal astrocytes was higher. Exposing astrocytes to high-rate overpressures likely has an effect on proliferation as the day 17 blasted condition has much lower variability compared to the control. GFAP expression between blast and control is similar between conditions and does not favor the blasted astrocytes. It was hypothesized that the blasted astrocytes would express higher levels of GFAP. Astrocytes may have started to express GFAP during 2D cell culture or pipetting which can cause shear stress on the cells. Although there are similar expression levels of GFAP, the modulation of the ECM is different as shown by figure 5.3 (A). These results point in the direction that GFAP is a poor marker for the phenotype astrocytes develop following a simulated mTBI. Future studies should identify potential markers that better track the level of reactivity that causes alterations to the surrounding matrix.

Laminin is shown to be similar at the day 5-time point but increases much more in the control gels by day 17. Figure 5.6 (B) and (C) leads to the belief that a secondary cascade response due to exposure to a simulated mTBI minimizes the production of laminin. Collagen on the other hand shows a decrease in expression at both days 5 and 17 in hydrogels seeded with blasted cells. The decreased expression of both laminin and collagen IV may lead to long-term neurodegenerative diseases as both ECM proteins provide vital functions within the brain.

The semi-quantitative MMP antibody array assay showed expression of MMP-1, TIMP-1, and TIMP-2. Of these enzymes, there was a downregulation in MMP-1 and TIMP-2 in the

supernatant collected from blasted cells. TIMP regulates ECM degradation in vascular walls by inhibiting the activity of MMPs [86]. The absence of MMP expression can be explained by the high TIMP expression. TIMP-1 has been shown to also correlate with the progression of inflammatory diseases which includes cancer [87]. Further studies will need to be executed to link the dysregulation of TIMP expression to the progression of neurodegeneration.

Chapter 6

Conclusion

The cellular mechanisms that underlie the pathogenesis of mTBI and the contribution of mechanical forces that result in prolonged brain damage are yet to be comprehensively elucidated. To address this knowledge gap, this study was undertaken with the objective of developing and utilizing an *in vitro* mTBI platform to investigate the intricate mechanical interplay between ECM and astrocytes following a simulated mTBI. The platform facilitated an in-depth exploration of the mechanistic complexity underlying the ECM-astrocyte interaction, thereby providing new insights into mTBI pathologies.

An innovative platform has been devised to accommodate *in vitro* tissue-engineered models for investigating the mechanical influence of reactive astrocytes on the surrounding matrix. The platform has been efficaciously designed to fulfill all user requirements and has been validated as a technique to subject hydrogels to high-rate overpressures while preserving their sterility and accessibility.

The present study successfully devised mechanical characterization techniques for tissue-engineered models utilizing atomic force microscopy and rheology. These methods facilitate accurate measurement of mechanical features up to nanoscale resolution. Changes in the composition and structure of the ECM can have a significant impact on the mechanical properties of the hydrogel as well as the behavior of cells that interact within it. The developed techniques have enabled the detection of any alterations in the ECM.

The study investigated the impact of subjecting human astrocytes to high-rate overpressure on their mechanical properties and relevant protein expression. Results revealed that astrocytes exposed to the overpressure had altered mechanical properties of their surrounding matrix, as evidenced by increased shear modulus in hydrogels seeded with the affected cells. Furthermore, exposure to a simulated mTBI resulted in decreased expression of laminin and collagen IV, which are critical to brain function and may contribute to pathologies associated with exposure to injury. These findings suggest that astrocytes modulate their surrounding matrix following high-rate overpressure exposure, and further research is needed to elucidate the mechanisms underlying this phenomenon.

Bibliography

[1] 5 Interesting Facts about Traumatic Brain Injury (TBI).

[2] Douglas I Katz, Sara I Cohen, and Michael P Alexander. Mild traumatic brain injury DEFINITIONS AND DIAGNOSTIC CRITERIA Mild traumatic brain injury. Technical report, 2015.

[3] Get the Facts About TBI. Technical report.

[4] Christopher A. Taylor, Jeneita M. Bell, Matthew J. Breiding, and Likang Xu. Traumatic Brain Injury–Related Emergency Department Visits, Hospitalizations, and Deaths — United States, 2007 and 2013. *MMWR. Surveillance Summaries*, 66(9):1–16, 3 2017.

[5] David B Arciniegas, C Alan Anderson, Jeannie Topkoff, and Thomas W McAllister. Mild traumatic brain injury: a neuropsychiatric approach to diagnosis, evaluation, and treatment. *Neuropsychiatric disease and treatment*, 1(4):311–27, 12 2005.

[6] Harvey S. Levin and Ramon R. Diaz-Arrastia. Diagnosis, prognosis, and clinical management of mild traumatic brain injury, 5 2015.

[7] Katarina Bohman, Kristy B. Arbogast, and Ola Boström. Head injury causation scenarios for belted, rear-seated children in frontal impacts. *Traffic Injury Prevention*, 12(1):62–70, 2 2011.

[8] Department of Health, Human Services, and Centers for Disease Control. Centers for Disease Control and Prevention Prevention and Control SURVEILLANCE REPORT Surveillance Report of Traumatic Brain Injury-related Emergency Department

Visits, Hospitalizations, and Deaths TBI: SURVEILLANCE REPORT ACKNOWLEDGEMENTS. Technical report.

[9]) Carroll, Cassidy, L Kraus, and J Coronado. Terms and conditions Privacy policy Methodological issues and research recommendations for mild traumatic brain injury: The WHO Collaborating Centre Task Force on Mild Traumatic Brain Injury. Technical Report 43, 2004.

[10] Vigneswaran Veeramuthu, Vairavan Narayanan, Tan Li Kuo, Lisa Delano-Wood, Karuthan Chinna, Mark William Bondi, Vicknes Waran, Dharmendra Ganesan, and Norlisah Ramli. Diffusion tensor imaging parameters in mild traumatic brain injury and its correlation with early neuropsychological impairment: A longitudinal study. *Journal of Neurotrauma*, 32(19):1497–1509, 10 2015.

[11] Erin D. Bigler. Neuropsychological results and neuropathological findings at autopsy in a case of mild traumatic brain injury, 9 2004.

[12] Michael V. Sofroniew and Harry V. Vinters. Astrocytes: Biology and pathology, 1 2010.

[13] Gui Lian Yu, Ying Zhang, and Bin Ning. Reactive Astrocytes in Central Nervous System Injury: Subgroup and Potential Therapy, 12 2021.

[14] Michael M. Halassa, Tommaso Fellin, Hajime Takano, Jing Hui Dong, and Philip G. Haydon. Synaptic islands defined by the territory of a single astrocyte. *Journal of Neuroscience*, 27(24):6473–6477, 6 2007.

[15] K Ogata and T Kosaka. Structural and quantitative analysis of astrocytes in the mouse hippocampus. *Neuroscience*, 113(1):221–33, 2002.

[16] Raphaela Almeida Chiareli, Gustavo Almeida Carvalho, Bruno Lemes Marques, Lennia Soares Mota, Onésia Cristina Oliveira-Lima, Rodrigo Mello Gomes, Alexander

Birbrair, Renato Santiago Gomez, Fabrício Simão, Friederike Klempin, Marcel Leist, and Mauro Cunha Xavier Pinto. The Role of Astrocytes in the Neurorepair Process. *Frontiers in Cell and Developmental Biology*, 9, 5 2021.

[17] Carole Escartin, Elena Galea, András Lakatos, James P. O'Callaghan, Gabor C. Petzold, Alberto Serrano-Pozo, Christian Steinhäuser, Andrea Volterra, Giorgio Carmignoto, Amit Agarwal, Nicola J. Allen, Alfonso Araque, Luis Barbeito, Ari Barzilai, Dwight E. Bergles, Gilles Bonvento, Arthur M. Butt, Wei-Ting Chen, Martine Cohen-Salmon, Colm Cunningham, Benjamin Deneen, Bart De Strooper, Blanca Díaz-Castro, Cinthia Farina, Marc Freeman, Vittorio Gallo, James E. Goldman, Steven A. Goldman, Magdalena Götz, Antonia Gutiérrez, Philip G. Haydon, Dieter H. Heiland, Elly M. Hol, Matthew G. Holt, Masamitsu Iino, Ksenia V. Kastanenka, Helmut Kettenmann, Baljit S. Khakh, Schuichi Koizumi, C. Justin Lee, Shane A. Liddelow, Brian A. MacVicar, Pierre Magistretti, Albee Messing, Anusha Mishra, Anna V. Molofsky, Keith K. Murai, Christopher M. Norris, Seiji Okada, Stéphane H. R. Oliet, João F. Oliveira, Aude Panatier, Vladimir Parpura, Marcela Pekna, Milos Pekny, Luc Pellerin, Gertrudis Perea, Beatriz G. Pérez-Nievas, Frank W. Pfrieger, Kira E. Poskanzer, Francisco J. Quintana, Richard M. Ransohoff, Miriam Riquelme-Perez, Stefanie Robel, Christine R. Rose, Jeffrey D. Rothstein, Nathalie Rouach, David H. Rowitch, Alexey Semyanov, Swetlana Sirko, Harald Sontheimer, Raymond A. Swanson, Javier Vitorica, Ina-Beate Wanner, Levi B. Wood, Jiaqian Wu, Binhai Zheng, Eduardo R. Zimmer, Robert Zorec, Michael V. Sofroniew, and Alexei Verkhratsky. Reactive astrocyte nomenclature, definitions, and future directions. *Nature Neuroscience*, 24(3):312–325, 3 2021.

[18] Shane A. Liddelow and Ben A. Barres. Reactive Astrocytes: Production, Function, and Therapeutic Potential. *Immunity*, 46(6):957–967, 6 2017.

[19] Philip Hasel, Indigo V. L. Rose, Jessica S. Sadick, Rachel D. Kim, and Shane A. Liddelow. Neuroinflammatory astrocyte subtypes in the mouse brain. *Nature Neuroscience*, 24(10):1475–1487, 10 2021.

[20] Ila P Karve, Juliet M Taylor, and Peter J Crack. The contribution of astrocytes and microglia to traumatic brain injury. *British Journal of Pharmacology*, 173(4):692–702, 2 2016.

[21] Joseph T. Neary, Yuan Kang, Minh Tran, and Jonathan Feld. Traumatic Injury Activates Protein Kinase B/Akt in Cultured Astrocytes: Role of Extracellular ATP and P2 Purinergic Receptors. *Journal of Neurotrauma*, 22(4):491–500, 4 2005.

[22] Nora Hlavac, Fernanda Guilhaume-Corrêa, and Pamela J. VandeVord. Mechanostimulation initiated by extracellular adhesion and cationic conductance pathways influence astrocyte activation. *Neuroscience Letters*, 739:135405, 11 2020.

[23] Stefka Gyoneva and Richard M. Ransohoff. Inflammatory reaction after traumatic brain injury: therapeutic potential of targeting cell–cell communication by chemokines. *Trends in Pharmacological Sciences*, 36(7):471–480, 7 2015.

[24] Dingfei Qian, Linwei Li, Yuluo Rong, Wei Liu, Qian Wang, Zheng Zhou, Changjiang Gu, Yifan Huang, Xuan Zhao, Jian Chen, Jin Fan, and Guoyong Yin. Blocking Notch signal pathway suppresses the activation of neurotoxic A1 astrocytes after spinal cord injury. *Cell Cycle*, 18(21):3010–3029, 11 2019.

[25] Doris Lam, Heather A. Enright, Jose Cadena, Sandra K.G. Peters, Ana Paula Sales, Joanne J. Osburn, David A. Soscia, Kristen S. Kulp, Elizabeth K. Wheeler, and Nicholas O. Fischer. Tissue-specific extracellular matrix accelerates the formation of neural networks and communities in a neuron-glia co-culture on a multi-electrode array. *Scientific Reports*, 9(1), 12 2019.

[26] Charles Nicholson and Eva Syková. Extracellular space structure revealed by diffusion analysis. *Trends in Neurosciences*, 21(11):470, 11 1998.

[27] Renato Frischknecht and Eckart D. Gundelfinger. The Brain's Extracellular Matrix and Its Role in Synaptic Plasticity. pages 153–171. 2012.

[28] Inseon Song and Alexander Dityatev. Crosstalk between glia, extracellular matrix and neurons. *Brain Research Bulletin*, 136:101–108, 1 2018.

[29] Cesario Borlongan, Sandra Acosta, Ike de la Pena, Naoki Tajiri, Yuji Kaneko, Diego Lozano, and Gabriel Gonzales-Portillo. Neuroinflammatory responses to traumatic brain injury: etiology, clinical consequences, and therapeutic opportunities. *Neuropsychiatric Disease and Treatment*, page 97, 1 2015.

[30] Matthew A. Hemphill, Stephanie Dauth, Chung Jong Yu, Borna E. Dabiri, and Kevin Kit Parker. Traumatic Brain Injury and the Neuronal Microenvironment: A Potential Role for Neuropathological Mechanotransduction. *Neuron*, 85(6):1177–1192, 3 2015.

[31] Naijil George and Herbert M. Geller. Extracellular matrix and traumatic brain injury. *Journal of Neuroscience Research*, 96(4):573–588, 4 2018.

[32] Hao Cui, Craig Freeman, Glenn A. Jacobson, and David H. Small. Proteoglycans in the central nervous system: Role in development, neural repair, and Alzheimer's disease. *IUBMB Life*, 65(2):108–120, 2 2013.

[33] Jae-Hyuk Yi, Yasuhiro Katagiri, Bala Susarla, David Figge, Aviva J. Symes, and Herbert M. Geller. Alterations in sulfated chondroitin glycosaminoglycans following controlled cortical impact injury in mice. *The Journal of Comparative Neurology*, 520(15):3295–3313, 10 2012.

[34] Richard A. Asher, Daniel A. Morgenstern, Penny S. Fidler, Kathryn H. Adcock, Atsuhiko Oohira, Janet E. Braistead, Joel M. Levine, Richard U. Margolis, John H. Rogers, and James W. Fawcett. Neurocan Is Upregulated in Injured Brain and in Cytokine-Treated Astrocytes. *The Journal of Neuroscience*, 20(7):2427–2438, 4 2000.

[35] Esther Steiner, Gaby U. Enzmann, Ruth Lyck, Shuo Lin, Markus A. Rüegg, Stephan Kröger, and Britta Engelhardt. The heparan sulfate proteoglycan agrin contributes to barrier properties of mouse brain endothelial cells by stabilizing adherens junctions. *Cell and Tissue Research*, 358(2):465–479, 11 2014.

[36] Guoqiang Xing, Ming Ren, and Ajay Verma. Divergent Temporal Expression of Hyaluronan Metabolizing Enzymes and Receptors with Craniotomy vs. Controlled-Cortical Impact Injury in Rat Brain: A Pilot Study. *Frontiers in Neurology*, 5, 9 2014.

[37] Dianhua Jiang, Jiurong Liang, and Paul W. Noble. Hyaluronan as an Immune Regulator in Human Diseases. *Physiological Reviews*, 91(1):221–264, 1 2011.

[38] Melissa D. Laird, John R. Vender, and Krishnan M. Dhandapani. Opposing roles for reactive astrocytes following traumatic brain injury, 2 2008.

[39] Richard F Keep, Ningna Zhou, Jianming Xiang, Anuska V Andjelkovic, Ya Hua, and Guohua Xi. Vascular disruption and blood–brain barrier dysfunction in intracerebral hemorrhage. *Fluids and Barriers of the CNS*, 11(1):18, 2014.

[40] Barbara Pijet, Marzena Stefaniuk, and Leszek Kaczmarek. MMP-9 Contributes to Dendritic Spine Remodeling Following Traumatic Brain Injury. *Neural Plasticity*, 2019:1–12, 5 2019.

[41] Orr Hadass, Brittany N. Tomlinson, Major Gooyit, Shanyan Chen, Justin J. Purdy, Jennifer M. Walker, Chunyang Zhang, Andrew B. Giritharan, Whitley Purnell, Christo-

pher R. Robinson, Dmitriy Shin, Valerie A. Schroeder, Mark A. Suckow, Agnes Simonyi, Grace Y. Sun, Shahriar Mobashery, Jiankun Cui, Mayland Chang, and Zezong Gu. Selective Inhibition of Matrix Metalloproteinase-9 Attenuates Secondary Damage Resulting from Severe Traumatic Brain Injury. *PLoS ONE*, 8(10):e76904, 10 2013.

[42] Takuro Hayashi, Yuji Kaneko, SeongJin Yu, EunKyung Bae, Christine E. Stahl, Takeshi Kawase, Harry van Loveren, Paul R. Sanberg, and Cesar V. Borlongan. Quantitative analyses of matrix metalloproteinase activity after traumatic brain injury in adult rats. *Brain Research*, 1280:172–177, 7 2009.

[43] Guangyuan Han, Lijuan Song, Zhibin Ding, Qing Wang, Yuqing Yan, Jianjun Huang, and Cungen Ma. The Important Double-Edged Role of Astrocytes in Neurovascular Unit After Ischemic Stroke. *Frontiers in Aging Neuroscience*, 14, 4 2022.

[44] Ciro De Luca, Anna Maria Colangelo, Lilia Alberghina, and Michele Papa. Neuro-Immune Hemostasis: Homeostasis and Diseases in the Central Nervous System. *Frontiers in Cellular Neuroscience*, 12, 11 2018.

[45] Alain Goriely, Marc G. D. Geers, Gerhard A. Holzapfel, Jayaratnam Jayamohan, Antoine Jérusalem, Sivabal Sivaloganathan, Waney Squier, Johannes A. W. van Dommelen, Sarah Waters, and Ellen Kuhl. Mechanics of the brain: perspectives, challenges, and opportunities. *Biomechanics and Modeling in Mechanobiology*, 14(5):931–965, 10 2015.

[46] Bryan Kolb and Ian Q. Whishaw. BRAIN PLASTICITY AND BEHAVIOR. *Annual Review of Psychology*, 49(1):43–64, 2 1998.

[47] Silvia Budday, Timothy C. Ovaert, Gerhard A. Holzapfel, Paul Steinmann, and Ellen Kuhl. Fifty Shades of Brain: A Review on the Mechanical Testing and Modeling of

Brain Tissue. *Archives of Computational Methods in Engineering*, 27(4):1187–1230, 9 2020.

[48] William J. Tyler. The mechanobiology of brain function. *Nature Reviews Neuroscience*, 13(12):867–878, 12 2012.

[49] Clara Karton and T. Blaine Hoshizaki. Concussive and subconcussive brain trauma: the complexity of impact biomechanics and injury risk in contact sport. pages 39–49. 2018.

[50] Joshua E. Burda, Alexander M. Bernstein, and Michael V. Sofroniew. Astrocyte roles in traumatic brain injury. *Experimental Neurology*, 275:305–315, 1 2016.

[51] Leon Islas, Herminia Pasantes-Morales, and Jorge A. Sanchez. Characterization of stretch-activated ion channels in cultured astrocytes. *Glia*, 8(2):87–96, 6 1993.

[52] Candace L. Floyd, Fredric A. Gorin, and Bruce G. Lyeth. Mechanical strain injury increases intracellular sodium and reverses Na+/Ca2+ exchange in cortical astrocytes. *Glia*, 51(1):35–46, 7 2005.

[53] WHITEPAPER 2 A Basic Introduction to Rheology Shear Flow. Technical report.

[54] Terri Chen. Rheology: Basic Theory and Applications Training Section #1. Technical report.

[55] Atomic Force Microscopy Working Principle — AFM Explained - Nanosurf.

[56] Marcos Penedo, Ayhan Yurtsever, Keisuke Miyazawa, Hirotoshi Furusho, Kiyo-Aki Ishii, and Takeshi Fukuma. Photothermal excitation efficiency enhancement of cantilevers by electron beam deposition of amorphous carbon thin films. *Scientific Reports*, 10(1):17436, 10 2020.

[57] jpk-app-elastic-modulus.14-1.

[58] Caleb Jensen and Yong Teng. Is It Time to Start Transitioning From 2D to 3D Cell Culture? *Frontiers in Molecular Biosciences*, 7, 3 2020.

[59] Carolyn E Hampton, Chevon N Thorpe, Christopher A Sholar, Beverly A Rzigalinski, and Pamela J VandeVord. A novel bridge wire model of blast traumatic brain injury - biomed 2013. *Biomedical sciences instrumentation*, 49:312–9, 2013.

[60] Scott B. Campbell, Qinghua Wu, Joshua Yazbeck, Chuan Liu, Sargol Okhovatian, and Milica Radisic. Beyond Polydimethylsiloxane: Alternative Materials for Fabrication of Organ-on-a-Chip Devices and Microphysiological Systems. *ACS Biomaterials Science & Engineering*, 7(7):2880–2899, 7 2021.

[61] Lianchao Jia, Zhiyong Li, and Qingquan Wei. Bubble generation and growth mechanism in PMMA microfluidic chip. *AIP Advances*, 12(5):055106, 5 2022.

[62] F Fixe, M Dufva, P Telleman, and C B V Christensen. Functionalization of poly(methyl methacrylate) (PMMA) as a substrate for DNA microarrays. *Nucleic acids research*, 32(1):e9, 1 2004.

[63] Mohammad M. Faghih and M. Keith Sharp. Solvent-based bonding of PMMA–PMMA for microfluidic applications. *Microsystem Technologies*, 25(9):3547–3558, 9 2019.

[64] Jiri Suder, Zdenko Bobovsky, Jakub Mlotek, Michal Vocetka, Zdenek Zeman, and Michal Safar. EXPERIMENTAL ANALYSIS OF TEMPERATURE RESISTANCE OF 3D PRINTED PLA COMPONENTS. *MM Science Journal*, 2021(1):4322–4327, 3 2021.

[65] Ji Eun Song, Wha Soon Song, Sang Young Yeo, Hye Rim Kim, and So Hee Lee. Covalent immobilization of enzyme on aminated woven poly (lactic acid) via ammonia

plasma: evaluation of the optimum immobilization conditions. *Textile Research Journal*, 87(10):1177–1191, 6 2017.

[66] Matteo Minelli, Marco Giacinti Baschetti, Daniel T. Hallinan, and Nitash P. Balsara. Study of gas permeabilities through polystyrene-block-poly(ethylene oxide) copolymers. *Journal of Membrane Science*, 432:83–89, 4 2013.

[67] What are the glass transition temperatures for acrylic sheet_ - ACRYLITE®.

[68] Trotec eBook Advantages of laser cutting acrylic. Technical report.

[69] Ali Ansari, Rajiv Trehan, Craig Watson, and Samuel Senyo. Increasing silicone mold longevity: a review of surface modification techniques for PDMS-PDMS double casting. *Soft Materials*, 19(4):388–399, 10 2021.

[70] Alborz Amirsadeghi, Lance Brumfield, Junseo Choi, Emily Brown, Jae Jong Lee, and Sunggook Park. The role of hydrophobic silane coating on Si stamps in nanoimprint lithography. *Journal of Applied Physics*, 121(4):044909, 1 2017.

[71] Michael V. Lee, Ghaleb Husseini, Ken Sautter, and Matthew R. Linford. Gas Phase Deposition of Trichloro(1H,1H,2H,2H-perfluorooctyl)silane on Silicon Dioxide, by XPS. *Surface Science Spectra*, 17(1):87–92, 12 2010.

[72] Alexandra Borók, Kristóf Laboda, and Attila Bonyár. PDMS Bonding Technologies for Microfluidic Applications: A Review. *Biosensors*, 11(8):292, 8 2021.

[73] Ajith R Vancha, Suman Govindaraju, Kishore VL Parsa, Madhuri Jasti, Maribel González-García, and Rafael P Ballestero. Use of polyethyleneimine polymer in cell culture as attachment factor and lipofection enhancer. *BMC Biotechnology*, 4(1):23, 2004.

[74] Woojung Shin, Yoko M. Ambrosini, Yong Cheol Shin, Alexander Wu, Soyoun Min, Domin Koh, Sowon Park, Seung Kim, Hong Koh, and Hyun Jung Kim. Robust Formation of an Epithelial Layer of Human Intestinal Organoids in a Polydimethylsiloxane-Based Gut-on-a-Chip Microdevice. *Frontiers in Medical Technology*, 2, 8 2020.

[75] Amanda L. Placone, Patricia M. McGuiggan, Dwight E. Bergles, Hugo Guerrero-Cazares, Alfredo Quiñones-Hinojosa, and Peter C. Searson. Human astrocytes develop physiological morphology and remain quiescent in a novel 3D matrix. *Biomaterials*, 42:134–143, 2 2015.

[76] Chloe M. Hall, Emad Moeendarbary, and Graham K. Sheridan. Mechanobiology of the brain in ageing and Alzheimer's disease. *European Journal of Neuroscience*, 53(12):3851–3878, 6 2021.

[77] Jonathan M. Zuidema, Christopher J. Rivet, Ryan J. Gilbert, and Faith A. Morrison. A protocol for rheological characterization of hydrogels for tissue engineering strategies. *Journal of Biomedical Materials Research - Part B Applied Biomaterials*, 102(5):1063–1073, 2014.

[78] Anne S. G. van Oosten, Mahsa Vahabi, Albert J. Licup, Abhinav Sharma, Peter A. Galie, Fred C. MacKintosh, and Paul A. Janmey. Uncoupling shear and uniaxial elastic moduli of semiflexible biopolymer networks: compression-softening and stretch-stiffening. *Scientific Reports*, 6(1):19270, 1 2016.

[79] Rheology Theory and Applications. Technical report.

[80] Pavel Dutov, Olga Antipova, Sameer Varma, Joseph P. R. O. Orgel, and Jay D. Schieber. Measurement of Elastic Modulus of Collagen Type I Single Fiber. *PLOS ONE*, 11(1):e0145711, 1 2016.

[81] ab134004-Human MMP Antibody Array-Membrane Instructions for Use. Technical report.

[82] Michelle S. Mazzeo, Tiffanie Chai, Maryam Daviran, and Kelly M. Schultz. Characterization of the Kinetics and Mechanism of Degradation of Human Mesenchymal Stem Cell-Laden Poly(ethylene glycol) Hydrogels. *ACS Applied Bio Materials*, 2(1):81–92, 1 2019.

[83] Matilde Cescon, Peiwen Chen, Silvia Castagnaro, Ilaria Gregorio, and Paolo Bonaldo. Lack of collagen VI promotes neurodegeneration by impairing autophagy and inducing apoptosis during aging. *Aging*, 8(5):1083–1101, 4 2016.

[84] MONIQUE AUMAILLEY and NEIL SMYTH. The role of laminins in basement membrane function. *Journal of Anatomy*, 193(1):1–21, 7 1998.

[85] Juan F. Zapata-Acevedo, Valentina García-Pérez, Ricardo Cabezas-Pérez, Monica Losada-Barragán, Karina Vargas-Sánchez, and Rodrigo E. González-Reyes. Laminin as a Biomarker of Blood–Brain Barrier Disruption under Neuroinflammation: A Systematic Review. *International Journal of Molecular Sciences*, 23(12):6788, 6 2022.

[86] Tomohiro Aoki, Hiroharu Kataoka, Takuya Moriwaki, Kazuhiko Nozaki, and Nobuo Hashimoto. Role of TIMP-1 and TIMP-2 in the progression of cerebral aneurysms. *Stroke*, 38(8):2337–45, 8 2007.

[87] Celina Eckfeld, Benjamin Schoeps, Daniel Häußler, Julian Frädrich, Felix Bayerl, Jan Philipp Böttcher, Percy Knolle, Simone Heisz, Olga Prokopchuk, Hans Hauner, Enkhtsetseg Munkhbaatar, Ihsan Ekin Demir, Chris D. Hermann, and Achim Krüger. TIMP-1 is a novel ligand of Amyloid Precursor Protein and triggers a proinflammatory phenotype in human monocytes. *Journal of Cell Biology*, 222(2), 2 2023.

[88] Nanometer, Micrometer, and Millimeter Measurements in 1 System VK-X3000 Series. Technical report.

Appendices

Appendix A

Collagen I Hydrogel Synthesis

A.1 Protocol

All materials must be placed on ice throughout the procedure. All reagent volumes can be calculated using the equations listed in A.2. Collagen I (CB-40236, Thermo Fisher Scientific, Waltham, MA) is first transferred into a 15 mL tube. 10X PBS is then added and mixed. If using 10 mg/mL collagen mix with a spatula, otherwise use a pipette at lower concentrations. Add half of the NaOH volume calculated in equation A.3 then mix and repeat. If bubble formation occurs, centrifuge at 2500 rcf x 5 minutes at $4°C$. The cell suspension can then be added and mixed in. If creating hydrogels without cells, use media or 1X PBS. The hydrogel must then be seeded into wells and incubated for 30 minutes. The hydrogels must then be covered in media or PBS to incubate until ready for use.

A.2 Equations

$$C_V = (TG_V * DCC)/SCC \tag{A.1}$$

Where C_V = Collagen Volume (μL), TG_V = Total Gel Volume (μL), DCC = Desired Collagen Concentration (mg/mL) and SCC = Stock Collagen Concentration (mg/mL).

$$PBS_V = TG_V * 0.1 \tag{A.2}$$

Where PBS_V = 10X PBS Volume (μL).

$$NaOH_V = C_V * 0.02 \tag{A.3}$$

Where $NaOH_V$ = 1N NaOH Volume (μL).

$$CS_V = TG_V - NaOH_V - PBS_V Volume - C_V \tag{A.4}$$

Where CS_V = Cell Suspension Volume (μL).

Appendix B

Collagen I - HA Hydrogel Synthesis

B.1 Protocol

All materials must be placed on ice throughout the procedure. All reagent volumes can be calculated using the equations listed in B.2. Collagen I (CB-40236, Thermo Fisher Scientific, Waltham, MA) is first transferred into a 15 mL tube. 10X PBS is then added and mixed. Add half of the NaOH volume calculated in equation **??** then mix and repeat. DIW is the last reagent mixed into the collagen gel. The HA gel is synthesized by first adding the cell suspension to a new tube. If making a gel without cells, 1X PBS or media can be used. 5 mg/mL Glycosil (catalog number GS1004, Advanced Biomatrix Inc, San Diego, CA) is then mixed into the gel. The last component of the HA gel is the extralink. Once added, do not leave gel sitting for a long period of time as crosslinking will initiate. Once the 1 mg/mL HA gel is complete, transfer the gel into the 15 mL tube containing the 1 mg/mL collagen I gel and mix. The collagen I-HA gel can now be seeded into wells followed by 30 minutes of incubation for crosslinking to occur. Lastly, add media or 1X PBS on top of the gels and incubate until ready for use.

B.2 Equations

$$TCG_V = TG_V * 0.5 \tag{B.1}$$

Where TCG_V = Total Collagen Gel Volume (μL) and TG_V = Total Gel Volume (μL).

$$THAG_V = TG_V * 0.5 \tag{B.2}$$

Where $THAG_V$ = Total Hyaluronic Acid Gel Volume (μL).

$$C_V = (TCG_V * DCC)/SCC \tag{B.3}$$

Where C_V = Collagen Volume (μL), DCC = Desired Collagen Concentration (mg/mL) and SCC = Stock Collagen Concentration (mg/mL).

$$PBS_V = TCG_V * 0.1 \tag{B.4}$$

Where PBS_V = 10X PBS Volume (μL).

$$NaOH_V = C_V * 0.023 \tag{B.5}$$

Where $NaOH_V$ = 1N NaOH Volume (μL).

$$DIW = TG_V - NaOH_V - PBS_V Volume - C_V \tag{B.6}$$

Where DIW = Deionized Water (μL).

$$Gly = (DHAC * THAG_V)/(SHAC) \tag{B.7}$$

Where Gly = Glycosil Volume (μL), $DHAC$ = Desired Hyaluronic Acid Concentration

(mg/mL) and $SHAC$ = Stock Hyaluronic Acid Concentration (mg/mL).

$$Xlink = Gly/4 \tag{B.8}$$

Where $Xlink$ = Extralink Volume (μL).

$$CS_V = THAG_V - Gly - Xlink \tag{B.9}$$

Where CS_V = Cell Suspension Volume (μL).

Appendix C

ImageJ Anlaysis

C.1 Cell Viability

The viability of cells in different condition mediums was processed for analysis by completing the steps shown in figure C.1. First, each channel denoting propidium iodide and calcein green was split into two separate windows. This was followed by a threshold cutoff to determine the minimum level of intensity a pixel needs to express to be included in the analysis. It is best to determine the optimal value that removes back noise and use this value across all files being analyzed, otherwise, they cannot be effectively compared to each other. After setting the threshold, the analyze particle window is opened up. The most important parameter to consider is the range of particle size that will be included in the analysis. To develop a range, select the wand tool and click on the smallest particle you'd like to include then hit Ctrl M to measure the particle's area then repeat with the largest particle. The range you'll input should be a fair bit lower and higher than the values measured. Once ready, select OK and repeat for the other channel. The values will be shown like the last step and viability can be obtained by equation C.1.

$$CellViability(\%) = Count_{CG}/(Count_{CG} + Count_{PI}) \tag{C.1}$$

Where $Count_{CG}$ = Count Calcein Green and $Count_{PI}$ = Count Propidium Iodide

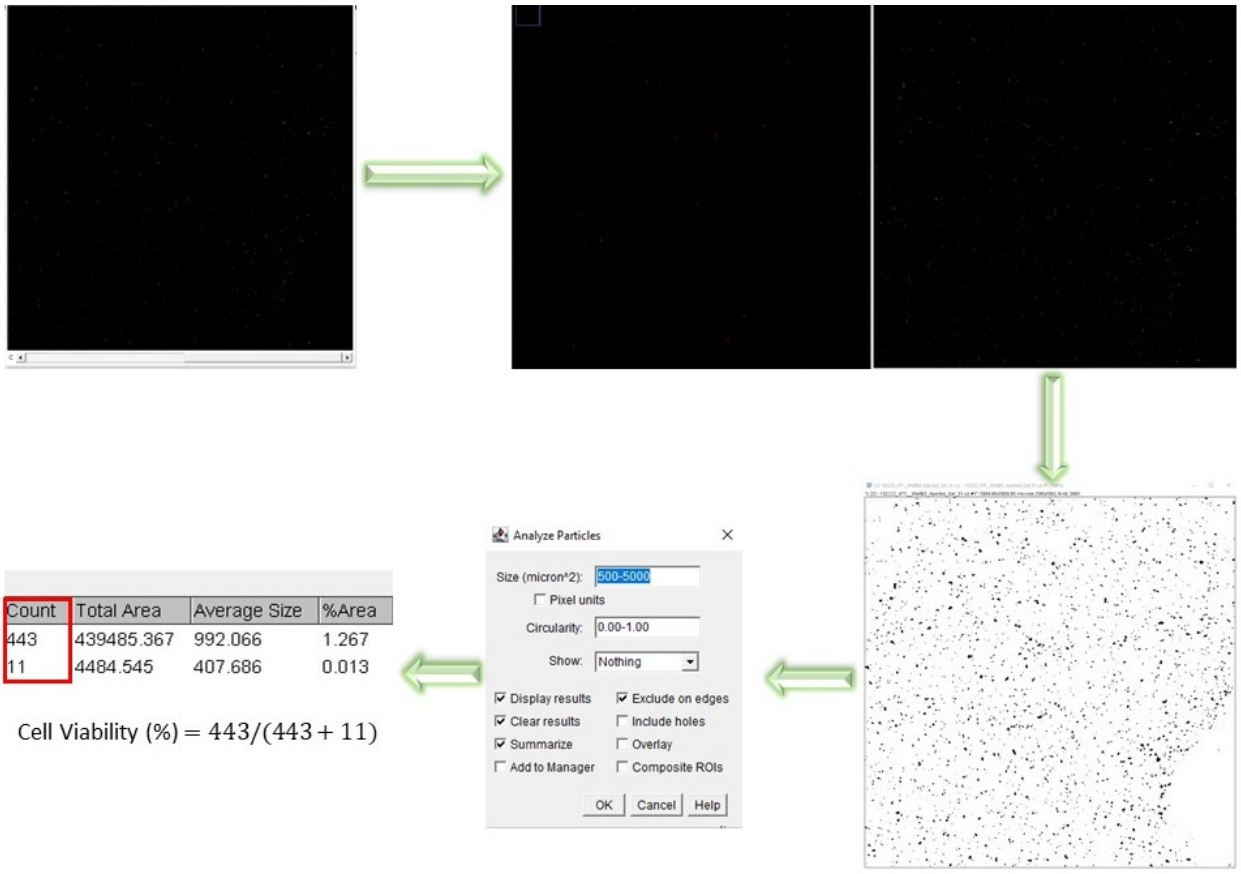

Figure C.1: Cell Viability Analysis in ImageJ

Appendix D

3D Surface Profilometer

The thickness of clear films can be measured by analyzing the light reflected between two edges of a transparent object [88]. To begin, place the sample on the stage and center the objective overhead. The film thickness measurement option needs to be selected as shown in figure D.1 (A). Next, located the top of the sample using a lower magnification objective and the laser option. Once located, the 20X objective should be used for more reliable results. Start at the top of the sample and click on the arrows pointing upward until there is no signal. Set the upper limit and proceed to click on the arrows pointing downward until the second boundary is found. Continue to descend a bit lower to ensure a safe margin and set the lower limit. To speed up acquisition and decrease noise from any interference within the sample e.g. cells in a hydrogel, select 1 line under the resolution tab shown on the bottom right of figure D.1 (A). Once the parameters are set, select start experiment. Measurements are obtained within the analysis software shown in section (B). Click on analyze data and proceed to select the point measurement shown in step (C). Select any point on the image where the intensity on the bottom boundary is visible. Next, on the point measure plot shown on the left of step (C), draglines 1 and 2 match the boundary locating from the image and verify they are at the correct location on the image as highlighted by the yellow rectangles. The thickness of the sample is then shown by the orange rectangle on the left side and a summary of all samples analyzed is shown within the main file (B).

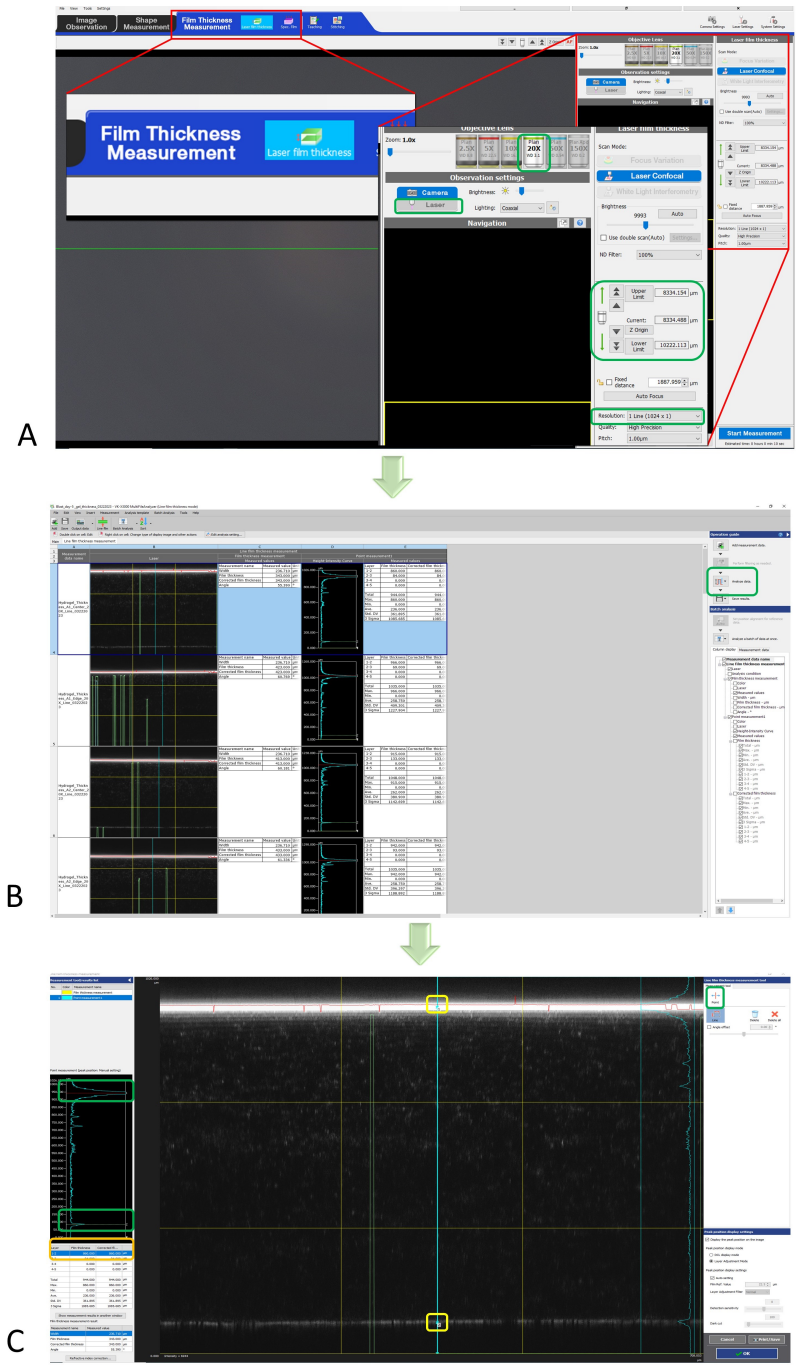

Figure D.1: Thickness measurement using Keyence 3D surface profilometer. Steps A-C depicts how to acquire thickness measurements and determine the thickness of a clear sample.